TECHNISCHE UNIVERSITÄT DRESDEN

Faculty of Forest, Geo and Hydro Sciences

Computational Hydrosystem Analysis: Applications to the Meijiang and Nankou Catchments in China

Dissertation for awarding the academic degree
Doctor of Natural Sciences (Dr. rer. nat.)

Submitted by
M.Sc. Feng Sun

Supervisor:

Prof. Dr. – Ing. Olaf Kolditz
Technische Universität Dresden
Helmholtz Centre for Environmental Research - UFZ

Prof. Dr. Rudolf Liedl
Technische Universität Dresden

Leipzig, January 2011

This is to certify that this copy is fully congruent with the original copy of the dissertation with the topic:

„ Computational Hydrosystem Analysis: Applications to the Meijiang and Nankou Catchments in China “

……
Place, Date

……
Signature (surname, first name)

Acknowledgments

First and foremost I would like to express my deep and sincere gratitude to my supervisor, Prof. Dr.-Ing. Olaf Kolditz. I appreciate all his contributions of time, ideas, and funding to make my Ph.D. experience productive and professional. The joy and enthusiasm he has for his research was contagious and motivational for me, even during the tough times in the Ph.D. pursuit. His wide knowledge and logical way of thinking have been of great value for me. His understanding, encouraging and personal guidance have provided a good basis for the present thesis.

I gratefully acknowledge the funding sources that made my Ph.D. work possible. I was funded by the China Scholarship Commission for the first year and the Helmholtz Association for the following two years. My work was also supported by Beijing Hydrological Center, China. I would also like to acknowledge the graduate school (HIGRADE) of Helmholtz Center for Environmental Research (UFZ), Leipzig which supplied me a lot of lectures and financed me for the international conferences.

The members of the Environmental Informatics group have contributed immensely to my personal and professional time at UFZ. The group has been a source of friendships as well as good advice and collaboration. I would especially like to acknowledge Dr. Wenqing Wang, Dr. Cui Chen and Dr. Haibing Shao for their invaluable hints and suggestions in my project work. Other past and present group members that I have had the pleasure to work with and would like to acknowledge are Dr. Chan-Hee Park, Dr. Thomas Kalbacher, Dr. Jens-Olaf Delfs, Dr. Joshua Taron, Dr. Yajie Wu and Dr. Karsten Rink.

My time at Leipzig was made enjoyable in large part due to the many friends and groups that became a part of my life. I am grateful for time spent with my roommates and friends, for my backpacking buddies and our memorable trips.

Lastly, I would like to thank my family for all their love and encouragement. For my parents who raised me with unconditional love and supported me in all my pursuits. For my sister who always gave me supportive and encouraging advices.

Of course, I would also like to thank anybody I missed who deserves a mention above. Thank you all!

Feng Sun
Leipzig
January 2011

Abstract

Hydrosystems are important elements of the hydraulic cycle. With population growth and climatic change impacting water resources, the existing water transport systems need to be reproduced in order to optimize the usage of the precious water resources. The individual flow process i.e. unsaturated soil flow and groundwater flow in porous and fractured media can be expressed by partial differential equations mathematically. The numerical models are generally used to give solutions of these equations with specific conditions.

In this work, the numerical solutions are carried out using the scientific software OpenGeoSys (OGS) based on the finite element method. The complex geometrical structure model domain can be imported into the numerical model with an implemented graphical interface. A GIS based relational database model GeoHydroDataBase (GHDB) designed to create a specialized set of geo- and hydro-objects is integrated with the numerical model.

The multi-field and detailed computational hydrosystem analysis methodology is applied to Meijiang catchment and Nankou site respectively. As an application, the case study for the Meijiang area with the focus on surface/subsurface water interaction and the recharge response from surface infiltration to groundwater with different time series discretization. In the Nankou case study, a 3-D regional groundwater flow model is developed. The hydrogeological system is reproduced according to sparsely distributed boreholes data. The model calibration and sensitivity analysis are accomplished with inverse methods by applying a model independent parameter estimation system (PEST). The results of the calibrated model show reasonable agreements with observed water levels. The transient groundwater flow simulations reflect the observed drawdown of the last 9 years and show the formation of a depression cone in an intensively pumped area. The well calibrated 3-D

groundwater model provides hydrogeological parameters and lateral fluxes from the adjacent mountain area for the following transport modeling and remediation scenarios analysis. In this study the method of capture zone type curves is used to estimate the pumping rate and the number of pumping wells needed for the contaminated aquifer cleanup. The analytical solutions of drawdown at the pumping wells (for both single pumping well and double wells) are compared with those calculated from the numerical model.

Symbols

Table 1: Latin symbols

Symbol	Meaning	Unit
C	Solute concentration	kg/m^3
D_d	Diffusion coefficient	m^2/s
g	Gravitational acceleration	m/s^2
h	Piezometric (hydraulic head)	m
κ	Permeability	m^2
K	Isotropic hydraulic conductivity	m/s
$\mathbf{K}$	Hydraulic conductivity tensor	m/s
K_d	Distribution coefficient	m^3/kg
M	Mass	kg
n	Porosity	m^3/m^3
p	Pressure	Pa
p_c	Capillary pressure	Pa
q	Darcy's flux	m/s
Q	Source/sink term	m^3/s
R	Retardation factor	-
S	Saturation	m^3/m^3
S_s	Volumetric specific storage	$1/m$
t	Time	s
x, y, z	Cartesian coordinates	m
$\mathbf{v}$	Velocity vector	m/s
V	Volume	m^3

Table 2: Greek and math symbols

Symbol	Meaning	Unit
α_T	Transverse dynamic dispersivity	m
α_L	Longitudinal dynamic dispersivity	m
β	Compressibility coefficient	$1/Pa$
θ	Moisture content	m^3/m^3
μ	Dynamic viscosity	$Pa \cdot s$
ρ	Material density	kg/m^3
ψ	Pressure head	m
ω	Tortuosity coefficient	-
Ω	Control volume, representative elementary volume (REV)	-
$\nabla()$	Gradient operator	
$\nabla \cdot ()$	Divergence operator	
∂	Partial differential	

Contents

List of Tables

List of Figures

Chapter 1

Introduction

1.1 State of the art

Hydrosystem is a term originally corned by Chow et al. [1988] to collectively describe the technical areas of hydrology, hydraulics and water resources including the application of economics, optimization, statistics and management. The terrestrial hydrosphere can be divided roughly into surface water, soil water and aquifer compartments [Kolditz et al., 2007]. The corresponding hydrological processes at the surface are lakes, rivers and overland flow during flooding, unsaturated soil flow in the subsurface and groundwater flow in porous and fractured media. Water exchange with the atmosphere occurs via evaporation and precipitation whereas root water uptake and transpiration represent links to the biosphere. Water in unsaturated soil is affected by suction gradients and its movement is subject to variations in conductivity resulting from changes in soil water content. Groundwater is recharged by percolation through the unsaturated zone, and the position of its surface (water table level) is determined by the relative rate of recharge versus outflow. From the view of mathematics and physics, those processes in the surface and subsurface compartments as well as their interactions can be described by partial differential equations.

An increasing realistic representation of hydrogeological processes by numerical modeling has been successively achieved during the last 30 years as the accuracy of numerical algorithms has continuously improved. Existing numerical codes for hydrosystem analysis are for instance MODFLOW2000 [Harbaugh et al., 2000], the Rainfall-Runoff

Model (TOPMODEL) [Bertoldi et al., 2004], Finite Element subsurface FLOW system (FEFLOW) [Wasy Software, 2004], MIKE-SHE emerged from European Hydrological System (SHE) [Abbott et al., 1986], HydroGeoSphere [Sudicky et al., 2003], Soil Water Assessment Tool (SWAT) [Arnold et al., 1998], Hydrologic Simulation Program Fortran (HSPF) [Gunduz and Aral, 2005] and OpenGeoSys (OGS) [Kolditz and Shao, 2010]. These models treat and couple different processes using a variety of simple to complex process descriptions, solution strategies and software concepts. They allow communication and data exchange between different hydrological simulation or data pre-/post- process tools with simple file interfaces to flexible interface manager. More discussions will be presented in the following sections.

1.2 Objective

Even though lots of efforts in the development of a new scientific software concept for integrated hydrological analysis, some challenges in the computational hydrosystem analysis when it is applied to the realistic sites still remain because of the complexity of hydrosystems in the reality. My PhD work focuses on tackling these challenges:

- Data Base System (DBS): The GeoHydroDataBase(GHDB) designed and constructed based on geographical information system (GIS) and Unified Modeling Language (UML), in which users can efficiently organize the integrated hydrosystem data, was coupled with OGS and applied to the Meijiang catchment.

- Geometrical modeling: The 3-D mesh generation of complicated hydrogeological structure with borehole data is based on Groundwater Modeling System (GMS), which also can communicate with OGS by means of the implemented interface.

- Numerical modeling: The complicated hydrological processes are described by mathematic equations and specific boundary conditions. These equations are solved with finite element method using OGS code. Some of benchmarks are presented following each part of the theories.

- Applications: OGS model calibration coupled with PEST, together with the geometrical model were applied to the Nankou project for the groundwater flow and mass transport simulation, as well as the scenario analysis providing the technical support for the future water management decision-making.

1.3 Dissertation organization

The dissertation is organized in the following structure. Chapter 2 describes the mathematical background of the flow and mass transport in the vadzones and aquifers, as well as some corresponding benchmark examples verified by OGS code. Chapter 3 documents the technical details regarding the data pre-processing and the implementation of the interface between GHDB/GMS and OGS. The calibration of OGS model coupled with PEST is also introduced in Chapter 3. The applications of the computational hydrosystem analysis to Meijiang and Nankou catchments in China are presented in Chapter 4. The summary and outlook of this work are concluded at the end.

Chapter 2

Hydrodynamics of the subsurface

The hydrological processes in the subsurface (i.e. infiltration, discharge, water flow as well as the transport of solutes) all occur in soils or rocks under actual meteorological conditions. The water flow in the interconnecting pores of the soil can be explained by the continuum soil physical concepts and theories. The essential part of these theories is the definition of a representative elementary volume (REV) [Bear, 1972] - the minimum volume of a soil sample required from which a given soil parameter measurement becomes independent of the size of the sample. That means in the macroscope view the soil physical properties such as porosity, permeability and dispersivity can be considered constant over this REV. In this thesis, the material properties and governing equations are based on this continuum concept.

2.1 Flow and mass transport in the vadose zone

2.1.1 Darcy's law

The Darcy's law was first formulated by Henry Darcy based on the results of experiments on the water flow through the sand bed in 1856. It is one of the basic equations in hydrogeological sciences on the description of the water movement in a porous media. Darcy's law is a simple mathematical formula. It indicates the proportional relationship between the flow rate and the head loss over a given distance. The formula can be expressed

as

$$q = -K\frac{\partial h}{\partial l} \tag{2.1}$$

where q is the flow rate $[LT^{-1}]$, K is the proportionality constant known as hydraulic conductivity $[LT^{-1}]$, $\frac{\partial h}{\partial l}$ is the hydraulic head gradient $[-]$. The negative symbol means that the flow direction is from the high hydraulic head position to the low one.

When the fluid is other material (i.e. oil or gas) than water flowing the same media, the conductivity in Eq. 2.1 can be replaced by the permeability κ $[L^2]$ of the porous media. The relationship between the hydraulic conductivity and the permeability is

$$K = \frac{\kappa \cdot \rho \cdot g}{\mu} \tag{2.2}$$

where ρ is the density of the fluid $[ML^{-3}]$, μ is the viscosity of the fluid $[ML^{-1}T^{-1}]$. Substitution of Eq. 2.2 into Eq. 2.1 yields the pressure formation of Dacy's law:

$$q = -\frac{\kappa}{\mu} \cdot \frac{\partial p}{\partial l} \tag{2.3}$$

2.1.2 Richards' equation

In the Darcy's experiment, the water is flowing in all pores of the sand under the hydraulic head gradient. In the field situation the soil in the vadose zone is unsaturated, and the water movement in the vadose zone is mathematically described by Richards' equation [Richards, 1931], which can be derived from the mass balance and Darcy's law.

The general form quoted for a mass balance is the mass that enters a system must, by conservation of mass, either leave the system or accumulate within the system, mass cannot be created or destroyed. For a given control volume with the edge length Δx, Δy and Δz (Fig. 2.1), the difference between the water flowing into the boundaries and that flowing out of the boundaries is equal to the difference of water content (θ) in the increment of time (Δt). The rate of inflow in the direction of the x axis is denoted by q_x. The change in q_x is assumed continuous, then the rate of outflow can be formulated by $q_x + \frac{\partial q_x}{\partial x}\Delta x$. The

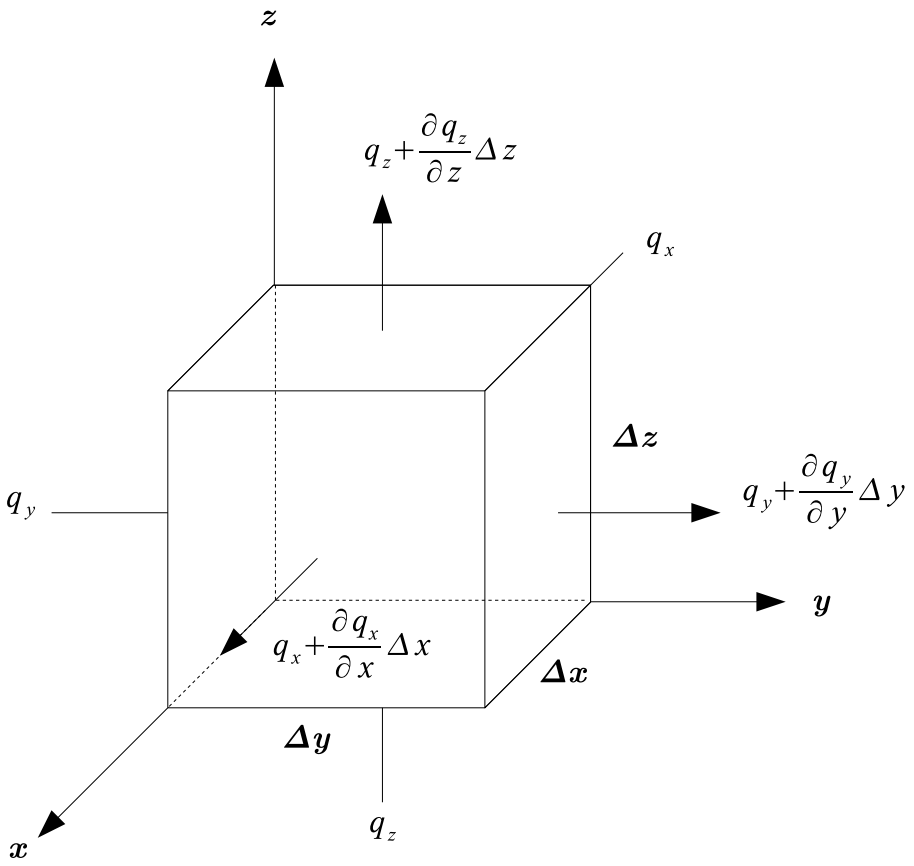

Figure 2.1: The control volume for water flow through porous media.

inflow volume is $q_x \Delta y \Delta z \Delta t$ and the outflow volume is $(q_x + \frac{\partial q_x}{\partial x}\Delta x)\Delta y \Delta z \Delta t$. Therefore the difference between inflow and outflow volumes (ΔQ_x) in the direction of x axis is expressed as

$$\Delta Q_x = q_x \Delta y \Delta z \Delta t - (q_x + \frac{\partial q_x}{\partial x}\Delta x)\Delta y \Delta z \Delta t = -\frac{\partial q_x}{\partial x}\Delta x \Delta y \Delta z \Delta t \qquad (2.4)$$

Similarly in the directions of the y axis and z axis, the differences between the inflow and the outflow volumes are expressed respectively as

$$\Delta Q_y = -\frac{\partial q_y}{\partial y}\Delta x \Delta y \Delta z \Delta t \qquad (2.5)$$

$$\Delta Q_z = -\frac{\partial q_z}{\partial z}\Delta x\Delta y\Delta z\Delta t \tag{2.6}$$

The sum of the above differences (Eq. 2.4, 2.5 and 2.6) equals to the change of the water content of the control volume, the water balance can be mathematically expressed as

$$\frac{\Delta\theta}{\Delta t}\Delta x\Delta y\Delta z\Delta t = -(\frac{\partial q_x}{\partial x} + \frac{\partial q_y}{\partial y} + \frac{\partial q_z}{\partial z})\Delta x\Delta y\Delta z\Delta t \tag{2.7}$$

Provided that $\theta(t)$ has a continuous derivative for $t > 0$, taking the limit as $\Delta t \to 0$, Eq. 2.7 can be formulated as

$$\frac{\partial\theta}{\partial t} = -(\frac{\partial q_x}{\partial x} + \frac{\partial q_y}{\partial y} + \frac{\partial q_z}{\partial z}) \tag{2.8}$$

Based on Eq. 2.1, the terms q_x, q_y and q_z can be replaced by $-K_x\frac{\partial h}{\partial x}$, $-K_y\frac{\partial h}{\partial y}$ and $-K_z\frac{\partial h}{\partial z}$, Eq. 2.8 becomes

$$\frac{\partial\theta}{\partial t} = \frac{\partial}{\partial x}(K_x\frac{\partial h}{\partial x}) + \frac{\partial}{\partial y}(K_y\frac{\partial h}{\partial y}) + \frac{\partial}{\partial z}(K_z\frac{\partial h}{\partial z}) \tag{2.9}$$

where K_x, K_y and K_z are the unsaturated hydraulic conductivities in the corresponding directions. As the soil is not saturated and flow occurs only in those pores filled with water, the value of K in the unsaturated situation will be smaller than the saturated hydraulic conductivity for the same soil. Therefore the unsaturated hydraulic conductivity is physically dependent upon the soil water content or saturation (S) and can be expressed by $K(\theta)$ or $K(S)$. For one-dimensional and vertical direction, the hydraulic head $h = \psi + z$, Eq. 2.9 can be expressed as

$$\frac{\partial\theta}{\partial t} = \frac{\partial}{\partial z}[K(\theta)(\frac{\partial\psi}{\partial z} + 1)] \tag{2.10}$$

where ψ is the pressure head $[L]$. If the porosity of the porous media is n, there is a relationship between the saturation and the water content

$$\theta = nS \tag{2.11}$$

Under the assumption that the air phase remains at constant pressure (atmospheric pressure) and the water phase is incompressible, the pressure change in the water is equal to the capillary pressure change in the opposite direction.

$$\Delta\psi = -\Delta p_c \tag{2.12}$$

Based on experimental data, simplified models [Brooks and Corey, 1964, van Genuchten, 1980] of capillary pressure as a function of water saturation can be constructed. There are also some empirical curves [Corey, 1954, Brooks and Corey, 1964, Lomeland et al., 2005] established based on the relationship between the relative permeability (κ_r) and water saturation. Give the z-axis is positive downwards, Eq. 2.10 can be transformed based on only saturation and pressure

$$n\frac{\partial S}{\partial p}\frac{\partial p}{\partial t} = \frac{\kappa_r \kappa_s}{\mu}(\frac{\partial p}{\partial z} - \rho g) \tag{2.13}$$

In the above equation, κ_s is the permeability of the porous media in the saturated situation.

2.1.3 Benchmark examples

Based on the above theory section, the processes in the hydrosystem can be expressed by partial differential equations (PDE). Only some of them with special initial and boundary conditions can be solved with analytical solutions. For the complicated PDEs, the finite element method (FEM) is used to find the approximate solutions. The following benchmark examples are intend to verify the numerical solutions applied FEM in OGS code with the analytical solutions, the observations or the results achieved from other numerical codes.

(A) Infiltration in homogeneous soil

• Problem definition

This case is a numerical modeling of the classical experiment by Warrick et al. [1971]. The solution is Richards' equation combining with uniform initial condition, fixed boundary condition without source term, and curve descriptions of homogeneous media properties.

As for the dimensional extension, line, triangle, quadrilateral, hexahedra, prism and tetrahedra mesh are used. The distinctions of different spacial discretization are presented in Fig. 2.5.

• Initial and boundary conditions

The uniform initial condition of the saturation in the whole domain is 0.455, which is -21500 Pa if it is expressed with the corresponding pressure. Boundary condition at the top is saturated and accordingly the pressure is 0. The pressure at the bottom is constant and equal to -21500 Pa in the simulation period. Details are illustrated in Fig. 2.2.

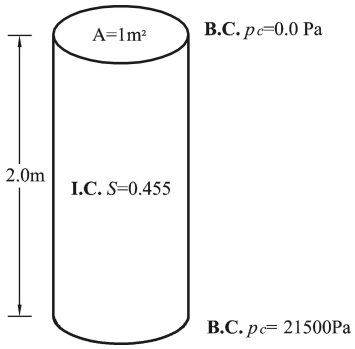

Figure 2.2: Illustration of numerical model and element test.

• Material properties

Homogeneous material properties are assumed within the whole domain. Table 2.1 gives the parameters.

Table 2.1: Parameters in the simulation of infiltration in homogeneous soil.

Parameter	Symbol	Setting	Unit
Porosity	n	0.38	-
Capillary pressure	$p(S)$	Curve in Fig. 2.3a	
Relative permeability	$\kappa_{rel}(S)$	Curve in Fig. 2.3b	
Saturated Permeability	κ_s	9.35e-12	m^2

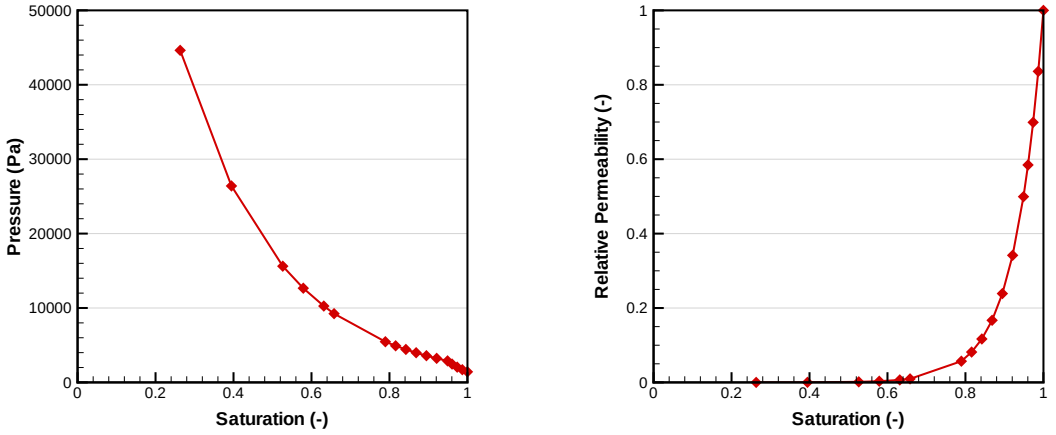

(a) $S - p_c$ (b) $S - \kappa_{rel}$

Figure 2.3: Relationships of capillary pressure-saturation and relative permeability-saturation.

• Results

Fig. 2.4 shows the distribution of saturation in the homogeneous soil column. The symbols in Fig. 2.4 are observed saturations by Warrick et al. [1971] and the solid lines are the calculated saturations. In Fig. 2.4 we also present the temporal evolution of the saturation in different colors.

Fig. 2.5 shows the distribution of saturation simulated with triangle or quadrilateral mesh respectively, the symbol-solid lines are 1-D results. When the mesh densities are

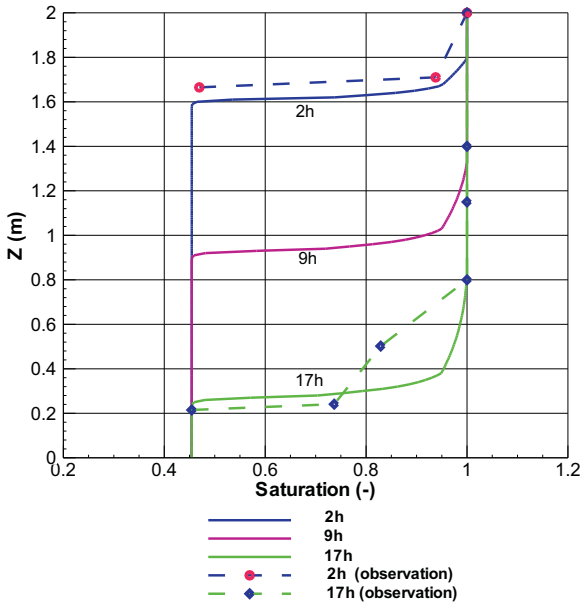

Figure 2.4: Comparison of observed and simulated saturation.

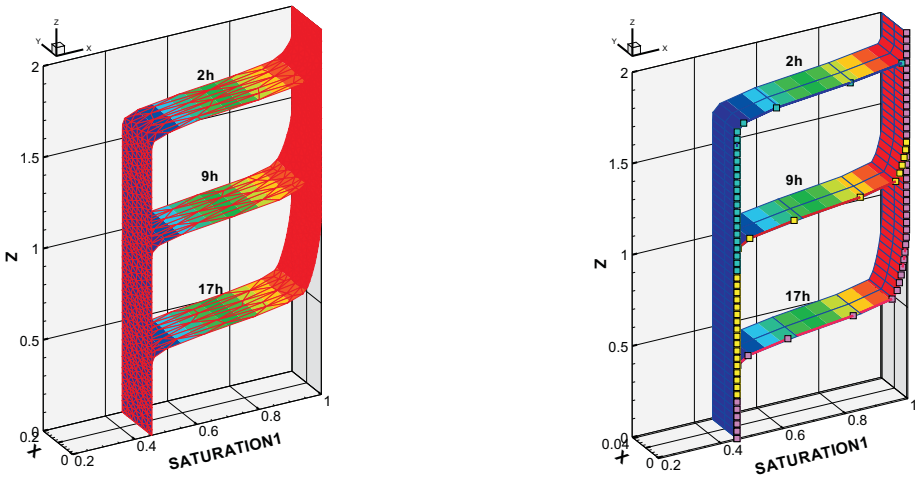

(a) triangle mesh

(b) quadrilateral mesh

Figure 2.5: Computed saturation with triangle and quadrilateral mesh compared with 1-D mesh (symbol-solid).

identical, the results are same; otherwise, there are distinctions.

(B) Conservative mass transport in unsaturated media

• Problem definition

This case is also a simulation of classical experiment by Warrick et al. [1971]. The solution is Richards' equation combining mass transport equation. For the hydraulic conditions, it is defined as the above section (A). For the mass transport, the tracer component goes inside from the top of the soil column.

• Initial and boundary conditions

Details of hydraulic conditions are illustrated in Fig. 2.2. The initial concentration of each component is 0, and the concentration changing in the simulation time at the top of the soil column is shown in Fig. 2.6.

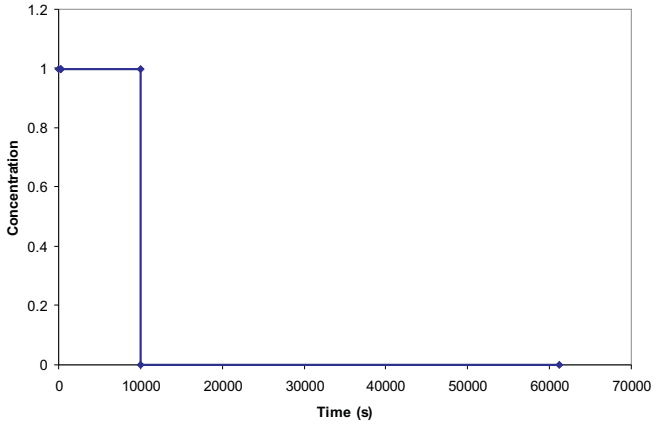

Figure 2.6: Boundary condition of the component.

• Material properties

Homogeneous material properties are assumed within the whole domain. Table 2.1 gives the parameters of material properties in this simulation.

• Component properties

Component properties are defined in Table 2.2.

Table 2.2: Parameters of component properties.

Component	Parameter	Symbol	Setting	Unit
	Mobile		1	
tracer	Transport phase water		0	
	Diffusion coefficient	D_d	6.0e-10	m^2/s
	Mobile		1	
	Transport phase water		0	
adsorb	Diffusion coefficient	D_d	6.0e-10	m^2/s
	Freundlich distribution coefficient	K_1	1e-3	
	Freundlich distribution coefficient	K_2	0.9	

• Results

The hydraulic features are shown in Fig.2.4. Fig. 2.7 shows the distribution of concentration. Points in the Fig.2.7 are observations.

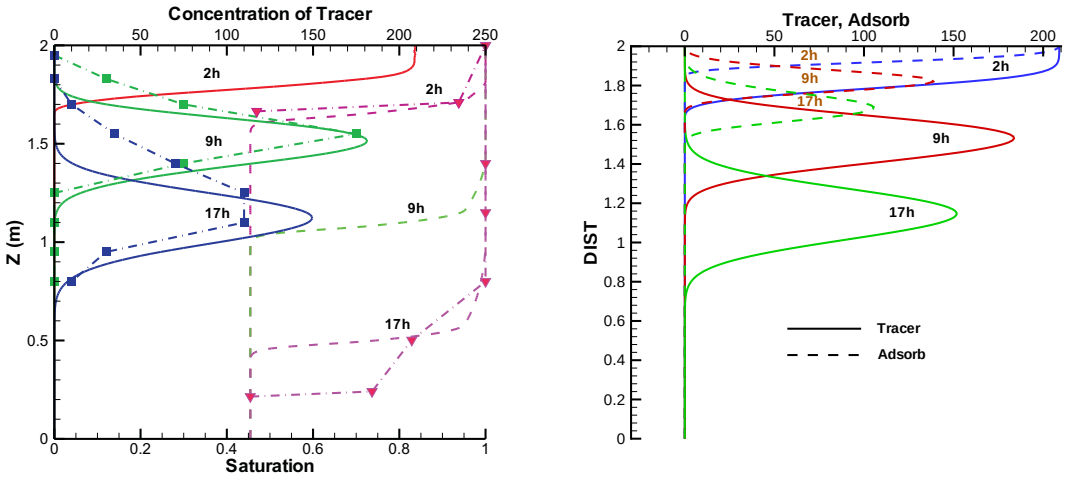

(a) (b)

Figure 2.7: Distribution of saturation and concentrations.

2.2 Flow and mass transport in groundwater

2.2.1 Groundwater flow equation

• Confined aquifer

The derivation of the groundwater flow equation is also based on the mass conservation and Dacy's law. For a given control volume, like we defined in Sec. 2.1.2, representing a small piece of confined aquifer, the water mass changing in an increment time (Δt) is equal to the difference between the water flowing into the boundaries and that flowing out of the boundaries

$$\frac{\Delta M_{storage}}{\Delta t} + W_{sink/source} = M_{inflow} - M_{outflow} \tag{2.14}$$

The confined aquifer is generally treated as saturated zone, then the water volume in it is equal to $n\Delta x\Delta y\Delta z$, where $n[-]$ is the porosity of the soil. Therefore, the water mass change in the given increment time is

$$\frac{\Delta M_{storage}}{\Delta t} = \frac{\partial M}{\partial t} = \frac{\partial}{\partial t}(\rho_w n dx dy dz) \tag{2.15}$$

Under most conditions, water can be considered incompressible (density does not depend on pressure). For the confined aquifer, the variation of the water mass storage in a control volume is because of the bulk aquifer material compressibility under the pressure. When the water and the aquifer are considered compressible, the water density ($\rho_w[M/L^3]$) and porosity of the aquifer will change as the pressure ($p[Pa]$) in the control volume changes. The compressibility of water, β_w can be defined as the rate of the relative change in density with regards to the pressure

$$\beta_w = \frac{1}{dp} \cdot \frac{d\rho_w}{\rho_w} \Rightarrow d\rho_w = \rho_w \cdot \beta_w \cdot dp \tag{2.16}$$

and if we assume the relative change of volume is only in the vertical direction, the bulk

aquifer material compressibility, β_a, can be given by

$$\beta_a = \frac{1}{dp} \cdot \frac{d(dz)}{dz} \Rightarrow \frac{d(dz)}{dz} = \beta_a \cdot dp \tag{2.17}$$

When the aquifer compresses or expands, the volume change of the solid part ($(1-n)dxdydz$) in the aquifer material is tiny enough to be neglected, that means

$$d[(1-n)dxdydz] = 0 \tag{2.18}$$

Differentiation of the above equation gives

$$d(1-n) \cdot dz + (1-n) \cdot d(dz) = 0 \Rightarrow dn = \frac{(1-n)d(dz)}{dz} \tag{2.19}$$

Substituting $d(dz)/dz$ with Eq. 2.17, Eq. 2.19 becomes

$$dn = (1-n)\beta_a dp \tag{2.20}$$

The differentiation of Eq. 2.15 is

$$\frac{\partial M}{\partial t} = (ndz \cdot \frac{\partial \rho_w}{\partial t} + \rho_w dz \cdot \frac{\partial n}{\partial t} + n\rho_w \cdot \frac{\partial (dz)}{\partial t})dxdy \tag{2.21}$$

Substituting $d\rho_w$, $d(dz)$ and dn with Eq. 2.16, 2.17 and 2.20 respectively, Eq. 2.21 becomes

$$\frac{\partial M}{\partial t} = \rho_w(n\beta_w + \beta_a) \cdot dxdydz \cdot \frac{\partial P}{\partial t} \tag{2.22}$$

Based on the derivation of Eq. 2.4, 2.5 and 2.6, the sum of volume differences between the water flowing into the control volume and that flowing out of the control volume is

$$-(\frac{\partial q_x}{\partial x}+\frac{\partial q_y}{\partial y}+\frac{\partial q_z}{\partial z})\Delta x\Delta y\Delta z\Delta t \tag{2.23}$$

Then the sum of the corresponding mass difference is

$$M_{inflow}-M_{outflow}=-\rho_w(\frac{\partial q_x}{\partial x}+\frac{\partial q_y}{\partial y}+\frac{\partial q_z}{\partial z})\Delta x\Delta y\Delta z \tag{2.24}$$

Combining Dacy's law (Eq. 2.1), Eq. 2.24 can be expressed by

$$M_{inflow}-M_{outflow}=\rho_w(K\frac{\partial^2 h}{\partial x^2}+K\frac{\partial^2 h}{\partial y^2}+K\frac{\partial^2 h}{\partial z^2})\Delta x\Delta y\Delta z \tag{2.25}$$

After the substitution of Eq. 2.25 and 2.22 into the water mass balance Eq. 2.14 and the replacement of the pressure differentiation ∂P with $\rho_w g\partial h$, the governing equation of the groundwater flow in a homogeneous aquifer is

$$\rho_w g(n\beta_w+\beta_a)\cdot\frac{\partial h}{\partial t}+W_s=K(\frac{\partial^2 h}{\partial x^2}+\frac{\partial^2 h}{\partial y^2}+\frac{\partial^2 h}{\partial z^2}) \tag{2.26}$$

In hydrogeology, the terms ($\rho_w g(n\beta_w+\beta_a)$) is defined as the volumetric specific storage (S_s[-]) [Freeze and Cherry, 1979], which is the aquifer material property that characterizes the capacity of releasing groundwater from storage in response to a decline of hydraulic head. Therefore a common formation of the groundwater flow equation in the homogeneous confined aquifer with sources or sinks in a 3-dimension is

$$S_s\frac{\partial h}{\partial t}+W_s=K(\frac{\partial^2 h}{\partial x^2}+\frac{\partial^2 h}{\partial y^2}+\frac{\partial^2 h}{\partial z^2}) \tag{2.27}$$

• Unconfined aquifer

Unconfined aquifers are those that have free water tables or phreatic surfaces in their upper boundaries. The phreatic surface fluctuates depending on the recharge/discharge rate of the aquifer. In a Cartesian coordinates system, the pressure head at any point (x, y, z) on this free surface Ω is equal to atmospheric pressure (where gauge pressure is equal to 0), that is

$$h(x, y, z, t) = z \quad x, y, z \in \Omega \tag{2.28}$$

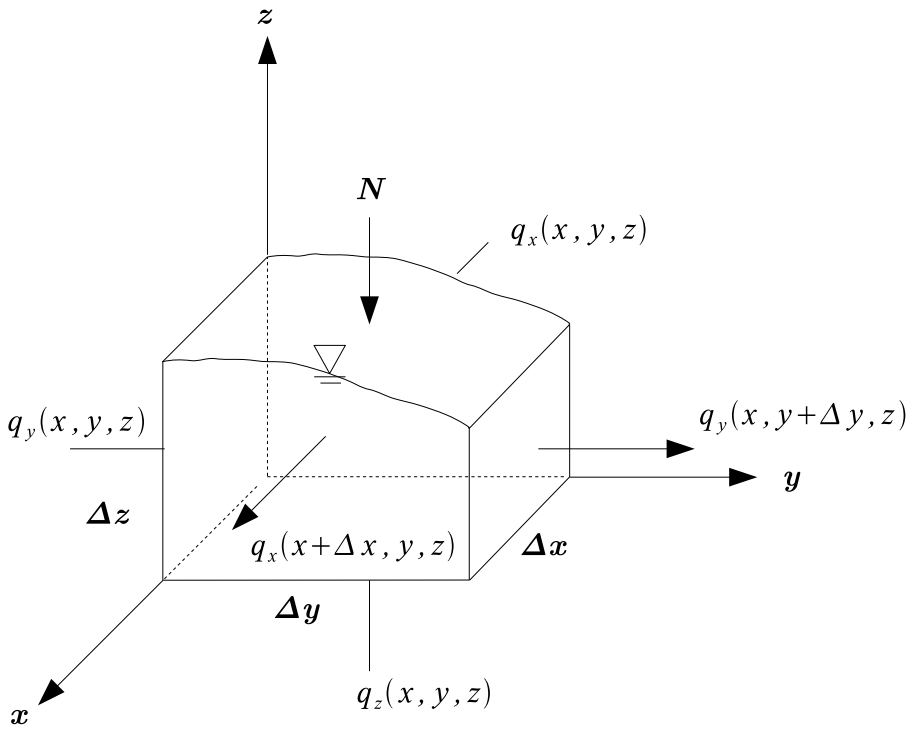

Figure 2.8: The control volume for water flow through the unconfined aquifer.

Considering a control volume inside the flow domain in an unconfined aquifer with the upper free surface (Fig. 2.8), the aquifer is assumed to be anisotropic and the vertical recharge/discharge rate is $N[LT^{-1}]$. Applying the mass conservation principle to this

unconfined control volume leads to:

$$\begin{aligned}
&[\Delta y(q_x\Delta z)\mid_{(x,y,z,t)} -\Delta y(q_x\Delta z)\mid_{(x+\Delta x,y,z,t)}]\Delta t\\
+&[\Delta x(q_y\Delta z)\mid_{(x,y,z,t)} -\Delta x(q_y\Delta z)\mid_{(x,y+\Delta y,z,t)}]\Delta t\\
&+(q_z+N)\Delta x\Delta y\Delta t\\
&=n_e(h\mid_{(x,y,z,t+\Delta t)} -h\mid_{(x,y,z,t)})\Delta x\Delta y
\end{aligned} \tag{2.29}$$

where q_x, q_y, q_z are Darcy's fluxes in the x, y,and z directions respectively, n_e is the effective porosity. When divided by $\Delta x\Delta y\Delta t$ on the both sides, Eq. 2.29 becomes

$$\begin{aligned}
&\frac{(q_x\Delta z)\mid_{(x,y,z,t)} -(q_x\Delta z)\mid_{(x+\Delta x,y,z,t)}}{\Delta x}\\
+&\frac{(q_y\Delta z)\mid_{(x,y,z,t)} -(q_y\Delta z)\mid_{(x,y+\Delta y,z,t)}}{\Delta y}\\
&+(q_z+N)\\
&=n_e\frac{h\mid_{(x,y,z,t+\Delta t)} -h\mid_{(x,y,z,t)}}{\Delta t}
\end{aligned} \tag{2.30}$$

When $\Delta t\to 0, \Delta x\to 0, \Delta y\to 0$, the differential form of Eq. 2.30 is

$$-\frac{\partial(q_x\Delta z)}{\partial x}-\frac{\partial(q_y\Delta z)}{\partial y}+q_z+N=n_e\frac{\partial h}{\partial t} \tag{2.31}$$

According to the chain rule of partial differentiation

$$\begin{aligned}
\frac{\partial(q_x\Delta z)}{\partial x}&=\Delta z\frac{\partial q_x}{\partial x}+q_x\frac{\partial\Delta z}{\partial x}\\
\frac{\partial(q_y\Delta z)}{\partial y}&=\Delta z\frac{\partial q_y}{\partial y}+q_y\frac{\partial\Delta z}{\partial y}
\end{aligned} \tag{2.32}$$

When $\Delta z\to 0$, $\Delta z\frac{\partial q_x}{\partial x}\to 0$ and $\Delta z\frac{\partial q_y}{\partial y}\to 0$. Combining Eq. 2.32, Eq. 2.31 becomes into

$$-q_x\frac{\partial(\Delta z)}{\partial x}-q_y\frac{\partial(\Delta z)}{\partial y}+q_z+N=n_e\frac{\partial h}{\partial t} \tag{2.33}$$

On the free surface Eq. 2.28 is true, then Eq. 2.33 can be written as

$$-q_x\frac{\partial h}{\partial x} - q_y\frac{\partial h}{\partial y} + q_z + N = n_e\frac{\partial h}{\partial t} \quad x, y, z \in \Omega \tag{2.34}$$

Based on Darcy's law $q_x = -K_x\frac{\partial h}{\partial x}$, $q_y = -K_y\frac{\partial h}{\partial y}$ and $q_z = -K_z\frac{\partial h}{\partial z} = -K_z(h = z)$, Eq. 2.34 becomes into the mathematic formation describing the free surface movement for a homogeneous unconfined aquifer

$$K_x(\frac{\partial h}{\partial x})^2 + K_y(\frac{\partial h}{\partial y})^2 - K_z + N = n_e\frac{\partial h}{\partial t} \quad x, y, z \in \Omega \tag{2.35}$$

2.2.2 Mass advection-dispersion equation

- Transport by concentration gradients

Solute particles in water will spread through random motion from regions of higher concentration to regions of lower concentration. This process is known as molecular diffusion or diffusion [Fetter, 1998]. Diffusion will occur as long as a concentration gradient exits, even if the fluid is not moving. The time dependence of the concentration statistical distribution in space can be expressed by Fick's second law, which can be derived from Fick's first law and the mass balance. The mass of fluid diffusing is proportional to the concentration gradient, which can be expressed as Fick's first law; in one dimension, it is

$$F = -D_d\frac{\partial C}{\partial x} \tag{2.36}$$

where F is the mass flux of solute per unit area per unit time $[ML^{-2}T^{-1}]$, D_d is the diffusion coefficient $[L^2T^{-1}]$, C is the solute concentration $[ML^{-3}]$ and $\frac{\partial C}{\partial x}$ is the concentration gradient $[ML^{-3}L^{-1}]$. Applied the mass balance of the solute to the control volume in one dimension,

$$\frac{\partial C}{\partial t}\Delta t = \frac{F - (F + \Delta F)}{\Delta x}\Delta t \tag{2.37}$$

When $\Delta x \longrightarrow 0$, Eq. 2.37 becomes

$$\frac{\partial C}{\partial t} = D_d \frac{\partial^2 C}{\partial x^2} \tag{2.38}$$

The above equation is known as Fick's second law, which was first derived by Adolf Eugen Fick in 1855. In porous media diffusion can not proceed as fast as it can in water because the ions must move along longer pathways as they travel around mineral grains. To account for this, an effective diffusion coefficient D^* is introduced to Eq. 2.38 instead of D_d, the relationship between them is

$$D^* = \omega D_d \tag{2.39}$$

where ω is a coefficient that is related to the tortuosity [Bear, 1972]. The value of ω is always less than 1 and can be achieved from diffusion experiments. According to Freeze and Cherry [1979], ω ranges from 0.5 to 0.01 for laboratory studies using geologic materials.

- Transport by advection

Dissolved solids are carried along with the flowing groundwater through the porous media. This process is called advective transport or convection. Based on Darcy's law, the quantity of groundwater flowing through a unit cross-sectional area of the porous media is

$$q_x = v_x n_e = -K \frac{\partial h}{\partial x} \tag{2.40}$$

Therefore, the one-dimensional mass flux F_x of advection is equal to the quantity of water flowing times the concentration of dissolved solids, which can be expressed as

$$F_x = v_x n_e C \tag{2.41}$$

where v_x is the average linear velocity in the x direction $[LT^{-1}]$.

- Transport by Mechanical dispersion

Groundwater is flowing at rates that are either greater or less than the average linear velocity due to the effects of individual pores in the granular aquifer. When the solute-containing water is invading to the aquifer at varied flow rates, mixing occurs along the flow path. This mixing is called mechanical dispersion, and it results in a dilution of the solute at the advancing edge of flow. The mixing that occurs along the direction of the flow path is called longitudinal dispersion and that in the direction normal to the flow path is called transverse dispersion. Although this mechanical dispersion process is very different to the diffusion, we can assume that it can been described mathematically by Fick's law as Eq. 2.36 and Eq. 2.38. Because the quantity of mechanical dispersion relates to the average linear velocity, the coefficient of mechanical dispersion in Eq. 2.36 can be expressed as a linear function of the average linear velocity:

$$\begin{aligned} D_{mL} &= \alpha_L v_i \\ D_{mT} &= \alpha_T v_i \end{aligned} \tag{2.42}$$

where D_{mL} is the coefficient of longitudinal mechanical dispersion, D_{mT} is the coefficient of transverse mechanical dispersion, α_L is the longitudinal dynamic dispersivity $[L]$, α_T is the transverse dynamic dispersivity $[L]$, v_i is the average linear velocity in the i direction.

- Hydrodynamic dispersion

The processes of molecular diffusion and mechanical dispersion in the flowing groundwater are not subjected to be separated from each other and can be grouped together to define a parameter called the hydrodynamic dispersion coefficient D. It can be given by

$$\begin{aligned} D_L &= \alpha_L v_i + D^* \\ D_T &= \alpha_T v_i + D^* \end{aligned} \tag{2.43}$$

where D_L is the hydrodynamic dispersion coefficient in the principle direction of the groundwater flow, D_T is the hydrodynamic dispersion coefficient in the direction normal to the principal groundwater flow.

In unfractured clay soils the coefficient of hydrodynamic dispersion is often controlled by the diffusion coefficient, and the coefficient of mechanical dispersion is negligible. In sandy soils and fractured layers the opposite is generally true and the mechanical dispersion dominates in the solute transport process except for the convection. The diffusion coefficient of solute in a porous media can be measured from laboratory diffusion experiments, and the dynamic dispersivity tends to be testing-scale dependent and is not a true property of the porous media [Gelhar et al., 1992].

- Advection-dispersion equation

The advection-dispersion transport equation is obtained by applying the mass balance of the solute to the control volume (Fig. 2.1) considering the solute fluxes transported by the advective and hydrodynamic dispersive processes. From Eq. 2.36 and Eq. 2.41, the solute flux through an aquifer with the porosity n_e can be expressed as

$$F_i = -D_i n_e \frac{\partial C}{\partial i} + v_i n_e C \tag{2.44}$$

The rate of the solute changing in an increment time in the control volume is

$$n_e \frac{\partial C}{\partial t} \Delta x \Delta y \Delta z \tag{2.45}$$

The total quantity of the solute entering the control volume is

$$F_x \Delta y \Delta z + F_y \Delta x \Delta z + F_z \Delta x \Delta y \tag{2.46}$$

The total quantity of the solute leaving the control volume is

$$(F_x + \frac{\partial F_x}{\partial x}\Delta x)\Delta y\Delta z + (F_y + \frac{\partial F_y}{\partial y}\Delta y)\Delta x\Delta z + (F_z + \frac{\partial F_z}{\partial z}\Delta z)\Delta x\Delta y \tag{2.47}$$

The difference between the mass of the solute entering the control volume and that leaving it is

$$-(\frac{\partial F_x}{\partial x} + \frac{\partial F_x}{\partial x} + \frac{\partial F_x}{\partial x})\Delta x\Delta y\Delta z \tag{2.48}$$

According to the law of mass conservation, the rate of mass change in the control volume must be equal to the difference in the mass of the solute entering and that leaving, that is

$$-(\frac{\partial F_x}{\partial x} + \frac{\partial F_x}{\partial x} + \frac{\partial F_x}{\partial x}) = n_e\frac{\partial C}{\partial t} \tag{2.49}$$

Substituting F_x, F_y and F_z with Eq. 2.44, Eq. 2.49 becomes

$$\begin{aligned}&[\frac{\partial}{\partial x}(D_x\frac{\partial C}{\partial x}) + \frac{\partial}{\partial y}(D_y\frac{\partial C}{\partial y}) + \frac{\partial}{\partial z}(D_z\frac{\partial C}{\partial z})]\\ &-[\frac{\partial}{\partial x}(v_xC) + \frac{\partial}{\partial y}(v_yC) + \frac{\partial}{\partial z}(v_zC)] = \frac{\partial C}{\partial t}\end{aligned} \tag{2.50}$$

If the Laplace operator is applied, the above equation can be written in a vector form as

$$\frac{\partial C}{\partial t} = \nabla\cdot(\mathbf{D}\cdot\nabla C) - \nabla\cdot(\vec{v}\ C) \tag{2.51}$$

Eq. 2.50 or Eq. 2.51 describes the advective-dispersive solute transport for a conservative solute through the porous media in three-dimensional without internal sources or sinks.

Solutes dissolved in groundwater are subject to be sorbed onto the surface of the mineral grains of the aquifer or organic carbon that might be present in the aquifer. As a result of sorption processes, some solutes will move much more slowly through the aquifer than the groundwater that is transporting them, this effect is called retardation. If there is a simple

linear relationship between the amount of a solute sorbed onto solid and the concentration of the solute, the retardation factor R can be defined as

$$R = 1 + \frac{\rho_b}{n} K_d \tag{2.52}$$

where ρ_b is the bulk density of the aquifer, n is the porosity and K_d is the distribution coefficient.

In addition to the adsorption processes through which the solutes can be removed from the aquifer, other reactions such as chemical reactions, biodegradation and radioactive decay might happen. If the effect of all these reactions can be assumed as a first order irreversible rate reaction, expressed by rate constant λ, the general equation for advective-dispersive transport incorporating equilibrium controlled linear sorption (Eq. 2.52) and first order irreversible reaction can be obtained as:

$$R\frac{\partial C}{\partial t} = \nabla \cdot (\mathbf{D} \cdot \nabla C) - \nabla \cdot (\vec{v}\, C) - \lambda R C \tag{2.53}$$

2.2.3 Benchmark examples

(A) Linear groundwater flow

(1) Flow in an anisotropic medium

• Problem definition

The aim of this example is to simulate the stationary groundwater flow in an anisotropic porous medium. In order to consider the anisotropy of permeability, a 2-D numerical model was built which contains a higher permeability in the vertical direction than that in the horizontal direction. The aquifer is assumed anisotropic, saturated and stationary.

• Model set-up of the 2-D numerical model

For the two-dimensional simulation, the cube consisting of a porous medium is simplified as a square with an area of 1 m^2. The calculation model includes 736 triangular

elements and 409 nodes. At the lower left corner of the model a constant pressure of 1000 Pa is specified along two polylines of the length of 0.3 m (Fig. 2.9). At the top and the right border the pressure is set to 0 in order to create the pressure gradient. As the porous medium is assumed to be anisotropic, which influences the groundwater flow, the values for permeability are equal to 1.0×10^{-15} m^2 in x-direction and 1.0×10^{-14} m^2 in y-direction. Other property of the anisotropic media is shown in Table. 2.3.

Table 2.3: The parameters defined in the anisotropic media.

Parameter	Symbol	Setting	Unit
porosity	n	0.2	–
permeability	κ_x	1.0×10^{-15}	m^2
permeability	κ_y	1.0×10^{-14}	m^2

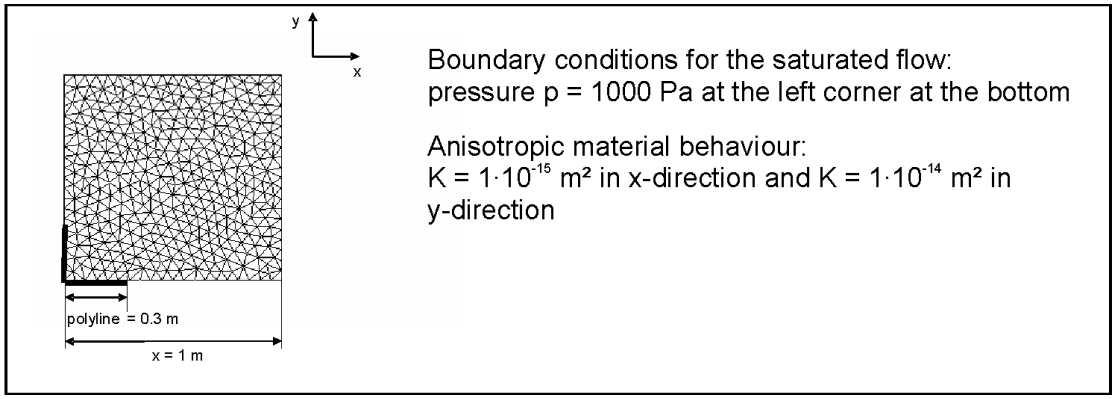

Figure 2.9: Calculation model (2-D) of the anisotropic media.

• Evaluation method

This test example is not made up to introduce a new process, but it shows the possibility for the OGS user to give a specific permeability for each direction. Therefore, the interpretation of OGS results comprises merely the comparison between pressure distributions due to anisotropic groundwater flow that were simulated by the use of RockFlow (RF) and OGS. This comparison is possible because both versions are developed separately concerning anisotropy of soils.

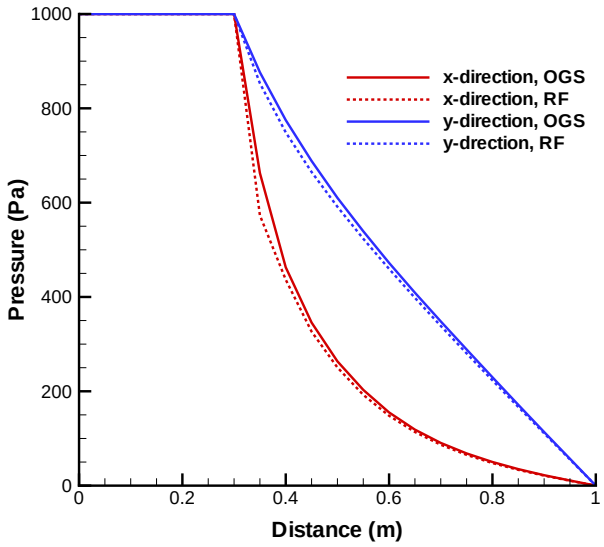

Figure 2.10: Pressure distribution caused by anisotropic saturated flow.

- Results

In Fig. 2.10 the horizontal and vertical pressure distributions of an anisotropic groundwater model which is developed using the program code RF are depicted next to those calculated from the above described anisotropic model with OGS. While presuming an anisotropic medium, an inhomogeneous pressure field is developing because the groundwater is not able to spread out uniformly. This can be recognized at the different curve gradients in x- and y-direction. There are slight differences between the curve characteristics of the RF and OGS simulation results. These differences are due to different element types (square in the RF model) and the resulting different x- or y-coordinates. Therefore, the pressure distributions obtained by the simulation with OGS are evaluated to be correct.

(2) Flow in an isotropic and heterogeneous medium

• Problem definition

The aim of this example is to simulate the stationary groundwater flow in an isotropic and heterogeneous porous medium. In order to consider the heterogeneous of hydraulic conductivity, a 2-D numerical model is built. The heterogeneous distribution of hydraulic conductivity is shown in Fig. 2.11. The aquifer is assumed isotropic, heterogeneous, saturated and stationary.

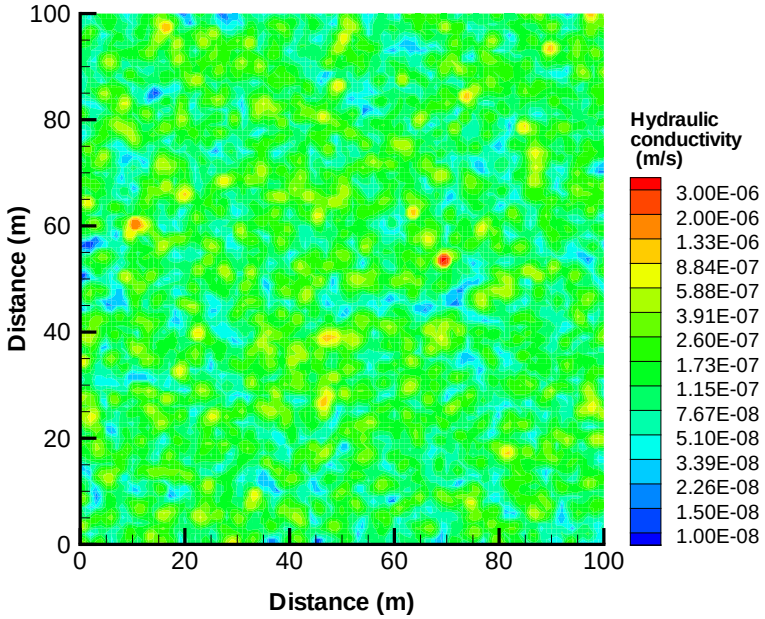

Figure 2.11: Calculation model (2-D): hetergeneous hydraulic conductivity distribution.

• Model set-up of the 2-D numerical model

For the two-dimensional simulation, the cube consisting of a porous medium is simplified as a square with an area of 10000 m^2. The calculation model includes 10000 quad elements and 10201 nodes. At the left boundary a constant head of 10 m and the right boundary a constant head of 9 m are specified in order to create a pressure gradient.

• Results

As shown in figure 2.12, the head distribution of the groundwater flow in a heterogeneous medium is depicted complying with the distribution of the hydraulic conductivity.

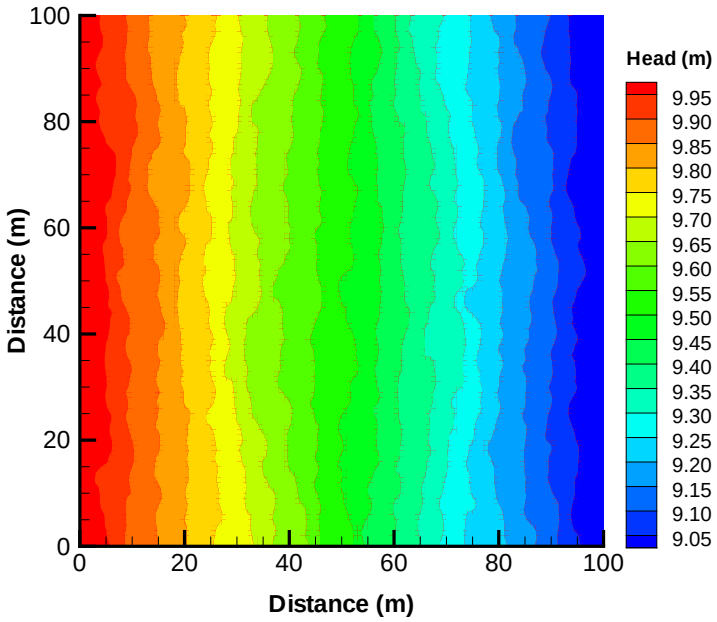

Figure 2.12: Head distribution in response to isotropic and heterogeneous medium.

• Model set-up of the 3-D numerical model

For the three-dimensional simulation, the aquifer is defined as a 100 m$\times$ 100 m$\times$ 50 m cuboid. The calculation model includes 60025 hex elements and 65000 nodes. A constant head of 10 m at the left surface and a constant head of 9 m at the right surface are specified in order to create a pressure gradient. The heterogeneous distribution of hydraulic conductivity is shown in Fig. 2.13.

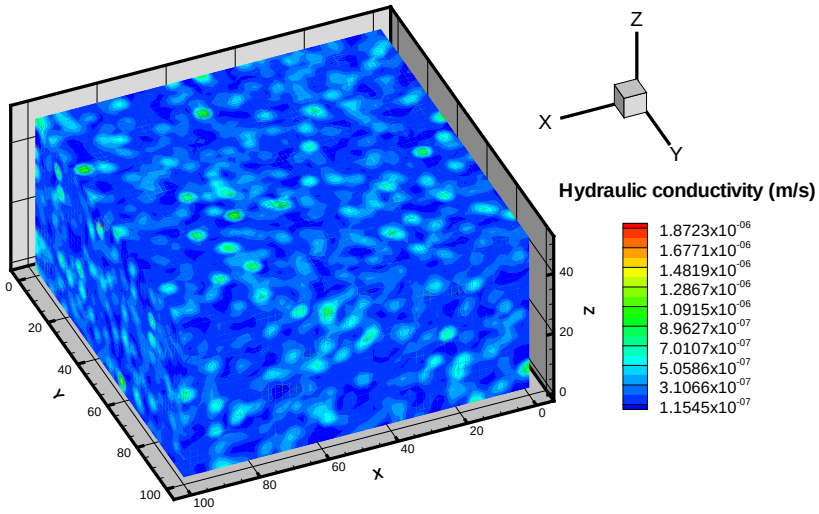

Figure 2.13: Calculation model (3-D): hetergeneous hydraulic conductivity distribution.

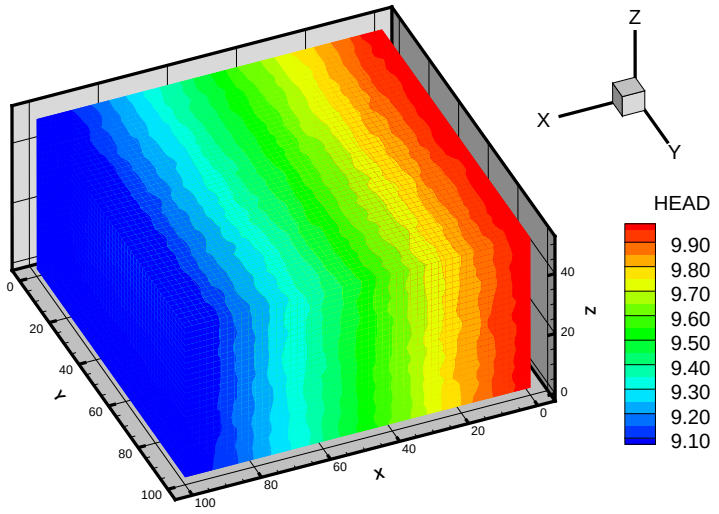

Figure 2.14: Head distribution in response to isotropic and heterogeneous medium (3-D).

• Results

As shown in figure 2.14, the 3-D head distribution of the groundwater flow in a heterogeneous medium is depicted in response to the distribution of the hydraulic conductivity.

(B) Confined aquifer

(1) Constant source term

• Problem definition

This example deals with an aquifer which is subject to a constant recharge line source. Glover [1978] presented an analytical solution for a constant line source in an infinite aquifer domain, which gives the groundwater head at any point of the source line by the following equation

$$h = q^{ex}\sqrt{\frac{\mu t}{\pi \rho g \kappa L S_y}} \tag{2.54}$$

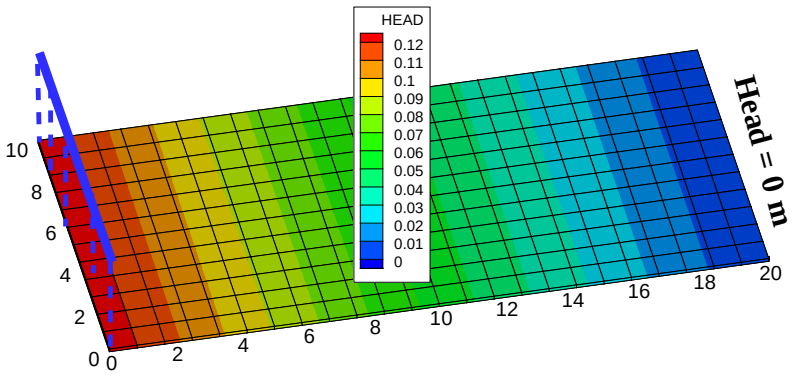

Figure 2.15: Computational domain and source term location.

• Initial and boundary conditions

In this benchmark, the aquifer size is 20 m$\times$ 10 m with the source term at the left boundary (See Fig. 2.15). The initial groundwater head is 0 m. The source term is $2.0\times10^{-4}\ m^2/s$ along the 10 m long channel, groundwater head is 0 m at the right boundary, and at the remaining parts there is no flow imposed. The simulation time is 30 minutes.

• Material properties

For the spatial discretization 24×12 quadrants are used. Material parameters are given in Table. 2.4.

Table 2.4: Parameters for the constant source term examples.

Parameter	Symbol	Setting	Unit
Storage	S	0.2	$-$
Viscosity	μ	1×10^{-3}	$Pa \cdot s$
Conductivity	K	1.0×10^{-3}	m/s
Thickness	L	25	m

• Results

Simulation results at the midpoint of left boundary are compared with the analytical solution in Fig. 2.16.

(2) Channel source term

• Problem definition

For this example the source term of the previous benchmark (Sec. *Constant source term*) is substituted by a corresponding channel source term. The integrated recharge flow that provides the link between the channel and the groundwater is defined by Eq. 2.55) [Gunduz and Aral, 2005]. The channel is assumed to be independent of the groundwater head and not affected by the water loss or the exchange flux. Therefore, the source term represents a steady and uniform channel located above the aquifer. The cross-section of

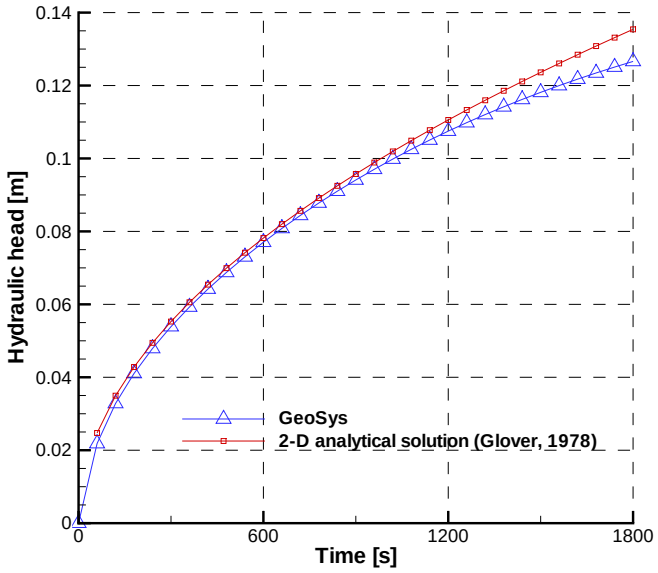

Figure 2.16: Simulation results and analytical solution for confined aquifer with line source term.

the channel is rectangular. The setup, spatial discretization, and calculated water head are shown in Fig. 2.15. The simulation time is 30 minutes.

$$q^{ex} = \begin{cases} -K_\Lambda P \frac{(h_r - h_g)}{a} & h_g > (z_r - a) \\ \\ -K_\Lambda P \frac{(h_r - (z_r - a))}{a} & h_g \leq (z_r - a) \end{cases} \tag{2.55}$$

where K_Λ is the channel bed conductivity, B is the channel width, a is the channel bed thickness, and h_r is the channel flow head, h_g is the groundwater table. The wetted perimeter $P = 2(h_r - z_r) + B$ for rectangular channel where z_r is the height of the top of the channel bed.

• Initial and boundary conditions

The initial groundwater head is 0 m. The channel source term is the boundary condition at one side, at the opposite boundary the head is fixed with 0 m. At the remaining boundaries no-flow is imposed.

• Material properties

For the spatial discretization either 24×12 quadrants or hexahedra are used as well prisms which are generated by cutting the hexahedra into two parts. The hexahedra or prism height is 1 m. The time step is 1 minute. Simulation parameters for the aquifer and the channel source term are given in Table. 2.5.

Table 2.5: Parameters for channel source term examples.

Parameter	Symbol	Setting	Unit
Aquifer			
Storage	S	0.2	$-$
Viscosity	μ	1.0×10^{-3}	$Pa \cdot s$
Conductivity	K	1.0×10^{-3}	m/s
Thickness	L	25	m
Channel source term			
Channel water surface	h_r	3	m
Bed top location	z_r	0	m
Bottom sediment thickness	a	0.3	m
Channel width	B	34	m
Bed conductivity	K_Λ	1.0×10^{-6}	m/s

A constant recharge value of $4.0 \times 10^{-4} m^2/s$ is obtained from Eq. 2.55 when the properties of the channel are defined as those values in Table. 2.5. Because this problem is symmetric for uniform and isotropic conditions in the aquifer and only half of the domain is taken into account. Therefore, the constant Neuman boundary condition is assigned with the half of the recharge value ($2.0 \times 10^{-4} m^2/s$).

• Results

Comparison of simulation results and analytical solution is given in Fig. 2.17 for quadrants and in Fig. 2.18 for hexahedra.

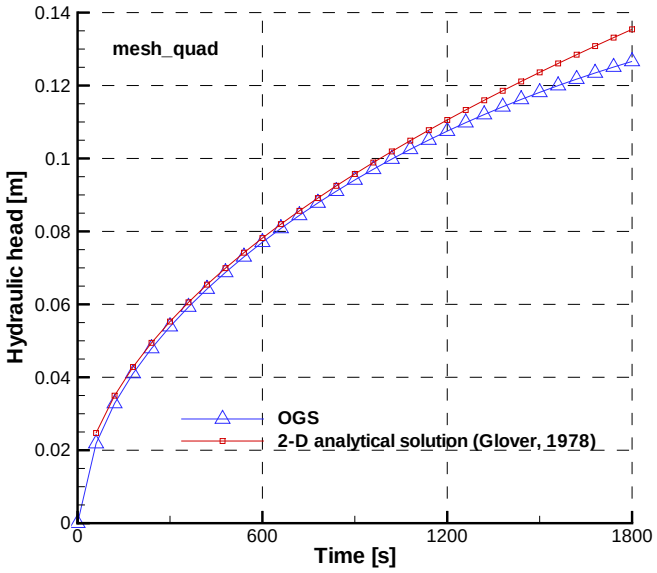

Figure 2.17: Results with quadratic elements and analytical solution for confined aquifer below uniform and steady channel.

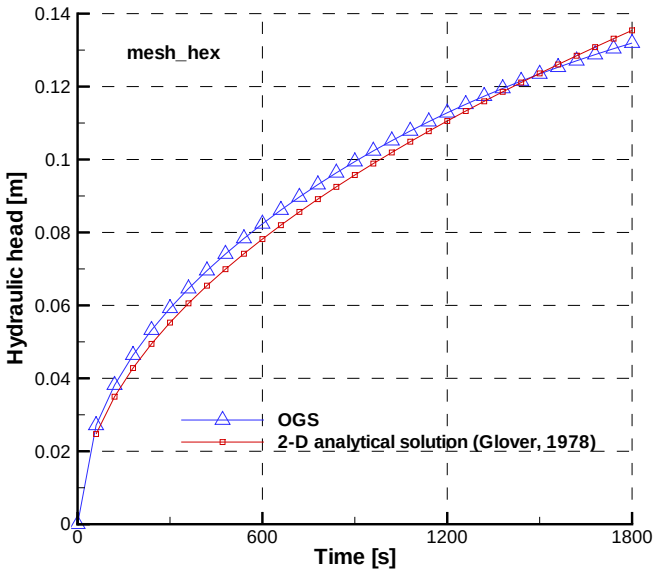

Figure 2.18: Results with hexahedral elements compared with the analytical solution for confined aquifer below uniform and steady channel.

(3) Channel sink term

• Problem definition

For this benchmark the channel of the previous example (Sec. *Constant source term*) is located under the surface of the aquifer so that the flow from the aquifer to the channel will take place. Therefore, the sink term represents a steady and uniform rectangular channel located in the aquifer. The simulation time is 30 minutes.

• Initial and boundary conditions

Initial groundwater head is 0 m. The channel sink term is the boundary condition at one side, at the opposite boundary the head is 0 m. At the other boundaries no-flow is imposed.

• Material properties

The domain is discretized with 24×12 quadrants. The time step size is 1 minute. Simulation parameters for the aquifer and the channel sink term are given in Table. 2.6.

Table 2.6: Parameters for the channel sink term example.

Parameter	Symbol	Setting	Unit
Aquifer			
Storage	S	0.2	$-$
Viscosity	μ	1.0×10^{-3}	$Pa \cdot s$
Conductivity	K	1.0×10^{-3}	m/s
Thickness	L	25	m
Channel sink term			
Channel water surface	h_r	-0.5	m
Bed top location	z_r	-0.7	m
Bottom sediment thickness	a	0.3	m
Channel width	B	59.6	m
Bed conductivity	K_Λ	1.0×10^{-6}	m/s

• Results

Simulation results are shown in Fig. 2.19.

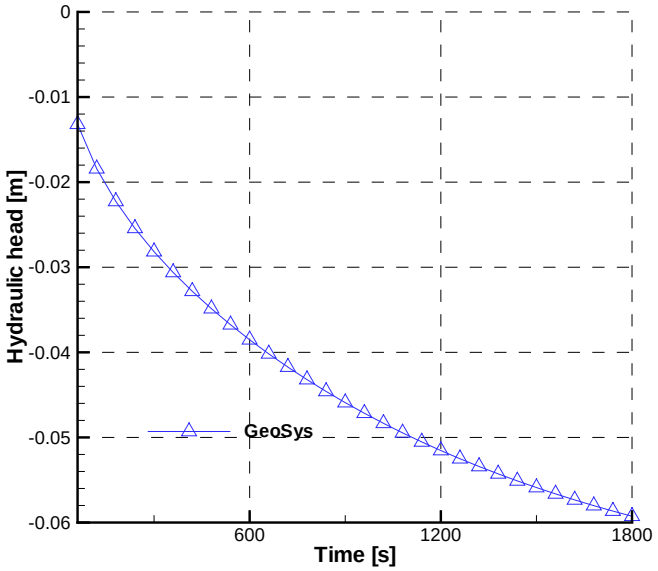

Figure 2.19: Simulation results for confined aquifer with a constant channel sink term.

(4) Theis' Problem

• Problem definition

Theis' problem examines the transient lowering of the water table induced by a pumping well. Theis' fundamental insight was to recognize that Darcy's law is analogous to the law of the heat flow by conduction, hydraulic pressure being analogous to temperature, pressure-gradient to thermal gradient.

• Assumptions

Aquifer: confined, infinite extended area, homogeneous, isotropic, uniform thickness, horizontal piezometric surface.

Well: constant discharge rate, well penetrates the entire thickness, well storage effects can be neglected.

• Analytical solution

The analytical solution of the drawdown as a function of time and distance is expressed by Eq. 2.56:

$$h_0 - h(t, x, y) = \frac{Q}{4\pi T} W(u) \tag{2.56}$$

$$u = \frac{(x^2 + y^2)S}{4Tt} \tag{2.57}$$

where h_0 is the constant initial hydraulic head $[L]$, Q is the constant discharge rate [L^3T^{-1}], T is the aquifer transmissivity [L^2T^{-1}], t is time $[T]$, x, y is the coordinate at any point $[L]$, S is the aquifer storage $[-]$.

• Initial and boundary conditions

The parameters and initial & boundary conditions are defined in Table. 2.7.

Table 2.7: The parameters defined in 1-D Theis' problem.

Parameter	Symbol	Setting	Unit
Initial conditions	$h(0, r)$	0	m
Well pumping rate	Q	1.2233$\times 10^3$	m^3/d
Boundary conditions	$h(t, 304.8)$	0	m
Flow materials			
-Hydraulic conductivity	K	9.2903$\times 10^{-4}$	m/s
-Storage coefficient	S	0.0010	-
-Wellbore radius	r	0.3048	m

• Results

Fig. 2.20 shows the comparison of analytically and numerically calculated drawdown of hydraulic head versus time at the distance of 9.639 m from the well.

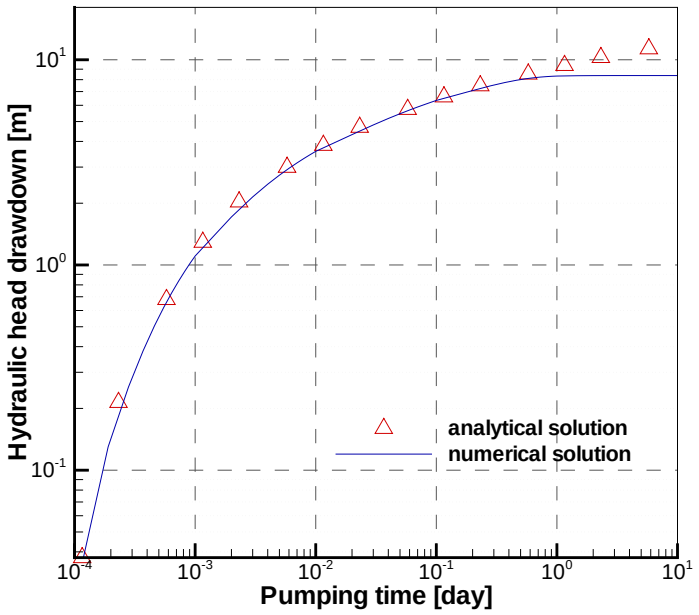

Figure 2.20: Calculated drawdowns at a distance of 9.639 m from the well.

• 2-D application

The 2-D application is solved in the following situation (Table. 2.8).

Table 2.8: The parameters defined in 2-D Theis' problem.

Parameter	Symbol	Setting	Unit
Discharge rate	Q	1000	m^3/d
Specific storage	S	1.0×10^{-5}	$1/m$
Transmissivity	T	1000	m^2/d
Thickness of aquifer	B	20	m

The aquifer horizontal domain size is 1000 m $\times$ 750 m with the pumping well at the location coordinate (500, 375). The discretization of space is 10 m $\times$ 10 m grid. The simulation time is 151.2 seconds and the time step is 1.036 seconds. The initial head is 20 m in the whole domain and the boundary condition is 0 m drawdown at the left and

right boundaries. There is no flux through the top and bottom boundaries. The cone of depression induced by the pumping well at the end of the simulation is plotted in Fig. 2.21.

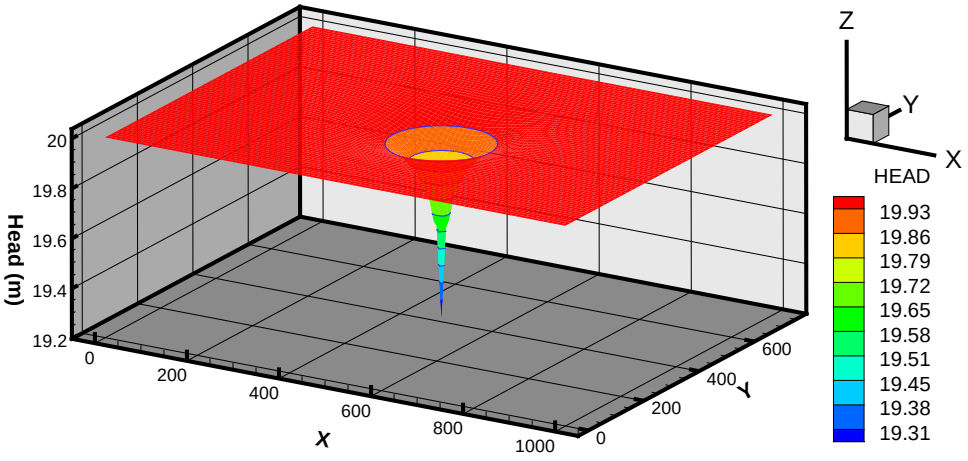

Figure 2.21: Cone of depression at the end of the simulation.

(C) Unconfined aquifer

Steady state case

• Problem definition

In this example the aquifer consists of a small strip with the size of 100 m $\times$ 2 m (see Fig. 2.22). At both ends the head is fixed and constant recharge is imposed on the whole domain which leads to steady state flow. This setting allows the comparison with an analytical solution.

• Initial and boundary conditions

Initial groundwater head is 0 m. At one end of the strip the head is 1 m at the other 5 m. At the top a source term is 1.0×10^{-8} m/s and at the remaining parts no-flow is imposed.

• Material properties

For the spatial discretization 100 equal quadrants and 410 triangles or prisms are used. In latter case, the three-dimensional unconfined groundwater equation (Eq. 2.35) is solved with elements adapting to the water height. One time step with the size of 100 s is used. The specific storage $S_s = 0$ m $^{-1}$ or specific yield $S_y = 0$ and a hydraulic conductivity K of 9.9×10^{-6} m/s is used.

• Results

Comparison of simulation results with prisms and analytical solution is shown in Fig. 2.22.

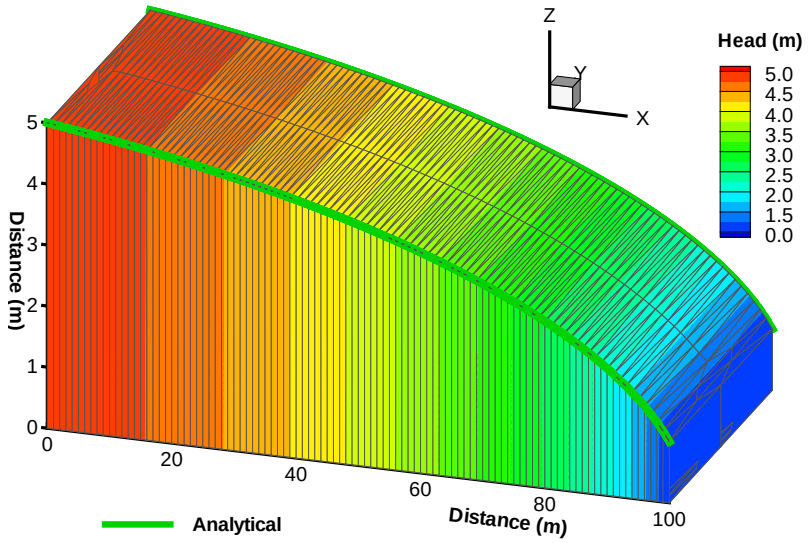

Figure 2.22: Benchmark example results of unconfined aquifer with prisms.

(D) Mass transport

(1) 1-D conservative transport with sorption and decay

• Problem definition

This benchmark describes conservative mass transport in a one-dimensional aquifer and has two aims. Firstly, a conservative component, a linearly retarded component and a decaying component at a first order decay rate are transported. The profiles and breakthrough curves are compared with the corresponding analytical solutions. This comparison is possible only using these simplified reaction types. Secondly, the benchmark is set up in a way that allows testing all element types in this simplified "quasi" one-dimensional setup.

The model aquifer has a length of 100 m in x direction and 1 m in both y and z direction. Discretization is in element sizes of 1 m in x direction, yielding 100 elements and 101 nodes for the line elements, 100 elements and 202 nodes for the quad elements, 200 elements and 202 nodes for the triangular elements, 100 elements and 404 nodes for the hexahedra elements, 200 elements and 404 nodes for the prism elements and 600 elements and 404 nodes for the tetrahedral elements. To make the boundary conditions consistent with all element types, surfaces in the y-z plane are used to define the boundary conditions at x=0 m and x=100 m.

The hydraulic conductivity is assumed to be isotropic and constant in the whole aquifer. Flow is from the left to the right (complying with the positive x axis), induced by fixed head boundary conditions at x=0 and x=100 and a total head difference of 1 m. All components have initial conditions of 0 and a constant concentration boundary condition of 1 at x=0. For the purpose of this benchmark, the concentration units are arbitrary and are therefore normalized. Transport velocity corresponds to 1 m/d, thus time step length is chosen accordingly as 86400 s (corresponding to 1 d). The total simulation time is 100 d. Thus the Courant number C = 1.0 and the grid Peclet number Pe = 4, keeping the effects of numerical dispersion as well as oscillations sufficiently small. All parameters used in this simulation are given in Table. 2.9.

Three components are used in this benchmark: the component `ConsTracer` denotes the conservative tracer, for which the advection - dispersion equation is solved; Component `Decay` is transported according to the advection - dispersion equation with a first order

decay rate λ; Component `SorbLin` is transported according to the advection - dispersion equation with a linear instantaneous sorption, which corresponds to a retardation of $R = 1 + \frac{1-n}{n}\rho_s K_d = 1 + \frac{0.5}{0.5} \cdot 2000 \cdot 0.001 = 3$. All components have the same aqueous phase diffusion coefficient.

Table 2.9: Parameters used for benchmark of 1-D conservative transport.

Parameter	Symbol	Setting	Unit
Porosity	n	0.5	–
Hydraulic conductivity	K	5.787×10^{-4}	m/s
Storage	S	0.0	-
Solid density	ρ_s	2000	kg/m^3
Density of water	ρ_w	1000	kg/m^3
Viscosity of water	μ	0.001	$Pa \cdot s$
Dispersion length	α_L	0.25	m
Diffusion coefficient	D_d	1.0×10^{-9}	m^2/s
First order decay rate in water	λ	1.0×10^{-7}	s^{-1}
Distribution coefficient	K_d	1.0×10^{-3}	m^3/kg

• Evaluation method

Model results are compared to the analytical solution for component profiles along x after a simulation time of 75 days, as well as for breakthrough curves at x=50 m for all components. To facilitate testing of all elements, a batch-file is provided (1D_all.bat) which reruns the benchmark for all element types by replacing the mesh file accordingly. Results can be viewed using the corresponding layout files by Tecplot.

The file of `companaProfile_*.lay` is used for displaying the profile results and `companaBTC_*.lay` is used for displaying the breakthrough curve results for element type `*`. The files `companalytBTC.lpk` and `companaProfile.lpk` save the simulation results for both types from an earlier OGS version for reference.

• Results

Results of the simulation and the comparison with the analytical solution are shown in Fig. 2.23 for the profiles and in Fig. 2.24 for the breakthrough curves. Numerical results using OGS are denoted by symbols, the analytical solution is denoted by the full lines. Correspondence is very good in both cases.

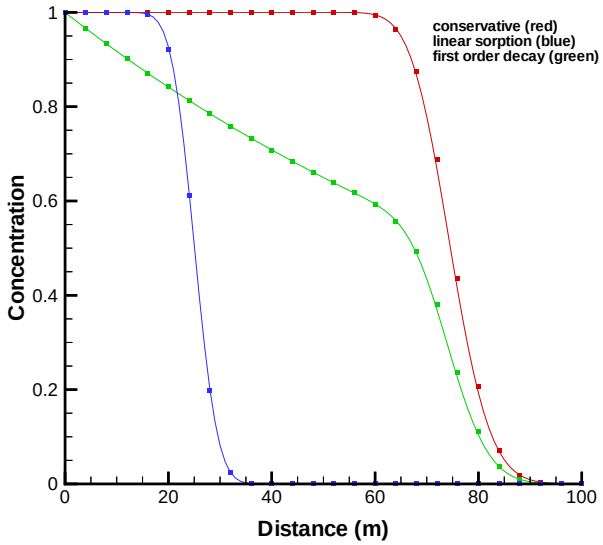

Figure 2.23: Comparison of analytical solutions and OGS simulated concentration profiles after 100 d.

(2) 2-D conservative transport

• Problem definition

This benchmark describes the conservative mass transport in a two-dimensional homogeneous aquifer. The main purpose is to compare the numerical results of a conservative mass transport simulation without any reactions with the suitable analytical solution.

The model aquifer has a length of 100 m in the x direction, 50 m in the y direction and 1 m in the z direction. The whole domain is discretized into 10560 triangular elements with a constant x and y dimension of 1 m (this value guarantees a Peclet number = 4), except at the boundaries of the injection area where a finer grid is chosen.

The aquifer is assumed to have a homogeneous and isotropic hydraulic conductivity and the constant head boundary conditions on the left (piezometric surface of 2 m) and right side (piezometric surface of 1 m) produce a steady state flow in the right direction.

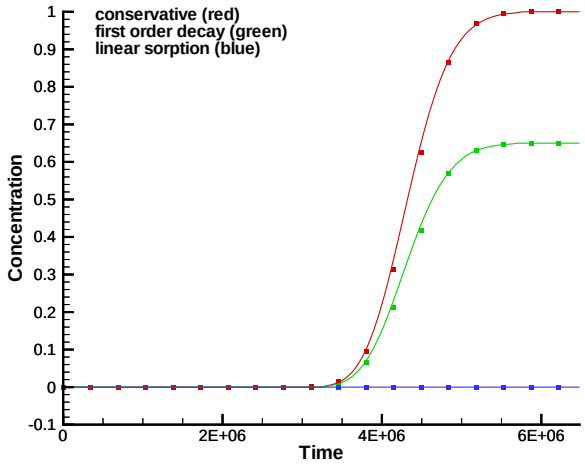

Figure 2.24: Comparison of analytical solution and OGS simulated concentration breakthrough curves at x = 50 m.

As the material has a constant porosity of 0.5 the resulting flow velocity is 1.1574 $\times 10^{-3}$ m/s. Both longitudinal and transversal dispersivity have a value of 0.25, consequently the total simulation time of 80 days is divided into 160 time steps to insure a Courant number lower than 1. The constant tracer is injected with a relative concentration value of 1.0 from a line source with an 8 m length set on the left boundary of the aquifer, while the initial concentration of the tracer is zero all over the aquifer domain. All parameters used in this simulation are given in Table. 2.10.

- Evaluation method

Model results are compared to the Hewson's analytical solution [Hewson, 1976] for a x-y planar view of the model domain as well as for breakthrough curves at x=60 m and x=80 m after a simulation time of 80 days. The Hewson's solution is more desirable for comparison of this benchmark than the solution by Domenico [1987], because it was developed for a finite width aquifer while the one of Domenico refers to an infinite width

aquifer.

Table 2.10: Parameters used for benchmark of 2-D conservative transport.

Parameter	Symbol	Setting	Unit
Porosity	n	0.5	–
Hydraulic conductivity	K	5.787×10^{-4}	m/s
Storage	S	0.0	-
Solid density	ρ_s	2000	kg/m^3
Density of water	ρ_w	1000	kg/m^3
Viscosity water	μ	0.001	$Pa \cdot s$
Longitudinal dispersivity	α_L	0.25	m
Transversal dispersivity	α_T	0.25	m
Diffusion coefficient	D_d	1.0×10^{-9}	m^2/s

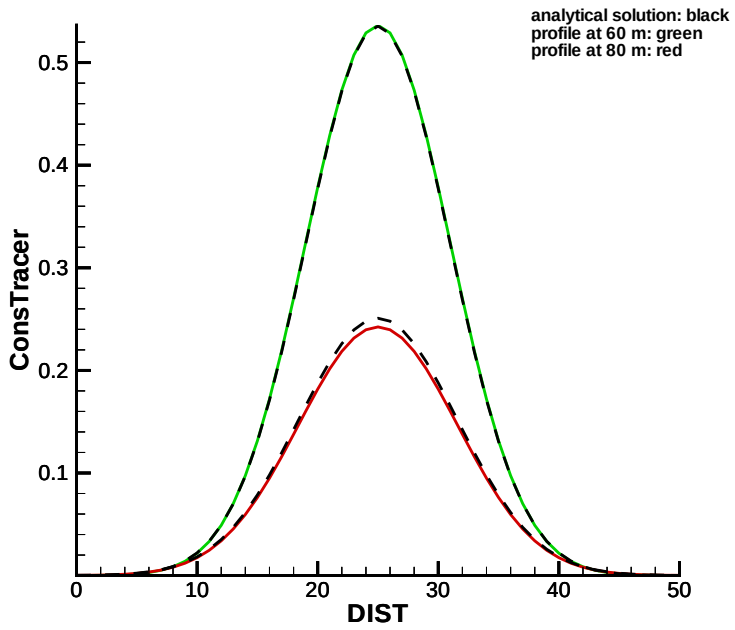

Figure 2.25: Comparison of analytical solution and OGS results with the profiles at 60 m and 80 m after 80 d.

• Results

Results of the simulation and the comparison with the analytical solution are shown in Fig. 2.25 for the profiles at 60 m and 80 m, and in Fig. 2.26 for the planar view. Numerical results using OGS are represented by the black line, while the Hewson's analytical solution is denoted by the red line. Correspondence is very good in both cases and from the x-y view we can also point out that the numerical simulation is able to properly reproduce the lateral and transversal spreading of the constant tracer.

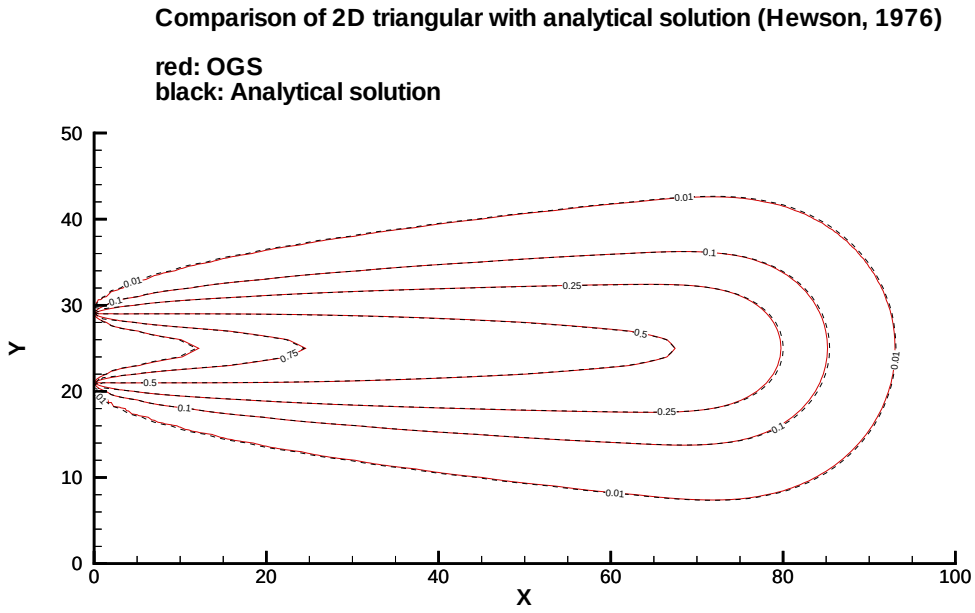

Figure 2.26: Comparison of analytical solution and OGS results (Planar x-y view after 80 d).

Chapter 3

Workflow and implementation of the model

3.1 Geometrical modeling

The Groundwater Modeling System (GMS) was first designed as a comprehensive graphical user environment for performing groundwater simulations in 1994. The entire GMS system consists of tools for site characterization, model conceptualization, mesh and grid generation and several models for groundwater simulations.

In this study, the modules of model conceptualization and mesh generation are used to do borehole data analysis and 3-D mesh creation. The procedure of the GMS based 3-D structure model analysis will be described in the following subsections.

3.1.1 Borehole data preparation

Generally, the borehole data contains site stratigraphic characteristics, which are used to represent soil layers. The soil layers are represented using contacts and segments in GMS as shown in Fig. 3.1. A contact is defined as the interface between two adjacent segments and the segments between contacts is associated with a soil type such as silt, sand or clay, etc. Each contact has a location (x, y, z), a horizon ID and two segment types (one for the material above and one for the material below the contact).

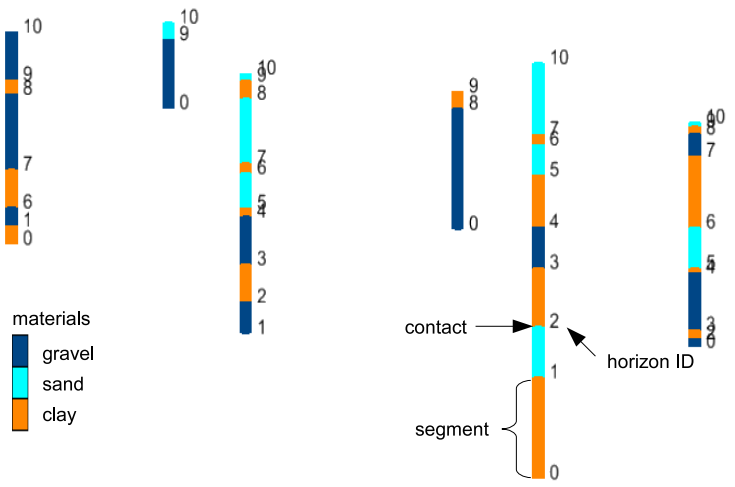

Figure 3.1: Boreholes representing soil stratigraphy with contacts, horizon ID and segments.

A horizon is defined as a surface representing the top of a geologic unit in a depositional sequence. The horizon IDs are assigned with numbers in the oder of this sequence in the borehole data file, starting at 1 and increasing from the bottom to the top, where 1 is associated with the top elevation of the bottom geologic layer (see Fig. 3.1).

3.1.2 Model boundary and primary TIN or 2-D mesh definition

The domain boundary can be directly defined by creating polygons in the “Map” module. Since polygons are defined by arcs, the first step in constructing a polygon is to create the arcs forming the boundary of the polygon. Once the arcs are created, they should be selected with the “Select Arc” tool, and the “Build Polygons” command can be applied from the “Feature Objects” menu. The other way to do this is to convert a shape file directly to a map coverage in the “GIS” module. By selecting the “GIS | ArcObjects → Feature Objects” command (with an ArcObjects license), or the “GIS | Shapes → Feature Objects” (without an ArcObjects license), a mapping wizard will be launched. Under this guidance, the process of converting GIS data to feature objects in a map coverage will be executed

step by step. A new active coverage with the attributes corresponding to the shape file should be created before this converting wizard starts.

After a domain boundary is constructed, there is a significant step before the primary TIN or 2-D mesh definition. It is to redistribute the vertices along the arcs because the density of the vertices will control the density of the triangles in the primary TIN or 2-D mesh. The spacing of the vertices can be adjusted at either a higher or lower density by using the command of “Redistribute Vertices” in the “Feature Objects” menu.

The primary TIN or 2-D mesh is a plan view or projection of the 3-D mesh. Each triangle in the 2-D mesh will result in a column of 3-D wedge elements (six node prism or five node pyramid). The “Map $\rightarrow$ 2D mesh or TIN” is the preferred method for mesh generation from a domain polygon with redistributed vertices in GMS.

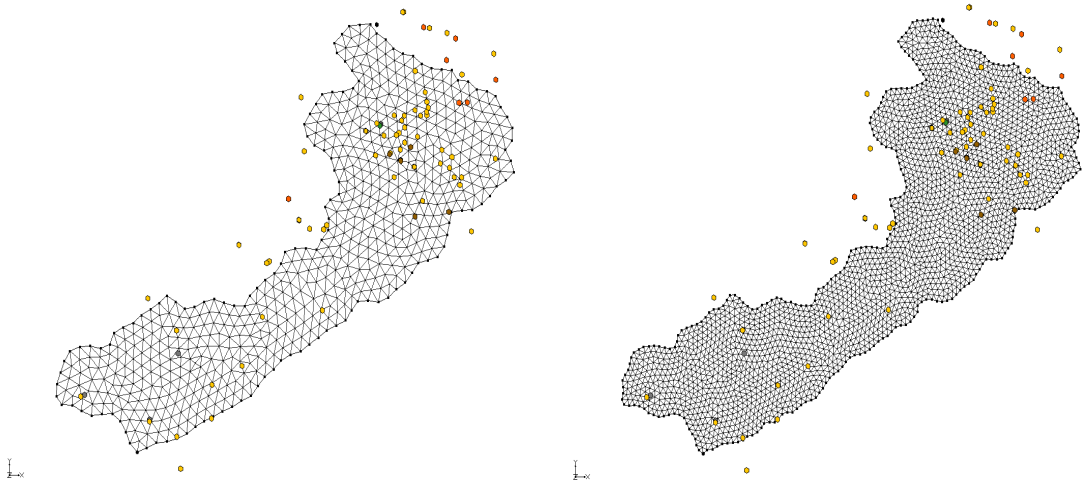

Figure 3.2: 2-D mesh with different density (spacing distance in the left is 1000 m, right is 500 m . Case study from the Selke catchment, Sachsen-Anhalt, Germany).

3.1.3 3-D mesh generation with horizon method

In GMS, 3-D finite element meshes are usually constructed in the “TINs” or “Boreholes” module and the applied method depends on available data. TINs for every horizon surfaces can be used directly to create a 3-D mesh by filling between TINs, otherwise only

with borehole data, the process should be started from the beginning step to assign horizon IDs to boreholes. After the horizon IDs are assigned to the boreholes and a primary 2-D mesh is created based on the research domain, the horizons wizard can be executed by selecting the "Horizons → 3D Mesh" command in the "Boreholes" or "TINs" menu.

When the "Horizons → 3D Mesh" command is executed, the horizons specified on the borehole contacts are converted to a set of scatter points with one data set for each horizon. The scatter points are then used to interpolate an elevation surface for each horizon with two optional interpolation methods: inverse distance weighted or natural neighbor. These horizon elevation surfaces are interpolated based on the primary 2-D mesh or TIN defined before, so every surface has the same number of nodes and topology with the primary 2-D mesh.

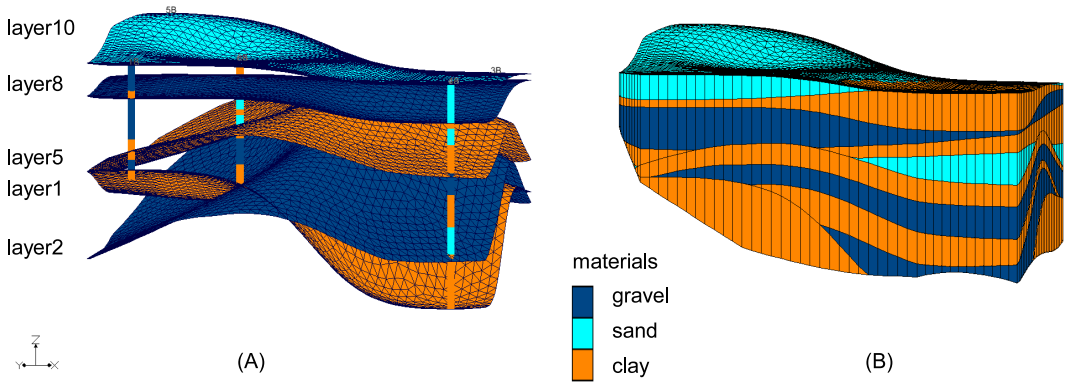

Figure 3.3: Example of layered mesh (A) and 3-D mesh (B).

In addition to the TINs defined by interpolating the horizon elevations, it is often very important to define two other TINs: a top surface TIN and a bottom TIN. The top TIN is usually imported from a raster file with the digital elevation model (DEM) of the research site, which is more accurate than that surface interpolated from the top elevations of the available boreholes. Likewise, the bedrock elevation data with high resolution for the bottom TIN is more accurate than that interpolated from the bottom elevations of boreholes.

Before a solid or 3-D mesh is build with horizon elevation surfaces, the primary 2-D mesh or TIN will be modified according to the intersecting horizon surfaces and the horizon

elevation have to be adjusted if the higher horizon has a lower elevation in some nodes than that in the next below horizon. The detailed modifications were described by Lemon and Jones [2003]. Each element in the 3-D Mesh will be represented by a material ID after the entire process is finished. Fig. 3.3 shows an example of layered mesh interpolated from scatter points in the different horizon groups and a 3-D mesh generated with borehole data.

3.1.4 Interface between GMS and OGS

OGS is a scientific open source code focused on the numerical simulation of thermo-hydro-mechanical-chemical (THMC) processes in porous and fractured media based on the finite element method. The 3-D mesh for hydrogeological model in OGS is generally mapped layer by layer with GIS raster data, and there is no function or module in it to create a 3-D spatial structure directly with borehole data. GMS with a series of powerful modules provides different interpolation methods to deal with the stratigraphic scattered points based on the borehole logs. The 3-D mesh created with GMS can be exported into an ASCII file with the extension of .3dm, which can be imported into OGS with the present implemented interface by rewriting the record of each node and element according to the syntax of OGS mesh file. This interface has been successfully used in several other case studies such as the Nankou area of Beijing Plain, China, the western Dead Sea Escarpment, Jordan and Selke catchment, Sachsen-Anhalt, Germany. The user interface implemented in OGS for importing GMS 3-D mesh is shown in Fig. 3.4.

3.2 Parameter estimation

Due to the complexity in geology of the study area, parameter identification is of great importance for groundwater modeling. To increase the model accuracy, an inverse method is often employed to calibrate the parameters by minimizing a user defined objective function. Poeter and Hill [1997] presented an introduction of inverse modeling by using simple nonlinear least-squares regression to calibrate transmissivity in a confined aquifer. Liu et al. [2009] combined the adjoint state, the gradient search and the least square error

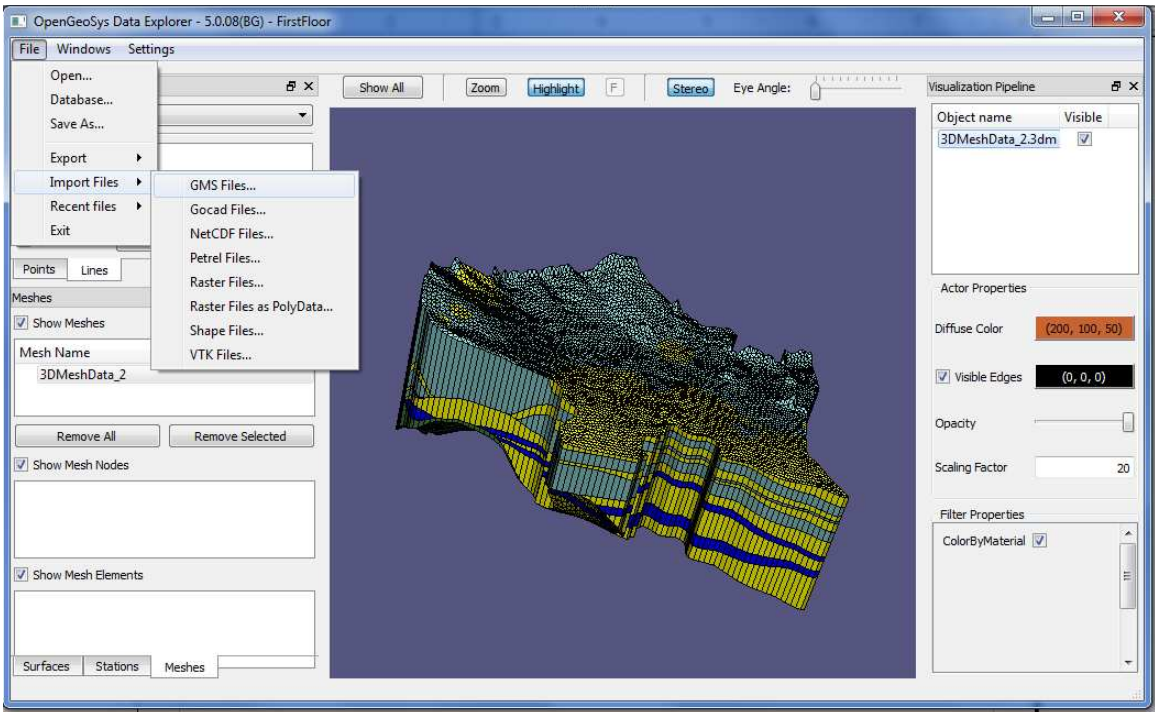

Figure 3.4: The interface for importing GMS 3-D mesh to OGS.

algorithm and applied them simultaneously to estimate aquifer parameters, initial conditions and boundary conditions for a confined aquifer. In order to accomplish the calibration procedure automatically, practical nonlinear least-squares inverse modeling softwares such as MODINV [Doherty, 1990], MODFLOWP [Hill, 1992], PEST [Doherty, 2004] and UCODE_2005 [Poeter et al., 2005] are well established and can be efficiently integrated with other groundwater modeling simulators. In this study, the model independent nonlinear parameter estimation code PEST was applied with OGS for parameters identification. In the following subsections, the mathematics of PEST and the OGS/PEST work flow will be introduced.

3.2.1 Mathematical theory

The goal of any model calibration is to minimize the differences between a set of observed values and model-generated values. In PEST an objective function Φ is defined as

the weighted sum of the squared differences between model-generated and observed values. The purpose of PEST is to achieve a minimal Φ by adjusting the parameters to be optimized iteratively.

• Linear Models

A linear model, i.e. in which observations are calculated from parameters through a matrix equation with constant parameter coefficients, can be described by the following equation

$$\mathbf{Xp} = \mathbf{h} \tag{3.1}$$

where $\mathbf{X}$ is a $m \times n$ matrix and the elements of $\mathbf{X}$ are constant as well as independent of the elements of vector $\mathbf{p}$, which is a vector of order n composed by system parameters. $\mathbf{h}$ is a vector of order m containing model-generated values corresponding to the observed values consisting of vector $\mathbf{h}_0$. If a weight is supplied with each observation, the objective function Φ can be expressed by

$$\Phi = \sum_{i=1}^{m} (w_i r_i)^2 \tag{3.2}$$

where w_i is the weight of the ith observation, r_i(the ith residual) is the difference between the model-generated and observed values for the ith sample point. Eq. 3.2 can be expressed in another way combined with Eq. 3.1

$$\Phi = (\mathbf{h}_0 - \mathbf{Xp})^T Q (\mathbf{h}_0 - \mathbf{Xp}) \tag{3.3}$$

where Q is a diagonal matrix whose ith diagonal element q_{ii} is the square of w_i, T is the matrix transpose operation.

• Nonlinear Models

Most models are nonlinear, such as Richards' equation for unsaturated water flow (Eq.2.13). If the relationship between parameters and model-generated observations for a particular model is represented by a continuously differential function M, which maps n-dimensional parameter space into m-dimensional observation space, the model system can be described by

$$\mathbf{h} = M(\mathbf{p}) \tag{3.4}$$

Supposed that for the set of parameters comprising the vector $\mathbf{p}_0$, the corresponding set of model-generated observations with function M is $\mathbf{h}_0$. If there is a parameter vector $\mathbf{p}$ that differs only slightly from $\mathbf{p}_0$, the nonlinear model can be linearised with Taylor's approximation

$$\mathbf{h} = \mathbf{h}_0 + \mathbf{J}_M(\mathbf{p} - \mathbf{p}_0) \tag{3.5}$$

where $\mathbf{J}_M$ is the Jacobian matrix of M, which is a $m \times n$ matrix comprised of $\mathbf{J}_{ij}$ (the derivative of the ith observation with respect to the jth parameter). Then the objective function Φ for nonlinear model can be defined by

$$\Phi = (\mathbf{h} - \mathbf{h}_0 - \mathbf{J}_M(\mathbf{p} - \mathbf{p}_0))^T Q(\mathbf{h} - \mathbf{h}_0 - J_M(\mathbf{p} - \mathbf{p}_0)) \tag{3.6}$$

Denoting $\mathbf{u}$ as the parameter upgrade vector $(\mathbf{p} - \mathbf{p}_0)$, it can be given by minimizing Φ in Eq. 3.6 as following

$$\mathbf{u} = (\mathbf{J}_M{}^T Q \mathbf{J}_M)^{-1} \mathbf{J}_M{}^T Q(\mathbf{h} - \mathbf{h}_0) \tag{3.7}$$

Eq. 3.7 explains that why we need an initial set of parameters supplied to start off the optimization process in PEST.

3.2.2 PEST parameter estimation work flow with OGS

PEST communicates with OGS through the model's own input/output files and the corresponding prepared template/instruction files. A PEST control file which "brings it all together", supplying PEST with the names of all template and instruction files together with the model input/output files to which they pertain. It also provides PEST with the model name, parameter initial estimates, field or laboratory measurements to which model outcomes must be matched, prior parameter information, and a number of PEST variables which control the implementation of the Gauss-Marquardt-Levenberg method. In the following subsections, some important basics of PEST will be described briefly.

- Templates of model input files

The PEST template files are prepared for those model input files containing parameters need to be adjusted. To construct a template file, simply start with a model input file and replace each space occupied by a parameter with a set of characters that both identify the parameter and define its width on the input file. Then whenever PEST runs the model it copies the template to the model input file, replacing each parameter space with a parameter value as it does so. Generally, the PEST template file should be saved as an ASCII file with the extension of *.tpl*.

Table 3.1: An example of OGS input file and the corresponding PEST template file.

OGS input file	PEST template file
	ptf !
GeoSys-MMP Material Medium Properties	GeoSys-MMP Material Medium Properties
#MEDIUM_PROPERTIES	#MEDIUM_PROPERTIES
$GEOMETRY_DIMENSION	$GEOMETRY_DIMENSION
3	3
$GEO_TYPE	$GEO_TYPE
DOMAIN	DOMAIN
$POROSITY	$POROSITY
1 0.3	1 0.3
$PERMEABILITY_TENSOR	$PERMEABILITY_TENSOR
ORTHOTROPIC 6.E-4 6.E-4 6.E-4	ORTHOTROPIC !Kh0! !Kh0! !Kz0!
#STOP	#STOP

See an example of OGS input file and the corresponding PEST template file in Table. 3.1. In the PEST template file, the first line must contain the letters “ptf” followed by a space and a single character (parameter delimiter, the example in Table 3.1 takes “!”). The “ptf” is a key word which stands for PEST template file. The name of parameter e.g. Kh0 is identified by the set of characters within the parameter space, between the parameter delimiters.

- Instructions to read model output files

In the process of PEST parameter estimation, the model-generated values which need to be compared with those corresponding observed or measured values are transfered to PEST under the directions built in an instruction file. In order to distinguish the instruction files from other types of file, they are provided with the extension of *.ins*. An example of OGS output file and the corresponding PEST instruction file is shown in Table 3.2.

Table 3.2: OGS output file and the corresponding PEST instruction file.

OGS output file	PEST instruction file
TITLE = “Time curves in points”	
VARIABLES = “TIME” HEAD	
ZONE T=“POINT=POINT320”	pif @
0.000000000000e+000 4.353690000000e+001	@0.000000000000e+000@
3.650000000000e+002 4.353227798740e+001	l1 $[head320_2]$21:40
7.310000000000e+002 4.351502506330e+001	l1 $[head320_3]$21:40
1.096000000000e+003 4.348890554506e+001	l1 $[head320_4]$21:40
1.461000000000e+003 4.345771440423e+001	l1 $[head320_5]$21:40
1.826000000000e+003 4.342239049354e+001	l1 $[head320_6]$21:40
2.192000000000e+003 4.338162501887e+001	l1 $[head320_7]$21:40
2.557000000000e+003 4.335789740162e+001	l1 $[head320_8]$21:40
2.922000000000e+003 4.335577804972e+001	l1 $[head320_9]$21:40
3.287000000000e+003 4.336647086600e+001	l1 $[head320_10]$21:40

Like in the PEST template file, the first line of a PEST instruction file must begin with

the three letters “pif” which stand for “PEST instruction file”. Then, after a single space, must follow a single character, the marker delimiter. The role of the marker delimiter in an instruction file is unlike that of the parameter delimiter in a template file. Its role is to define the extent of a marker; a marker delimiter must be placed just before the first character of a text string comprising a marker and immediately after the last character of the marker string. In the same way that each parameter must have a unique name, so must each observation be provided with a unique name, which is put between square brackets.

When PEST reads a model output file in the forward (top-to-bottom) direction, it looks at the instructions in the instruction file to check out what to do next. As shown in Table 3.2, firstly PEST records the line number where the marker delimiter is located by searching the whole output file. Then in the first line following the above marker, the characters between the position 21 and 40 are transferred to the observation variable head_320.

- The PEST control file

Once all the template and instruction files have been prepared for a particular case, a PEST ”control file” must be prepared which is a “command center” for every behavior of PEST. In particular, the control file must have an extension of *.pst*. Many of data items in the PEST control file are used to tune PEST’s operation to the case in hand; such items include parameter change limits, parameter transformation types, termination criteria etc. A PEST control file must begin with the letters “pcf”. A number of section headers (blue color) are scattered through the file as shown in Table 3.3. Further detailed discussion about the control file can be found in the PEST manual [Doherty, 2004].

Table 3.3: An example of PEST control file based on the case of OGS.

```
pcf
* control data
restart estimation
6 10 1 0 1
1 10 single point 1 0 0
10.0 2.0 0.3 0.01 8
5.0 5.0 1.0e-3
.1
30 .005 4 3 .01 3
1 1 1
* parameter groups
por relative .01 .00001 switch 1.5 parabolic
* parameter data
Kh0 log factor 6.25e-4 1.e-7 1.e-3 por 1.0 0.0 1
Kz0 log factor 6.25e-4 1.e-7 1.e-3 por 1.0 0.0 1
Kh1 log factor 3.7e-5 1.e-7 1.e-3 por 1.0 0.0 1
Kz1 log factor 1.85e-5 1.e-7 1.e-3 por 1.0 0.0 1
Kh2 log factor 2.89e-6 1.e-8 1.e-5 por 1.0 0.0 1
Kz2 log factor 1.45e-6 1.e-8 1.e-5 por 1.0 0.0 1
* observation groups
group_1
* observation data
head320 40.18 1 group_1
head321 34.35 1 group_1
head327 58.35 1 group_1
head329 45.68 1 group_1
head331 51.58 1 group_1
head337 47.76 1 group_1
head339 41.64 1 group_1
head343 30.76 1 group_1
head345 41.02 1 group_1
head346 52.69 1 group_1
* model command line
rf4.exe NKSteady > NKSteady.txt
* model input/output
NKSteady.tpl NKSteady.mmp
NKSteady.ins320 NKSteady_time_POINT320_GROUNDWATER_FLOW.tec
NKSteady.ins321 NKSteady_time_POINT321_GROUNDWATER_FLOW.tec
NKSteady.ins327 NKSteady_time_POINT327_GROUNDWATER_FLOW.tec
NKSteady.ins329 NKSteady_time_POINT329_GROUNDWATER_FLOW.tec
NKSteady.ins331 NKSteady_time_POINT331_GROUNDWATER_FLOW.tec
NKSteady.ins337 NKSteady_time_POINT337_GROUNDWATER_FLOW.tec
NKSteady.ins339 NKSteady_time_POINT339_GROUNDWATER_FLOW.tec
NKSteady.ins343 NKSteady_time_POINT343_GROUNDWATER_FLOW.tec
NKSteady.ins345 NKSteady_time_POINT345_GROUNDWATER_FLOW.tec
NKSteady.ins346 NKSteady_time_POINT346_GROUNDWATER_FLOW.tec
```

3.3 GeoHydroDataBase

Virtual Hydrologic Environment (VHE) is an integrated approach where two major data systems are included: integration of different types of GIS and water resources data, integration of data and modeling. The Unified Modeling Language (UML) [Booch et al., 2005] facilitates the design of GIS based relational database model GeoHydroDataBase (GHDB) and is used to create a specialized set of geo- and hydro-objects from both surface and subsurface hydrology in a consistent manner. Feather classes are created to store spatial data, such as sub-catchments and stream network. Tables are created to store time series and other parameters. Relationship classes are developed to link related objects. Furthermore, a graphical user interface is implemented as a link between object- and process-oriented numerical model OGS and GHDB for the pre-processing of model data and parameters.

3.3.1 Designing a GHDB model with UML

When designing a GHDB model, one has to define the main components in a hydrological system. Therefore, the first stage of the project is to establish the GHDB structure. The GHDB data model is a description on the characteristics of the hydrological system such as river networks, watersheds and channels, soil, precipitation, land use, geologic units, boreholes and so on. The data model is a set of concepts expressed in a data structure and describes a simplification of reality using tables and relationships within a database. It integrates spatial and temporal information into a defined structure.

The UML offers a standard way to visualize a system's architectural blueprint. Therefore the UML is suggested to develop the structure of the GHDB data model. The development of a UML based GHDB data model design follows five steps which are:

- Model the user's view of data
- Design objects and relationships
- Select geographic representation
- Match to GHDB elements

- Organize the GHDB structure

The data model specification is created using CASE tools and results in a diagram that uses UML clearly defining the structure of the model in a visual diagram (Fig. 3.5 and 3.6). The empty database schema of the data model is then tested with real data (e.g. Meijiang).

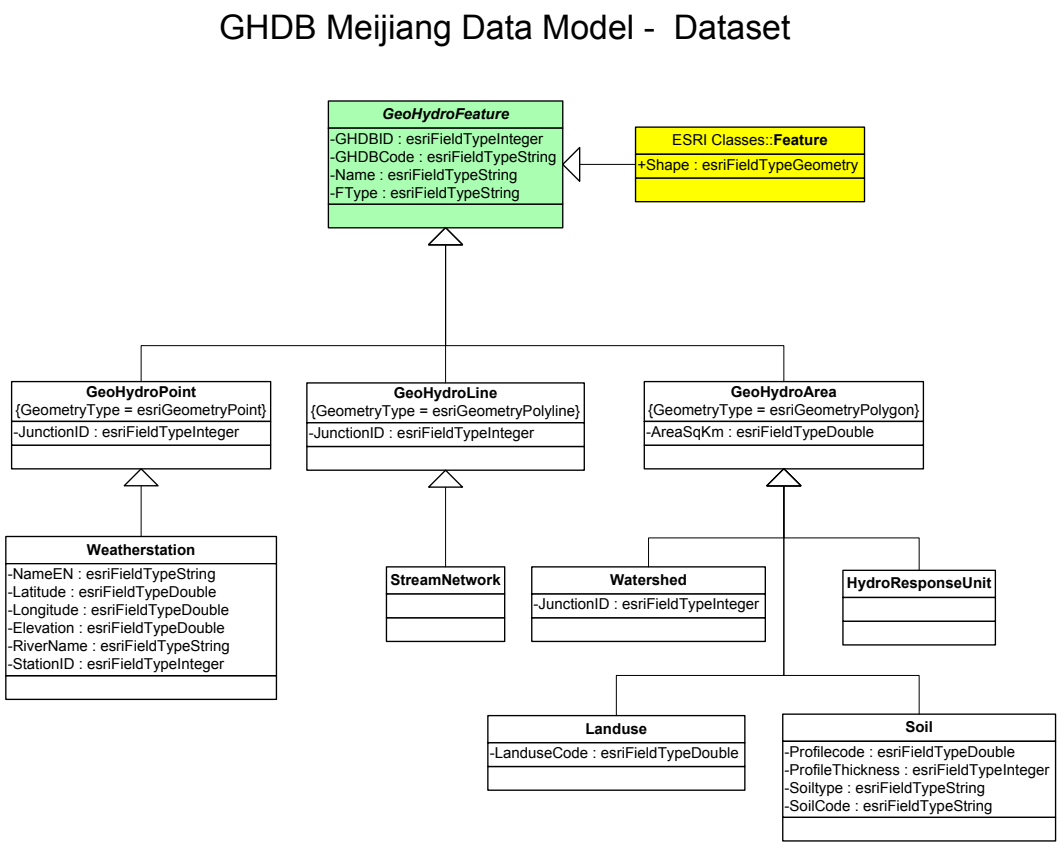

Figure 3.5: GHDB dataset model of Meijiang catchment.

In the process of constructing the data model, there are some requirements for an integrated GHDB database system as following:

- All data must be held in a same geographic coordinate system.
- The primary structure used for representation of a large region must be vector data (points, lines and areas), supported by raster and TIN surface data when necessary.

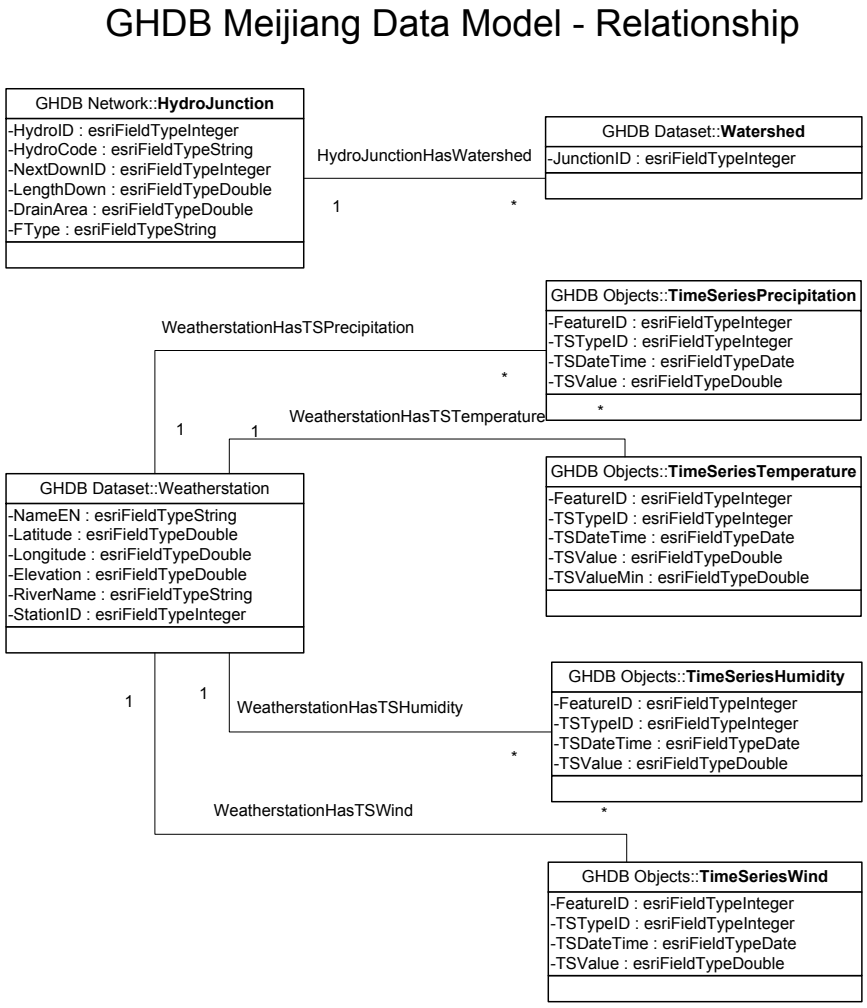

Figure 3.6: GHDB relationship model of Meijiang catchment.

- Relationships among geographic features in different data layers are needed to trace water movement from feature to feature through the landscape and underground.
- It is able to link geographic information with time series measurements to form a complete information system for water resources.

3.3.2 Filling GHDB with data

After the GHDB structure is set up, the second step of the project is to fill data into the empty database system. Geographic Information Systems/Remote Sensing (GIS/RS) and related technologies such as image processing can provide critical data and products for parameterizing the hydrologic models. The following activities are involved in this part concerning about the data processing:

- Extraction of hydrological data from remotely sensed images.
- Data preparation and pre-processing of data for modeling purposes.
- Hydro-parameterization, which is a process to derive parameters for hydrological models from the extracted data or measurements.

The data sources are from different data format, such as ArcGIS raster and vector map, Excel table, DataBase file, etc. After loading data into the GHDB database, it can be used as input data sources for the modeling purpose.

Modifying the schema is an extension for the process of creating GHDB. Depending on how the schema is created, relatively few or many modifications may be made in this phase.

- Adding or removing feature classes
- Modifying feature classes
- Adding or removing fields from tables
- Changing the relationship classes
- Associating domains with attributes

3.3.3 Interface between OGS and GHDB

Before the data can be used for the modeling purposes, it is necessary to set up a connection between GHDB and OGS, which includes the geometry and non-spatial data part, such as time series data. Two steps are involved in this process:

- The feature class together with its attribute data inside the GHDB will be read into OGS.
- The table and relationships will be handled using access ADO provider.

Geometry and soil elements

Geospatial Data Abstraction Library (GDAL) is a cross platform C++ translator library for raster and vector geospatial data formats that is released under an X/MIT style as Open Source license by the Open Source Geospatial Foundation. The related OGR is a part of the GDAL library providing a similar capability for simple features vector data. OGR optionally supports reading ESRI Personal GeoDatabase (.mdb files) via ODBC. This driver accesses the personal geodatabase via ODBC but does not depend on any ESRI middleware. The GHDB data model is the same as personal geodatabase format. The OGR library is used to access data from GHDB data model in this study. The graphical user interface (Fig. 4.3) which provides a link to GHDB is implemented in OGS.

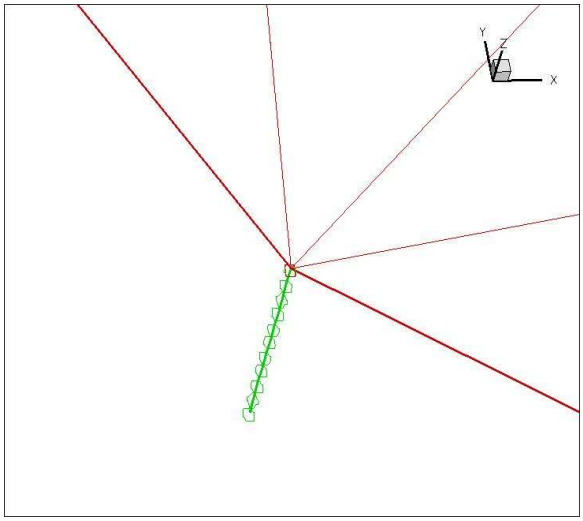

Figure 3.7: An example of soil line element.

Another important process is to generate soil line elements for regional hydrosystem analysis. Here the soil information, e.g. soil thickness and soil group, are read from the GHDB database tables. After identifying the nodes from the finite element meshes using the spatial operation functions in OGR library, the spatial distribution of soil groups is read from the soil map.

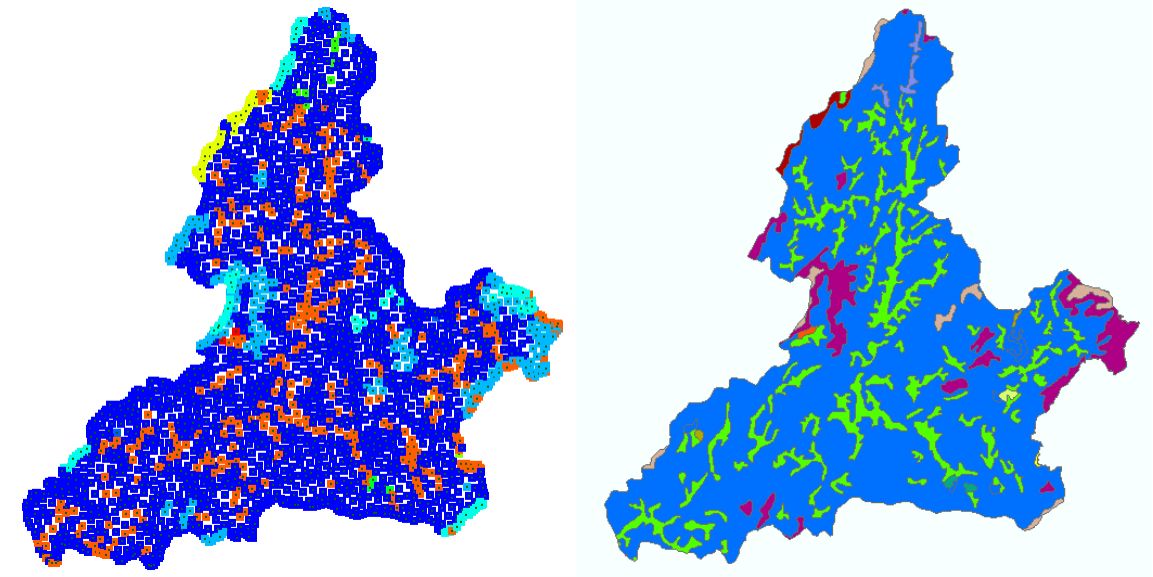

(a) OGS (b) ArcGIS

Figure 3.8: Comparison of visualization of soil elements in OGS and soil map in ArcMap.

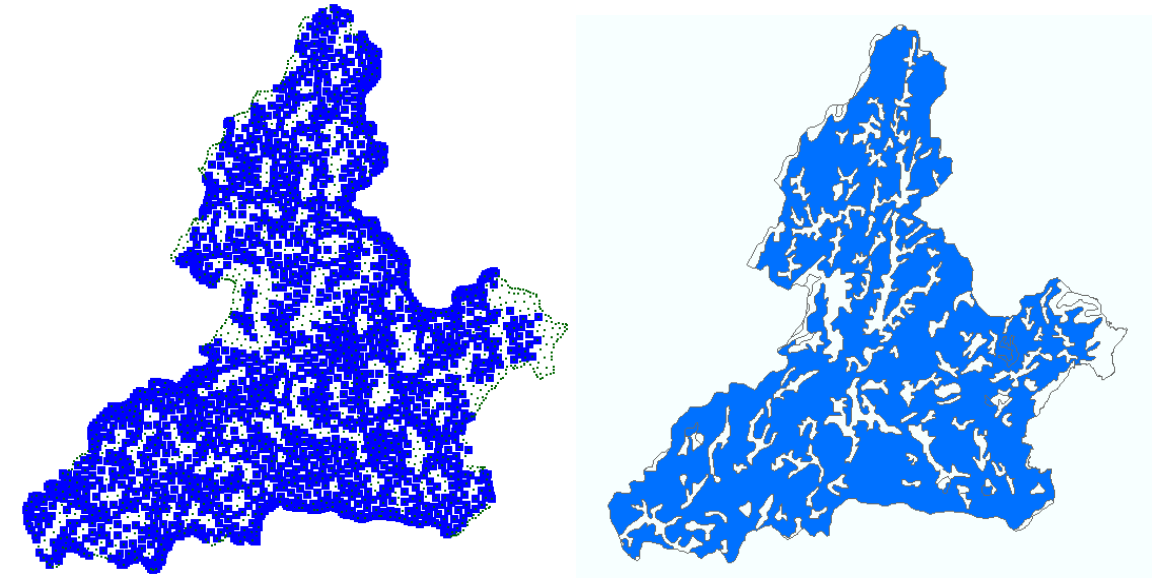

(a) OGS (b) ArcGIS

Figure 3.9: An example of soil element visualization with group S1 in OGS and in ArcMap.

Fig. 3.7 shows the generated one soil column - line elements. Visualization of soil elements with different color depends on the material groups (Fig. 3.8). Soil identified mesh elements and the soil map in ArcGIS about soil group S1 are displayed in Fig. 3.9.

Time series data

The non-spatial data, such as time series data from the GHDB data model is accessed using ADO (Microsoft ActiveX® Data Objects) provider. The following Fig. 3.10 shows the code implementation of accessing Microsoft Access database using ADO provider.

```
  Dim cnn As ADODB.Connection
  Set cnn = New ADODB.Connection

With cnn
  .Provider = "Microsoft.Jet.OLEDB.4.0"
  .Properties("Jet OLE DB:System Database") = _
  "\\MyComputer\MyShare\MySystem.mdw"
  .Open "\\MyComputer\MyShare\MyDatabase.mdb"
End With
```

Figure 3.10: ADO connection.

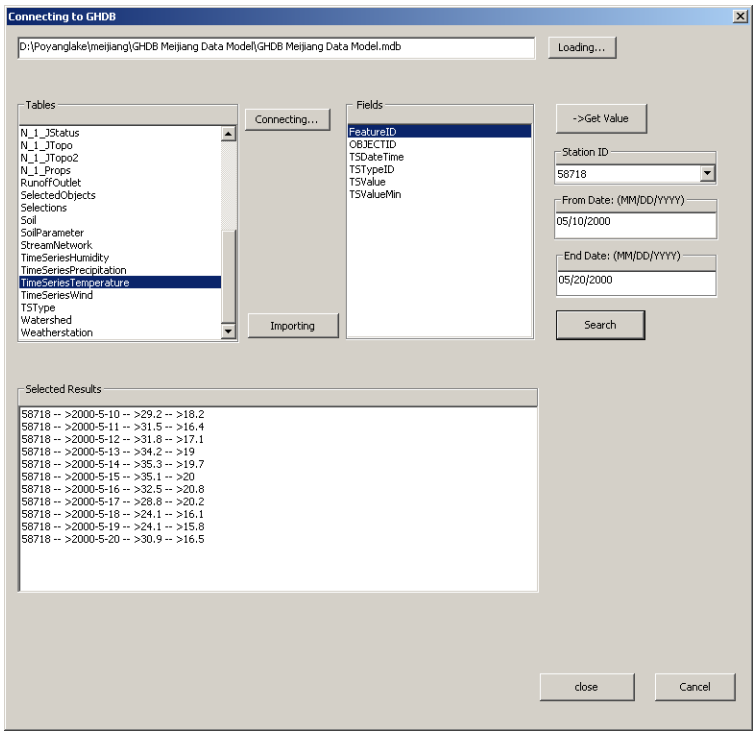

Figure 3.11: The graphical user interface of ADO access.

In addition to that, Structured Query Language (SQL) is used to search for the necessary data from the time series table. The graphical user interface is implemented as shown in Fig. 3.11. In this interface, the searching keyword can be: station ID, From Date, End Date. The queried results are displayed in the list box.

3.4 Visualization in 3-D Lab

Within the context of the presentation of complex hydrogeological structure and results, 3-D visualization plays a major role since it provides a clear picture of the involved problems, simulations and results. In order to enable scientists to examine large and structurally complex data sets and to be able to collaborate in work-groups with people of different backgrounds, a projection-based high resolution stereoscopic virtual environment driven by a workstation cluster (TESSIN-VISLab) is used to show the results of our project (Fig. 3.12a and 3.12b from the case study of Nankou (NK)).

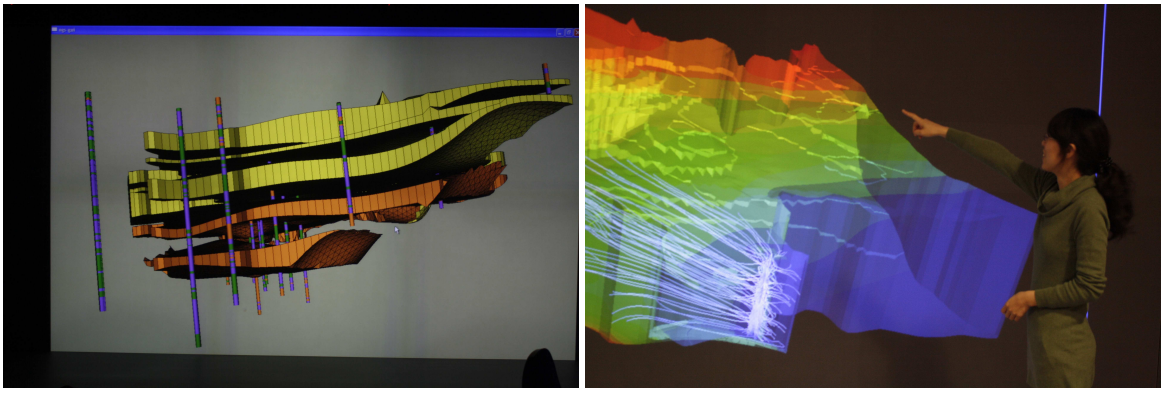

(a) hydrogeological structure (NK) (b) simulation result (NK)

Figure 3.12: Visualization of the complex hydrogeological structure and simulation result.

Chapter 4

Model applications

4.1 Regional hydrological analysis of Meijiang catchment

The Regional Hydrological Soil Model (RHSM) for regional soil water analysis was originally developed for Beerze-Reusel drainage basin in the southern part of the Netherlands [Kolditz et al., 2007]. A similar approach was used by [Eichhorn, 2010] for the slope soil in a mountain region. We further develop this methodology for hydrological modeling in particular combining GIS based structural 3-D modeling with data management as a pre-processing tool for the finite element analysis of hydrosystems. The 3-D structural modeling is based on typical geological layer information. The topography of all geological layers is represented by contour maps based on which stratified finite element meshes are mapped successively. The second new development is the integration of GIS database information into the finite element analysis within the scientific software OGS. Thus, for example, information about complex soil systems can be incorporated into the set-up of the corresponding finite element model for the soil compartment. As an application, we present a case study for the Meijiang area with the focus on surface/subsurface water interaction and the recharge response from surface infiltration to groundwater with different time series discretization. The numerical model was implemented within the framework of object-oriented programming.

4.1.1 Concept of the regional hydrologic soil/groundwater model

Conceptual model

The terrestrial hydrosphere can be divided roughly into surface water, soil water and aquifer compartments (Fig. 4.1). The corresponding hydrological processes at the surface are lakes, rivers and overland flow during flooding, unsaturated soil flow in the subsurface and groundwater flow in porous and fractured media. Water exchange with the atmosphere occurs via evaporation and precipitation whereas root water uptake and transpiration represent links to the biosphere. Water in unsaturated soil is affected by suction gradients and its movement is subject to variations in conductivity resulting from changes in soil water content. Groundwater is recharged by percolation through the unsaturated zone, and the position of its surface (water table level) is determined by the relative rate of recharge versus outflow. From the view of mathematics, those processes in the surface and subsurface compartments as well as their interactions can be described by partial differential equations.

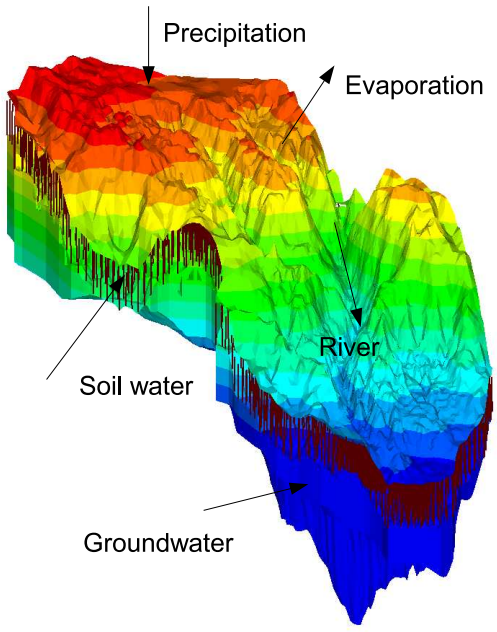

Figure 4.1: Concept model of the regional groundwater analysis.

Evaporation model

Precipitation is regarded as the main recharge to groundwater in this study, which is a time dependent boundary condition to the regional soil model. Before the precipitation infiltrates through the soil to groundwater, the evapotranspiration process should be decreased from the source term. The following simple balance formula, $I = P - ET$, is used, where I is infiltration, P is precipitation and ET is evapotranspiration, which is calculated by a modified Makkink's equation. The Makkink [1957] method for the estimation of potential evapotranspiration is based on radiation, which basically requires only two variables: global radiation and air temperature. de Bruin [1987] showed that an even more simple form of Makkink's equation yields reliable estimates of evaporation. The so-called modified Makkink's equation is given by Eq.4.1.

$$ET = C \cdot \frac{\Delta}{\Delta + \gamma} \cdot \frac{R_s}{\lambda} \tag{4.1}$$

where *ET* is the potential evapotranspiration [MJ m^{-2} d^{-1}], Δ is the slope of the vapor pressure curve [kPa $^\circ$C^{-1}] which is a function of temperature (T, the mean value of maximum and minimum temperature in one day in $^\circ$C), λ is the latent heat of vaporization [MJ kg^{-1}], γ is psychrometric constant [kPa $^\circ$C^{-1}], R_s is the solar radiation [MJ m^{-2} d^{-1}], C is an empirical constant of 0.8 compared with the results of de Bruin and Lablans [1998].

Infiltration model

In this paper, the regional hydrological soil model is developed in the framework of the compartment approach [Kolditz et al., 2007]. Multiple one-dimensional vertical Richards' equation was applied in each compartment,

$$n\frac{\partial S}{\partial t} + \frac{\partial q}{\partial z} = q_s \tag{4.2}$$

where n is soil porosity, S is soil water saturation, q_s is a source term, and $q$is the Darcy flux.

Groundwater model

The mathematical descriptions of groundwater flow are base on the water mass balance and Darcy's law:

$$\frac{\partial}{\partial x}\left(K_x\frac{\partial h}{\partial x}\right)+\frac{\partial}{\partial y}\left(K_y\frac{\partial h}{\partial y}\right)+\frac{\partial}{\partial z}\left(K_z\frac{\partial h}{\partial z}\right)+w=S_s\frac{\partial h}{\partial t} \tag{4.3}$$

where h is the hydraulic head, $t$is the time, $w$is a sink or source, S_s is the specific storage and$K$ is the hydraulic conductivity in different directions.

Influence area

In the present coupling model, the water recharge from soil to the aquifer is represented by the exchange of the Darcy flux between the Richards' equation and the groundwater equation.

To calculate such exchange in the finite element analysis, we need to know the influence area of each node on the surface between the soil and the aquifer. In the framework of the finite element, the influence area A_i of compartment i (shown in Fig. 4.2, top) is a face/volume integration of the corresponding shape function. Without losing the generality, we take compartment $i$in Fig. 4.2 as an example. Compartment i as an element node is shared by five elements A, B, C, D and E. With the finite element, the influence area of i, A_i can be calculated by

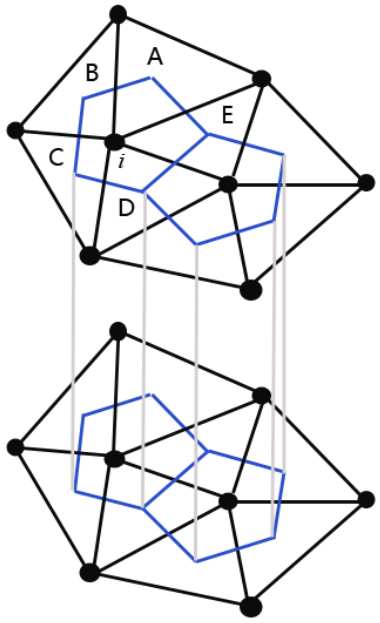

Figure 4.2: Calculation of influence area.

$$A_i=\sum_{K=A}^{E}\int N_j^K \mathrm{d}\Omega_K \tag{4.4}$$

where N_j is the interpolation function of node i with local index j in element K(= A, B, C, D or E), and Ω_K is the domain of element K. The regional groundwater recharge is calculated from the soil water Darcy velocities multiplied by the corresponding horizontal influence area of each soil profile.

Data model

Comprehensive datasets including geological, hydrological, soil and aquifer properties need to be preprocessed and integrated effectively before they can be used as input data to numerical simulators. Usually, most geometric data and attribute tables are stored and processed in a Geographic Information System (GIS). The proposed Geodatabase is a concept for data storage and management framework for ArcGIS. It combines "geo" (spatial data) with "database" (data repository) to create a central data depository for spatial data storage and management. Based on the Geodatabase of ArcGIS, a clearly understandable GHDB model structure is designed with the Unified Modeling Language (UML) in a visual format. The empty database schema of the data model is then tested with real data (e.g. present Meijiang case study).

Before the data sets can be used for simulation purposes, the geometry and non-spatial data part, such as time series data, will be imported into the simulator. The new graphical user interface (Fig. 4.3) between GHDB and OGS was developed to this purpose. Thus, e.g. information about complex soil systems can be easily incorporated into the set-up of the corresponding finite element model for the soil compartment.

Mapping procedure

The mapping of the prism layers is a procedure to position (vertical height) and modulate the prism elements according to topographic and stratigraphic information, which is provided by TIN (triangular irregular network) or grid files. Suppose a layer surface is defined by a regular grid on a horizontal plane with an elevation at each of its nodes, together with a 2-D mesh parallel to the horizontal plane (see Fig. 4.4a). Considering the horizontal plane is parallel to the plane of (x, y, 0) in the Cartesian system, the task of mapping

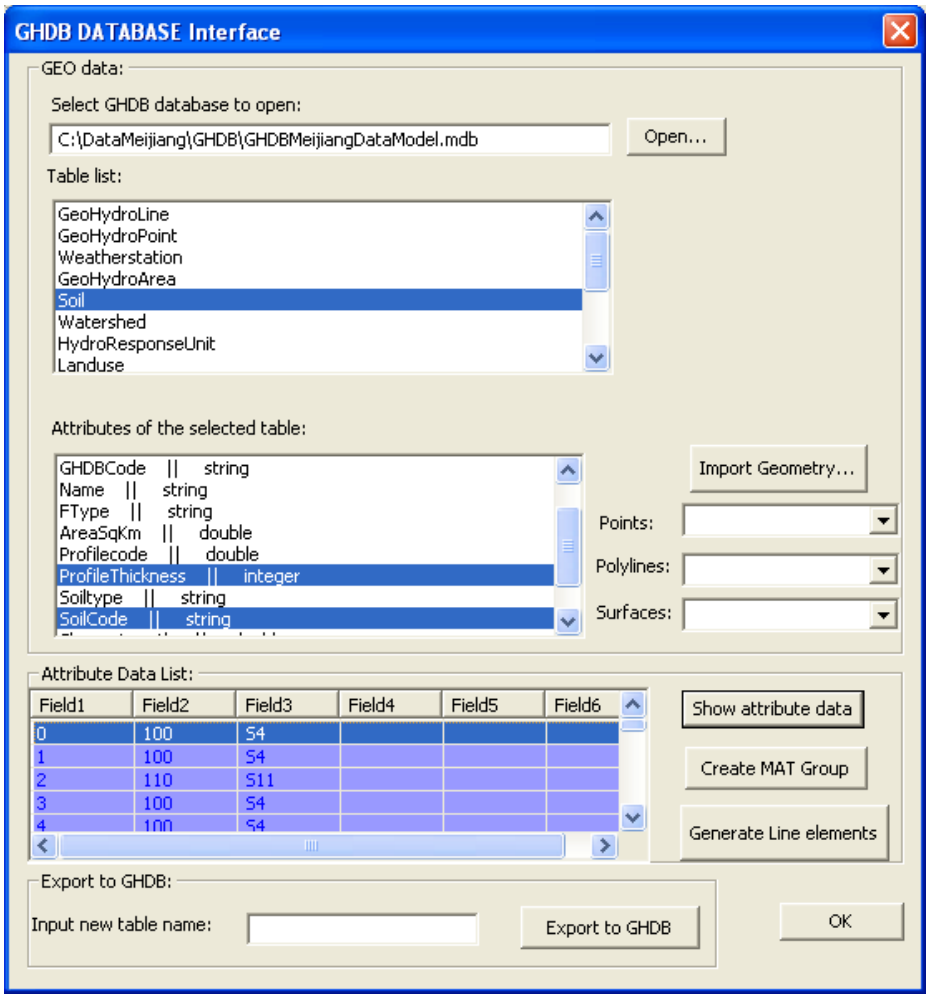

Figure 4.3: The graphical user interface between GHDB and OGS.

is to move each node of the 2-D mesh to the given surface without changing the x and y components of its coordinates (Fig. 4.4b).

The mapping approach is very simple. For each node n, we first locate the block in the grid with four grid points, i.e. i, j, k, l, and this block contains node n (Fig. 4.4a). The block can then be considered as a quadrilateral finite element with nodes, i, j, k, l,. Next, the local coordinate (ξ, η) of node n and corresponding values of the four finite element shape functions N_i, N_j, N_k and N_l are calculated. Assuming the elevations of the four

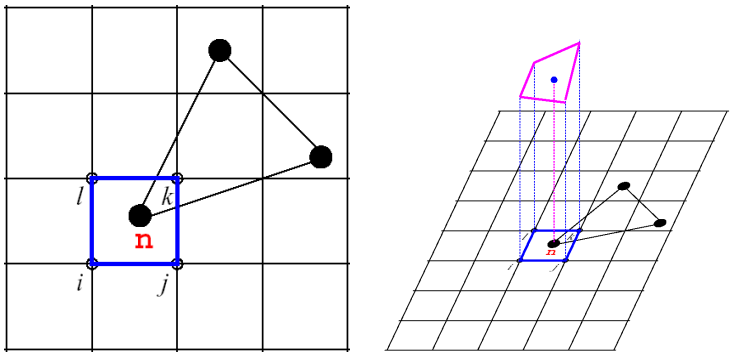

(a) (b)

Figure 4.4: Nodes of an element in the grid and mapping an element node to the surface [Miles et al., 2007].

points are z_i, z_j, z_k, z_l, the final step of the mapping is to interpolate a new z of n by

$$z_n = z_i N_i + z_j N_j + z_k N_k + z_l N_l \tag{4.5}$$

Using this method, the infiltration layers generated in ArcGIS with the kriging interpolation method are mapped to the catchment mesh layer as source terms for different single soil columns.

4.1.2 Application of the RHSM concept to Meijiang catchment

Site description

The study area (Meijiang catchment) lies in southeastern China and belongs hydrologically to the Yangtze River Basin (the longest river in China) and is one of major upper streams of Poyang Lake (Fig. 4.5). The extent of the study area is located at WGS84 coordinates 25 ˚ 57′53″N–27 ˚ 08′55″N and 115 ˚ 22′25″E–116 ˚ 38′07″E, and has an area of 6983 km^2. There are two major streams: Meijiang and Qinjiang, in the whole catchment. The Qinjiang flows from northeast to southwest and runs into the Meijiang at Meijiang County. The Meijiang continues flowing southwest and runs into the Gongshui. The Meijiang catchment is in the middle subtropical monsoon climate region of China, which is

characterized by distinct seasons, sufficient sunshine and rainfall. The average annual temperature is 18.3 ˚ C and 45–50% of precipitation falls between April and June, the average annual precipitation ranges from 1432 to 1614 mm/year.

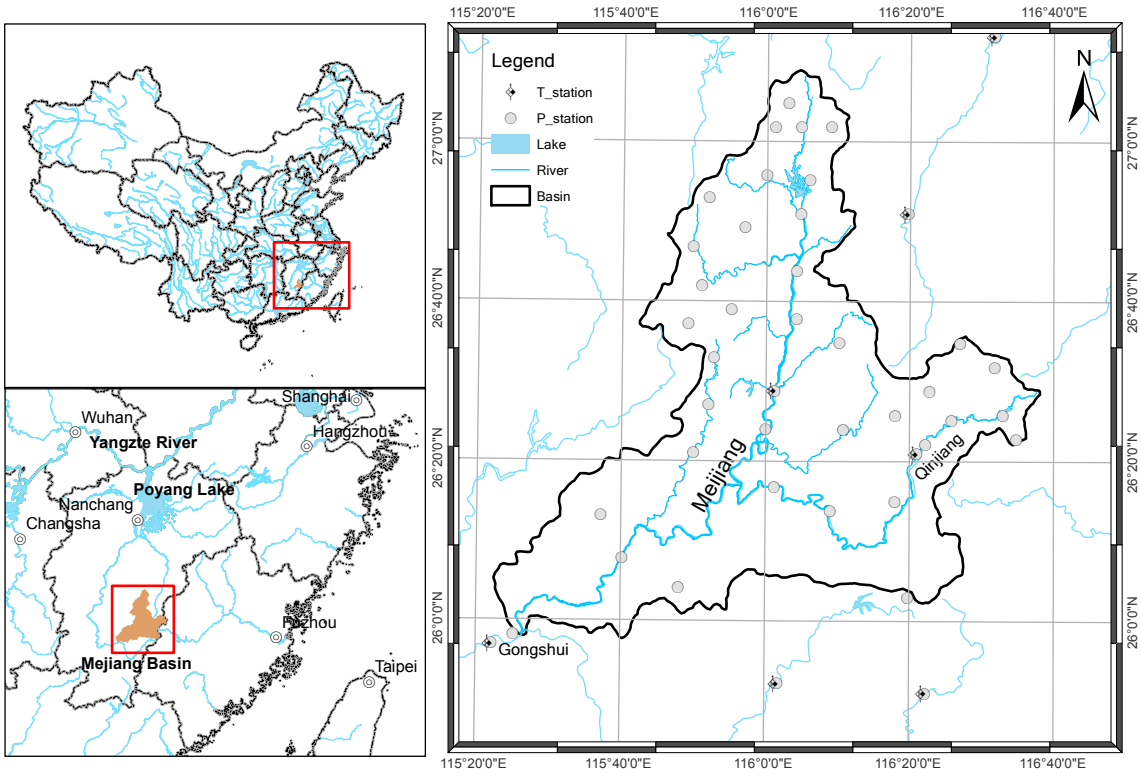

Figure 4.5: Location of the study area. Left top: China; left down: study area in the regional context; right: study area (the surface water catchment boundary of Meijiang is highlighted by the grey line).

Meteorological data

In this study, the precipitation and temperatures of 45 rainfall gauge stations and 8 meteorological gauge stations in 2000 (Fig. 4.5) are used to calculate the evapotranspiration (ET) and infiltration values. Daily extraterrestrial radiation (R_a) is estimated from the solar constant and the solar radiation is calculated based on the equations and recommendations given in Allen et al. [1998].

Soil properties

In order to get the parameters which are used to calculate the soil water characteristic curves, the SPAW (Soil–Plant–Air–Water) [Saxton and Willey, 2006] model is used. The SPAW model simulates the daily hydrology of agricultural fields and ponds including wetlands, lagoons and reservoirs. Data input and file selection are by graphical screens. Simulation results are both tabular and graphical. An estimating method for soil water characteristics has been developed and included. The technique is a set of generalized equations which describe soil tension and conductivity relationships versus moisture content as a function of sand and clay textures and organic matter.

The soil system of the Meijiang area can be subdivided into 12 groups depending on soil texture. The capillary pressure and relative permeability–saturation relationships with soil water content are calculated within SPAW.

Single soil column test

The RHSM was successfully applied to the Beerze-Reusel drainage basin under humid climate conditions. In the present study, we apply this methodology to the entire Meijiang catchment area using a higher column resolution. Before running the RHSM simulation, a single soil column was taken from Ningdu station as a test example, which is situated at 116 ° 01′12″E, 26 ° 28′48″N, at an elevation of 209.10 m. The thickness of soil column is 1.1m and is regarded as a homogeneous medium in this case. The mesh density is 11 cm. The top boundary condition is set as the transient infiltration in 2000 calculated in Section 4.1.1.

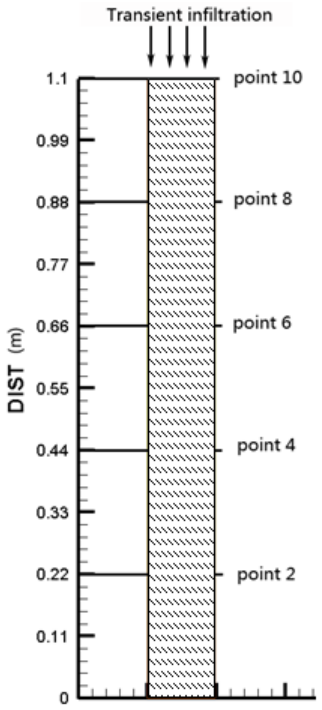

Figure 4.6: Single soil column model definition.

The time evolutions of soil water distribution responding to the infiltration variation at four different observation points (Fig. 4.6) chosen from the single

soil column are presented in Fig. 4.7a- 4.7d . It can be seen that different statistical methods (annual, 10 day, monthly and daily) of infiltration process result in different soil water distribution trends which comply with infiltration trends.

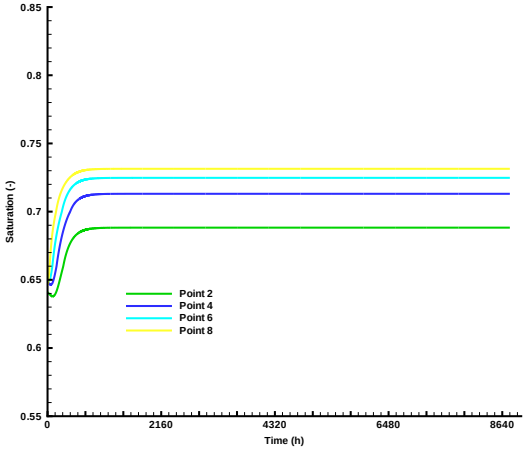

(a) daily infiltration constant

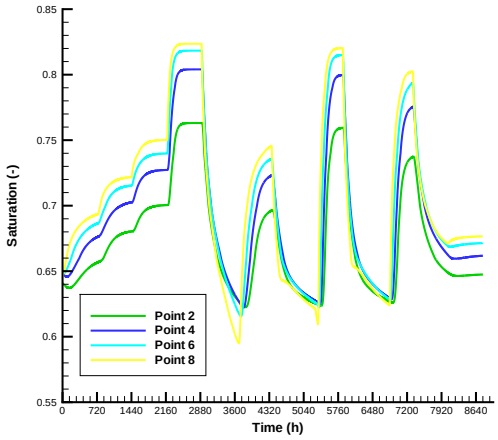

(b) monthly infiltration constant

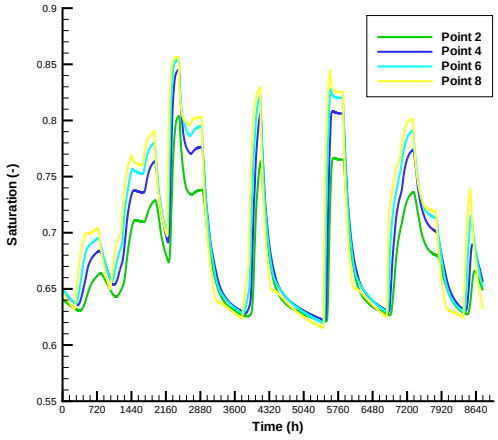

(c) 10 days infiltration constant

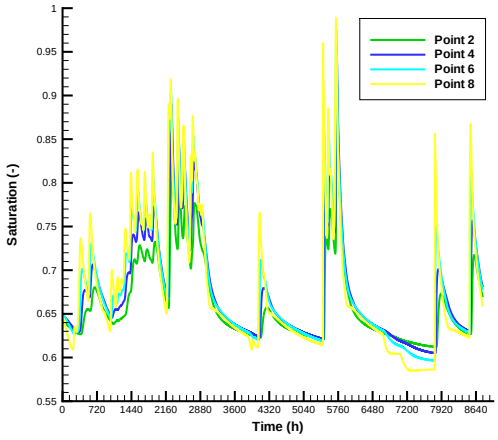

(d) daily change infiltration

Figure 4.7: The results for selected points.

Regional hydrological soil model

The regional evolution of soil water distributions at the end of 30 days and 180 days are shown in Fig. 4.8 and 4.9. It can be seen that the infiltration process into the soil compartment is very heterogeneous. It is the combined effect of the precipitation distribution in the region and the local variation of soil hydraulic properties. The regional groundwater recharge can be calculated from the soil water Darcy velocities multiplied by the corresponding horizontal influence area of each soil profile (Fig. 4.2).

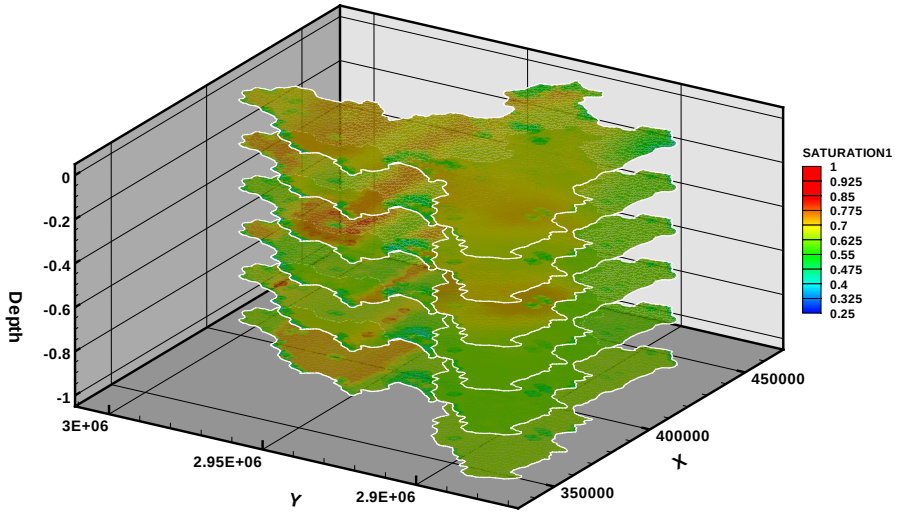

Figure 4.8: Regional soil water distribution at days 30 from the top surface to soil bottom.

4.1.3 Conclusion and future work

In this paper a Regional Hydrological Soil Model (RHSM) was developed and applied to the Meijiang catchment in China. A GIS-based relational database model GHDB was used as a preprocessing methodology for the finite element soil and groundwater analysis designed particularly for the case study area, and a new graphical data interface between GHDB and OGS was developed. A mapping procedure was used to create the different time-dependent hydrological input data for the numerical model. The soil water Darcy

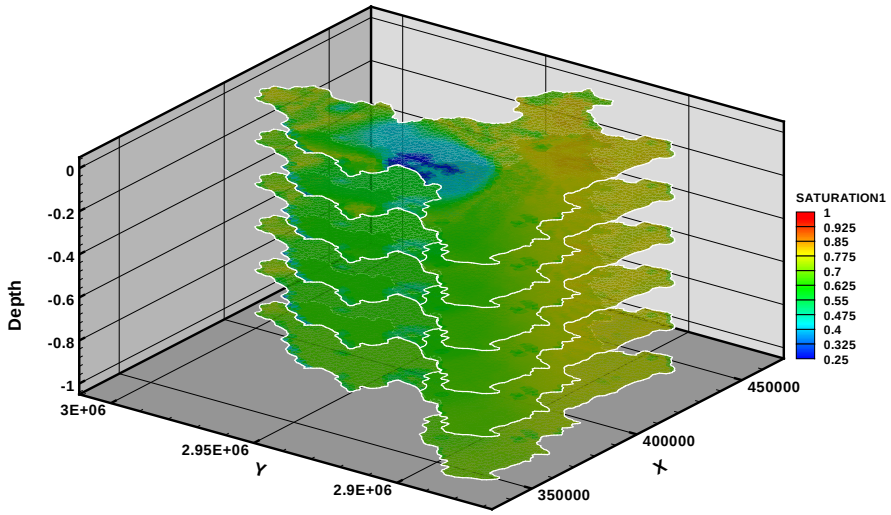

Figure 4.9: Regional soil water distribution at days 180 from the top surface to soil bottom.

velocities achieved from RHSM were used as source terms for calculating groundwater recharge by using a numerical integration scheme. To demonstrate the advantage of the present methodology, the regional soil water distribution in Meijiang area was studied. Compared to the case study for the Beerze-Reusel drainage basin [Kolditz et al., 2007], which is in similar humid climate conditions to Meijiang, the RHSM concept in the present case study allows the realization of high resolution soil models ($\sim$10 cm in vertical direction, Fig. 4.6) for a much larger catchment ($\sim$6980 km^{2}the Meijiang basin). The next step of our work is to extend the present RHSM concept to mass transport (e.g. nitrate fluxes) in large-scale catchments.

4.2 Groundwater drawdown at Nankou site of Beijing Plain

Water shortage and groundwater pollution have become two primary environmental concerns to Beijing since the 1990s. The local aquifers, as the dominant sources for domestic and agricultural water supply, are depleting due to groundwater abstraction and continuous drought in recent years with rapid urbanization and increasing water consumption. Therefore, understanding the hydrogeological system is fundamental for a sustainable water resources management. In this paper, the numerical analysis of a 3-D regional groundwater flow model for the Nankou area is presented. The hydrogeological system is reproduced according to sparsely distributed boreholes data. The numerical analysis is carried out using the scientific software OGS, which is based on the finite element method. The model calibration and sensitivity analysis are accomplished with inverse methods by applying a model independent parameter estimation system (PEST). The results of the calibrated model show reasonable agreements with observed water levels. The transient groundwater flow simulations reflect the observed drawdown of the last 9 years and show the formation of a depression cone in an intensively pumped area.

4.2.1 Introduction

Nankou is located at the northwest edge of the Beijing Plain (Fig. 4.10), covering a total area of 197.55 km^2. Since the 1990s, a large part of the area was urbanized, leading to a significant increase of water consumption. According to Beijing Water Authority, about 70% of the drinking water supply comes from the local aquifer. Meanwhile, the annual precipitation from 1998 to 2008 was 428 mm, i.e. 28% below the long-term average value of 1956 to 2000 [Probe International Beijing Group, 2008]. The local aquifer is under enormous stress. On the quantity side, increased pumping activities caused a drawdown of the groundwater table (Fig. 4.11) and on the quality side, the water hardness increased subsequently. The local municipality has introduced several measures to resolve these problems. Between the years 2003 and 2008, about 600 million m^3 surface water were diverted from reservoirs in the neighboring Shanxi and Hebei provinces [Probe International Beijing Group, 2008]. The South-North diversion project will be completed in 2010 to deliver annually around 1200 million m^3 of water to Beijing [Duan, 2005]. In June

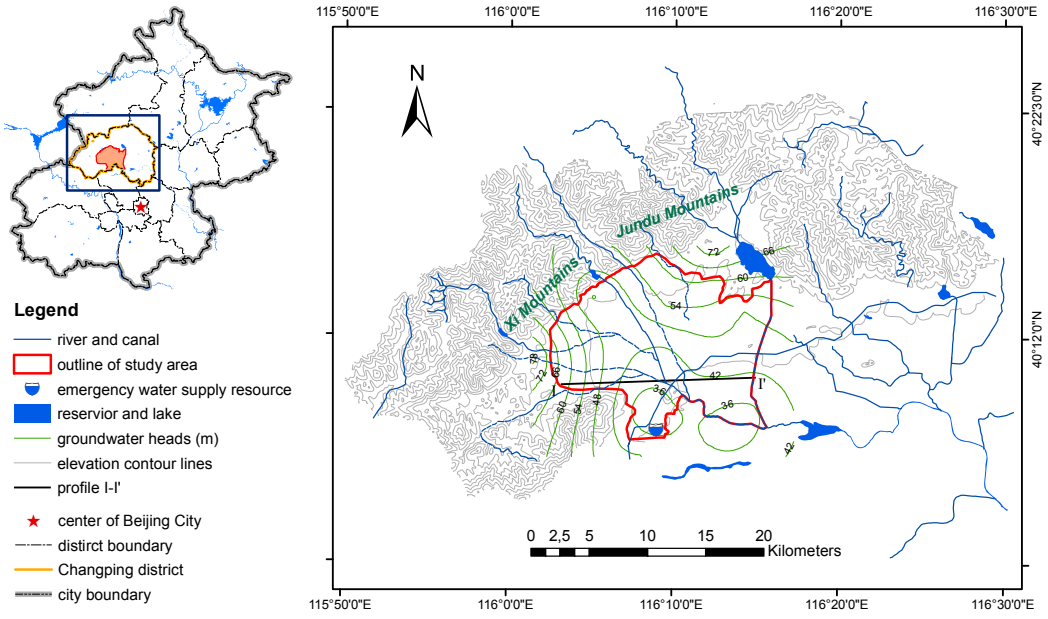

Figure 4.10: The location of study area.

2006, a groundwater supply project in the south side of the Nankou area (Fig. 4.10) was completed as an emergency water resource for Beijing City, supplying 300 $\sim$ 400 million m^3 water monthly [Xie et al., 2009] and causing a groundwater level drawdown in the surrounding area. Based on a long term measurement of groundwater quality in this site, a heavily contaminated patch with high concentration nitrate was found in the north of this site. For the above reasons, the Nankou area was chosen as a research site for the contamination remediation and water resources management. Therefore, it is necessary to have a better understanding of the local hydrogeological system. The well-calibrated groundwater model will provide hydrogeological parameters and boundary conditions for the following transport modeling and remediation scenarios analysis. The present work is focused on developing a numerical model for transient groundwater flow in the study area, which is fundamental to the understanding of the local hydrogeological system.

In the last few decades, large-scale groundwater models based on MODFLOW [McDonald and Harbaugh, 1988] have been developed for the North China Plain to address water scarcity and management optimization issues [Liu et al., 2008, Wang et al., 2008]. In the Sino- Netherlands co-operation project on groundwater monitoring and information management, launched in 2000, groundwater models [Xu, 2006, Wang et al., 2009a] in Beijing, Shandong, and Xinjiang have been established with groundwater modeling system (GMS) [Owen et al., 1996]. Despite the increasing concerns on the depleting groundwater in Beijing area, there is still limited knowledge on the groundwater flow regime in the Nankou area.

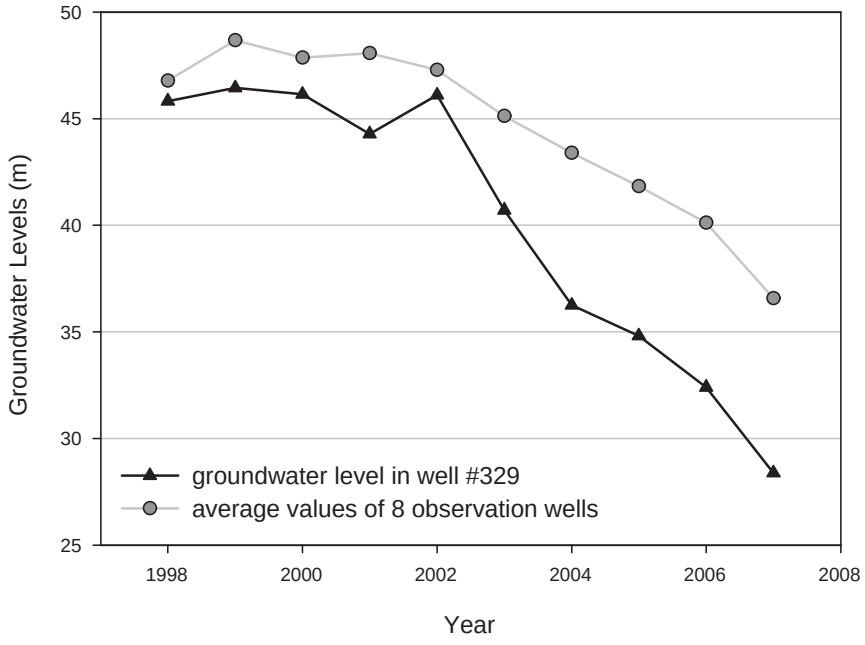

Figure 4.11: Ground water level changes in the Nankou Area (well locations shown in Fig. 4.17).

In this work, the groundwater model for the Nankou area was developed using the software OpenGeoSys (OGS) [Kolditz and Shao, 2010]. It is a scientific open source project for the development of numerical methods to simulate THMC processes in porous and fractured media based on the finite element method. With the object-oriented structure of OGS, it is possible for users to develop their own model by integrating OGS directly into pre- or post data process tools such as geographic information system (GIS) and GMS. For the sake of computational efficiency, OGS has been parallelized [Wang et al., 2009b] to deal with computationally intensive tasks in the modeling of complex problems such as the present 3-D model of the Nankou area. Chen et al. [2005] and Miles et al. [2007] have successfully applied high-resolution finite element models in groundwater simulation using OGS in central Jordan and eastern Germany regions. Kolditz et al. [2008] presented multi-field coupled hydrosystems within the framework of OGS at the Borden site in Canada and the Beerze-Reusel drainage basin in the Netherlands.

Due to the complexity in geology of the study area, parameter identification is of great importance for groundwater modeling. To increase the model accuracy, an inverse method is often employed to calibrate the parameters by minimizing a user defined objective function. Poeter and Hill [1997] presented an introduction of inverse modeling by using simple nonlinear least-squares regression to calibrate transmissivity in a confined aquifer. Liu et al. [2009] combined the adjoint state, the gradient search and the least square error algorithm and applied them simultaneously to estimate aquifer parameters, initial conditions and boundary conditions for a confined aquifer. In order to accomplish the calibration procedure automatically, practical nonlinear least-squares inverse modeling softwares such as MODINV [Doherty, 1990], MODFLOWP [Hill, 1992], PEST [Doherty, 2004] and UCODE_2005 [Poeter et al., 2005] are well established and can be efficiently integrated with other groundwater modeling simulators. In this paper, the model independent nonlinear parameter estimation code PEST was applied with OGS for parameters identification.

This paper is organized in the following sequence. Section 2 introduces the geology and meteorology of the Nankou area. Sections 3 describe the conceptual and numerical approaches for groundwater modeling. Section 4 presents the calibrated simulation results with discussion, followed by conclusions and outlook for the future work.

4.2.2 Study site and hydrogeologic setting

The Nankou area lies in a geographical unit commonly known as Wenyuhe catchment and belongs to Changping administrative district. In WGS84 (World Geodetic System, dating from 1984 and last revised in 2004) coordinates, the site is located at 116°02'32.53"E $\sim$116°15'55.28"E and 40°07'14.15"N $\sim$ 40°15'51.98"N. The elevation ranges from 40 to 197 m (calculated from topography counter map (1:10000), provided by Beijing Hydrological Center (BHC)). The study area has a continental monsoon climate. The precipitation in the Nankou area varies greatly with seasons and nearly 75% of rainfall occurs during a short flood season from June to August. Long-term (1960-2000) meteorology data shows that the regional annual mean precipitation is 551.9 mm, mean evaporation is 2080 mm, and mean temperature is 11.6°C.

The study area is surrounded by mountains in both north and west directions. The Jundu and Xi Mountains (see Fig. 4.10) in the north and west of the Nankou area control the distribution of Quaternary sediments and the lithofacies characteristics. The thickness of Quaternary sediments decreases from the southeast (about 600m in the deepest spot) to the northwest (only 15m the shallowest). In the opposite direction, the aquifer material varies gradually from gravel to fine sand, and the water table is shallower, respectively. The sediments change from a one-layer phreatic aquifer to an unconfined-confined multilayered system (Fig. 4.12), from the northwest to the southeast.

The primary discharge in the study area is the groundwater abstraction, the secondary discharge includes the groundwater outflow through the southern border. Since 1958, the flow in Dongsha River has been blocked by the dam in the upstream. Therefore, the river-groundwater exchange at the eastern border was not considered in the model.

In this paper, the groundwater model focuses on the shallow Quaternary aquifer. Horizontal boundaries of the model domain are defined by the mountain fronts in the northwest, Dongsha River in the east and two small channels together with a segment of Beisha River in the south. For the ground surface, elevation data is interpolated from the topography contour map. The domain bottom is approximated, mainly following the boundary of Quaternary sediment and partially according to the deepest aquitard (clay) recorded in borehole

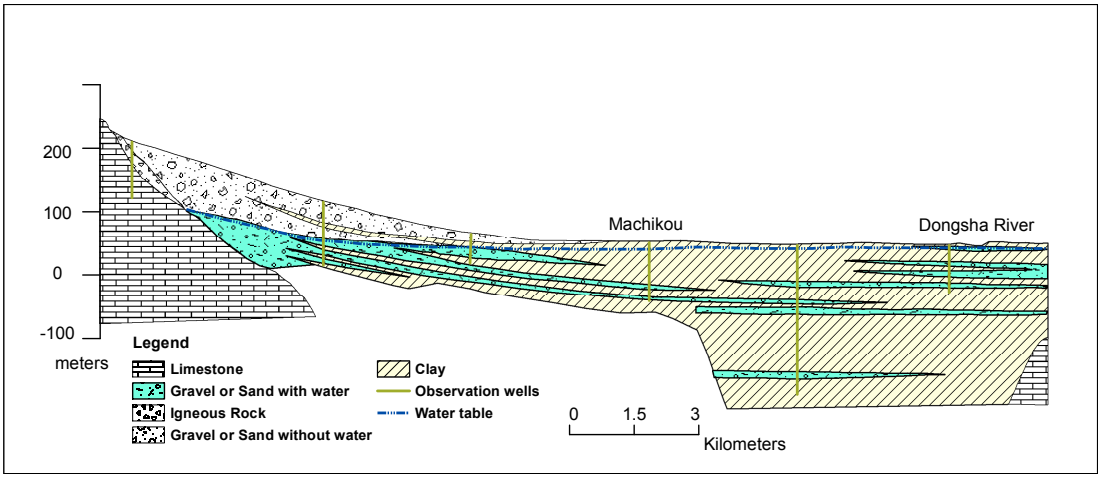

Figure 4.12: Hydrogeological profile for the Nankou area (see Fig. 4.10 for the location of I-I', modified from Beijing Hydrogeological Maps [Beijing Hydrogeology & Engineering Geology Center, 1980]).

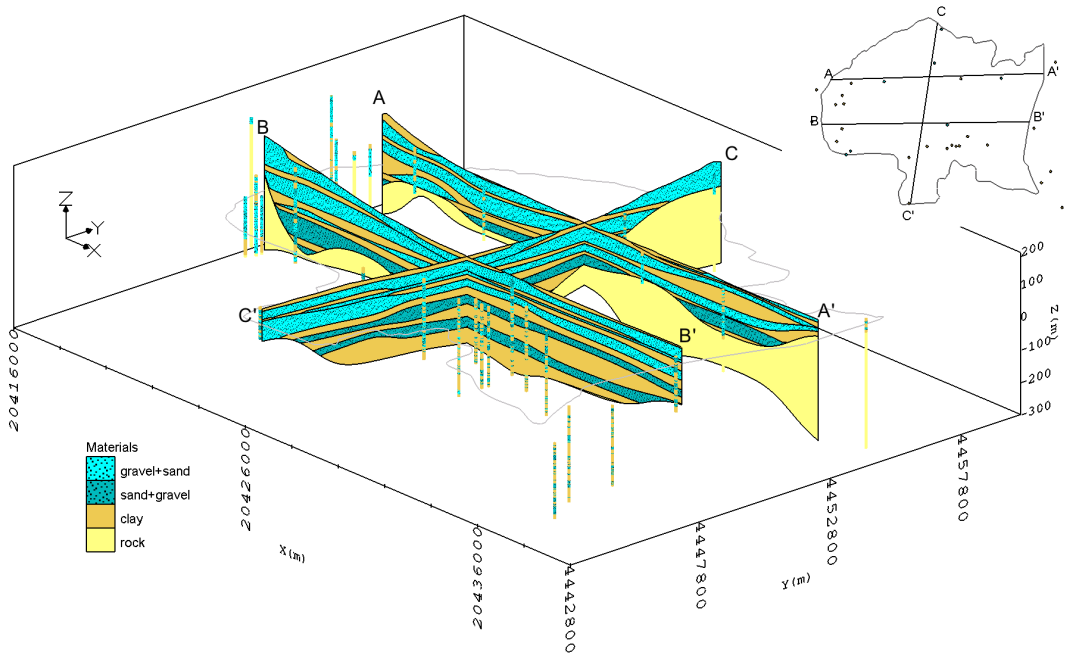

Figure 4.13: Intersections of geological profiles in 3-D solid model.

logs. The mathematical meaning of the conceptual boundary conditions is described in section 3 regarding the numerical site model.

Most of the wells in the Nankou area were designed for pumping purposes. Among

them, a total of 38 borehole logs is available. According to these logs, nearly 20 aquifer/aquitard types can be found in the sediments with a complex stratigraphy. Based on their grain size and hydrologic characteristics, these aquifer/aquitard layers were simplified into 4 groups, i.e. gravel, sand, clay and rock. The contacts between different soil layers in the borehole logs are numbered with horizon IDs consecutively from the bottom up, following the strata deposition order. Then the inverse distance weighting (IDW) method was employed to interpolate a surface for each scatter points dataset with the same horizon IDs. Starting with the lowest numbered horizon, the surface was extruded down to the bottom surface to create a solid. The surface corresponding to the next horizon was then extruded down to the bottom surface to create another solid. This process was repeated for each surface. At each step, the soil layer for the current horizon was created by subtracting all previously defined solids from that layer, resulting in an incremental build-up of the stratigraphy from the bottom to the top. The entire process was performed in GMS and a 3-D hydrogeological solid model was created with each horizontal layer represented by a material ID. It contains in total 6 clay layers and 5 gravel-sand layers. As an example, Fig. 4.13 shows three cross sections taken from the solid model for the Nankou area.

4.2.3 Model development

The development of a numerical groundwater model aims to analyze the hydrological behaviors over time in the geometrical domain with mathematical equations.

Governing equation

The conceptual hydrogeologic model can be described mathematically, using the ground water flow equation in porous media [Freeze and Cherry, 1979, Fetter, 1998]:

$$S_s \frac{\partial h}{\partial t} = \nabla \cdot (\mathbf{K} \nabla h) - W \tag{4.6}$$

where $\mathbf{K}$ is the hydraulic conductivity tensor [L/T] in three orthogonal directions, h is the hydraulic head [L], W is the volumetric flux per unit volume [1/T] and represents the

groundwater recharge/discharge, i.e. source/sink term for groundwater, S_s is the specific storage capacity [1/L] of the porous medium and t is the time. In our model, W is a function of space and time, depending on variations of recharge and discharge. The above equation, with initial and boundary conditions, is solved at each time step by the finite element code OGS.

Spatial and temporal discretization

Based on the solid model (Sec. 4.2.2), the model domain is spatially discretized into three types of elements, i.e. triangular prism, tetrahedron and five node pyramid using GMS. Because all elements of the GMS generated mesh are conforming, we divided each pyramid with a square or rectangular base into two tetrahedra, so that pyramidal elements are avoided while the total number of nodes is not changed. For this purpose, a function was implemented to convert each pyramid element into two tetrahedra when the 3-D mesh file was imported into OGS. After the meshing procedure is finished, the whole study area is divided into a total of 73324 elements including prisms and tetrahedra. Every horizontal layer contains 4597 nodes with a mesh density of about 200 m (Fig. 4.14). The numerical scheme for coupling multi-dimensional finite elements was described in detail in Kolditz [1995].

In the present study, we simulated the groundwater flow in the Nankou area for the time period from 1998 to 2007. The deviation between the water recharge from precipitation and the abstraction is a minimum of -2.73$\times$ 10^{-4} m/d in 1998. Therefore, the groundwater flow model in 1998 is first calibrated under the assumption of a steady-state. Afterwards, the steady-state flow field is used as initial conditions for the transient simulation from 1999 to 2007. The stress period of the transient simulation is defined as one year according to available data. Starting in June 2006, the emergency and preparative water source (Fig. 4.10) is introduced as the sink term in equation(4.6), so that the model is more close to reality. In the transient simulation, fixed time step size was used for temporal discretization. Considering the upper limit defined by Courant's criterion [Wylie and Streter, 1978] for numerical stability, we set the time step size equal to one day.

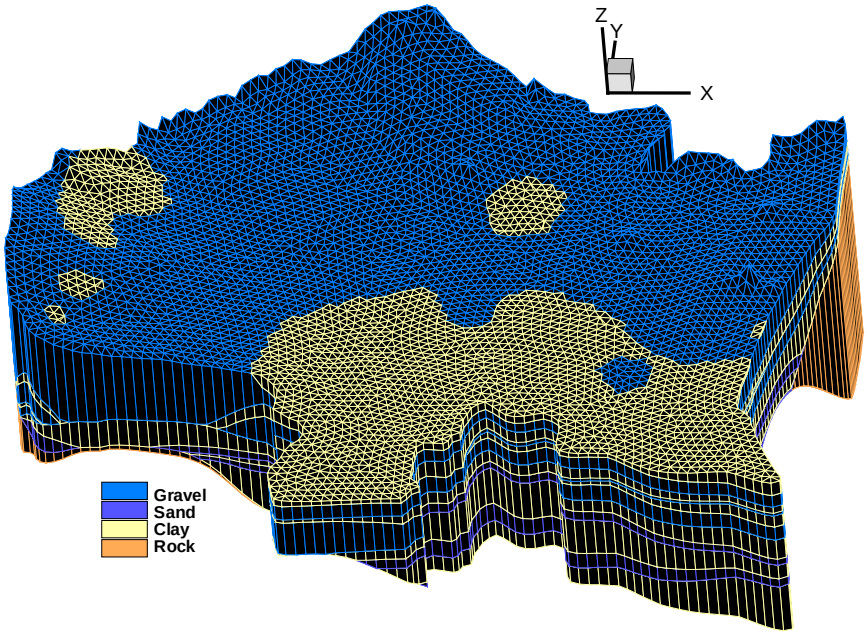

Figure 4.14: The 3-D discretized hydrogeological structure model.

Boundary conditions

The boundaries on the western and northern part of the model domain follow the contact zone between the Beijing Plain Quaternary sediments and limestone formations of the mountain terrains. On this interface, the mountain-front recharge enters laterally into the study area. Thus most of the western and northern edges were assigned with specified flux boundary conditions except for the ones parallel to the flow direction, which were defined as no flow boundaries in the model. The initial values of the specified fluxes were estimated according to Darcy's law, and they are listed in Table 4.1.

According to the groundwater level contour map (Fig. 4.10) from Beijing Hydrological Center, the eastern border and the regional groundwater flow are nearly parallel. Therefore, we can treat approximately the eastern edge as a no-flow boundary. In the south, the regional groundwater flows out of the model domain but reverses its direction if excessive

pumping occurs. This behavior is represented by imposing general head dependent boundaries along this border. The head values of these boundaries were achieved by interpolation using the contour map and the measured water levels in the nearby monitoring wells.

The top boundary is recharge and discharge from precipitation, phreatic evaporation losses and groundwater abstraction. The infiltration of precipitation is represented in the model by an average factor of 0.25 [Xu, 2006]. The quantity of phreatic evaporation decreases as the drawdown continues. According to a previous study in the Beijing Plain [Xu, 2006], the phreatic evaporation nearly stops as the groundwater level drops beyond 2.5m below the land surface. Therefore, we can ignore the quantity of the phreatic evaporation because the shallowest groundwater depth is 4m in our study area. As for the groundwater abstraction, an average pumping rate was given for the whole domain because of the data scarcity. The water recharge from precipitation and pumping rates from 1998 to 2007 are shown in Fig. 4.15. The bottom boundary is formed by the deepest aquitard (clay or limestone) of the Quaternary sediments and we assume no water fluxes through the bottom boundary.

Workflow of GMS/OGS/PEST integration

As mentioned in Sec. 4.2.2, OGS is a scientific open source code focused on the numerical simulation of THMC processes in porous and fractured media based on the finite element method. The 3-D mesh for hydrogeological model in OGS is generally mapped layer by layer with GIS raster data, and there is no function or module in it to create a 3-D spatial structure directly with borehole data. GMS with a series powerful modules provides different interpolation methods to deal with the stratigraphic scattered points based on the borehole logs. The 3-D mesh created with GMS can be exported into an ASCII file with the extension of .3dm, which can be imported into OGS with the present implemented interface by rewriting the record of every nodes and elements according to the syntax of OGS mesh file. This interface has been successfully used in several other case study such as the western Dead Sea Escarpment, Jordan and Selke catchment, Sachsen-Anhalt, Germany. The parameter estimation code PEST has been integrated in some popular commercial groundwater modeling sofware e.g. Visual MODFLOW and GMS. The advantages of applying such an model independent parameter estimation system in the model calibration process

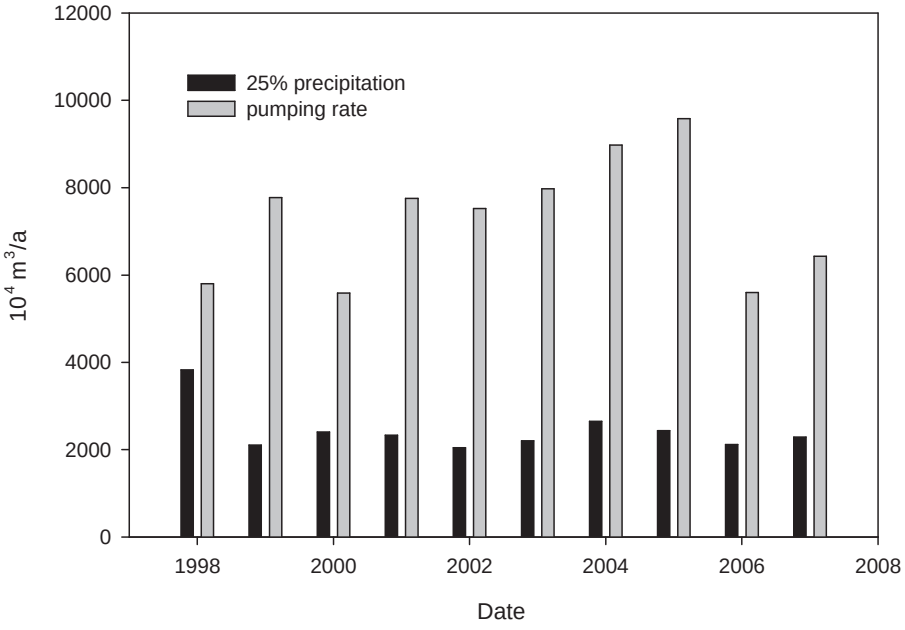

Figure 4.15: The water recharge from precipitation and pumping rates in the Nankou site from 1998 to 2007.

have been described in many publications [Hill, 1992, 1998, Poeter and Hill, 1997]. In this study, PEST was directly applied to OGS by preparing the control file and the input/output exchange files. The PEST control file puts all components together, which include the names of all template and instruction files (Fig. 4.16) as well as the model input/output files to which they pertain. It also provides PEST with the model name, parameter initial estimates, measurement values to which model outcomes must be matched, prior parameter information, and a number of PEST variables which control the implementation of the Gauss-Marquardt-Levenberg method [Doherty, 2004]. The data exchanges between PEST template/instruction files and model input/output files happen at each iterative step until an objective function minimum is achieved as shown in Fig. 4.16.

4.2.4 Results and discussion

The accuracy of the groundwater model depends not only on the input data but also on the parameters. In Sec. 4.2.3, available input data (precipitation, pumping rates, initial and boundary conditions) have been assembled in the model. The detailed process of parameter identification will be described in the following subsections .

Inverse parameter estimation

The goal of the calibration is to obtain an optimal fit between the computed and observed values by parameter estimation using inverse modeling. Besides the hydraulic conductivities of different porous media groups (Fig. 4.14), the groundwater recharges from adjacent mountain aquifers are also calibrated. The well-known PEST code (Doherty 2005) is applied for parameter estimation. The initial values and ranges (Table 4.1) for each parameter are defined in the PEST control file before calling the OGS model iteratively. The initial horizontal hydraulic conductivities and specific storages for the three material types were estimated from the pumping tests in the previous investigation [Zhang and Fei, 2009]. As the sedimentary rocks are generally much more permeable in the horizontal direction, a vertical anisotropy factor of 0.1 (K_v/K_h) was assumed for all the materials [Freeze and Cherry, 1979]. For all parameters a range of $\pm 50\%$ of the estimated value was used in the first calibration run. If there were some optimised parameter values approaching to the upper or lower boundary of the range, the ranges were extended wider (i.e. kz2 in Table 4.1) than before for the second calibration run.

During the run of PEST, parameter values were adjusted according to the control settings until model-generated heads fit observed heads as accurately as possible. Therefore, PEST searches a parameter set until the sum of squared deviations between calculated and measured values at the observation wells are reduced to a minimum.

The steady-state model considers the groundwater heads of the available observation wells in 1998. Considering all available 8 control points from the observation wells (Fig. 4.17), the optimized objective function, i.e. the sum of squared weighted residuals is 55.27 m^2 and the mean value of non-zero weighted residuals is -0.3139 m. The minimum residual is -0.198m (observation well #327, Fig. 4.17). The correlation coefficient, as a measure of

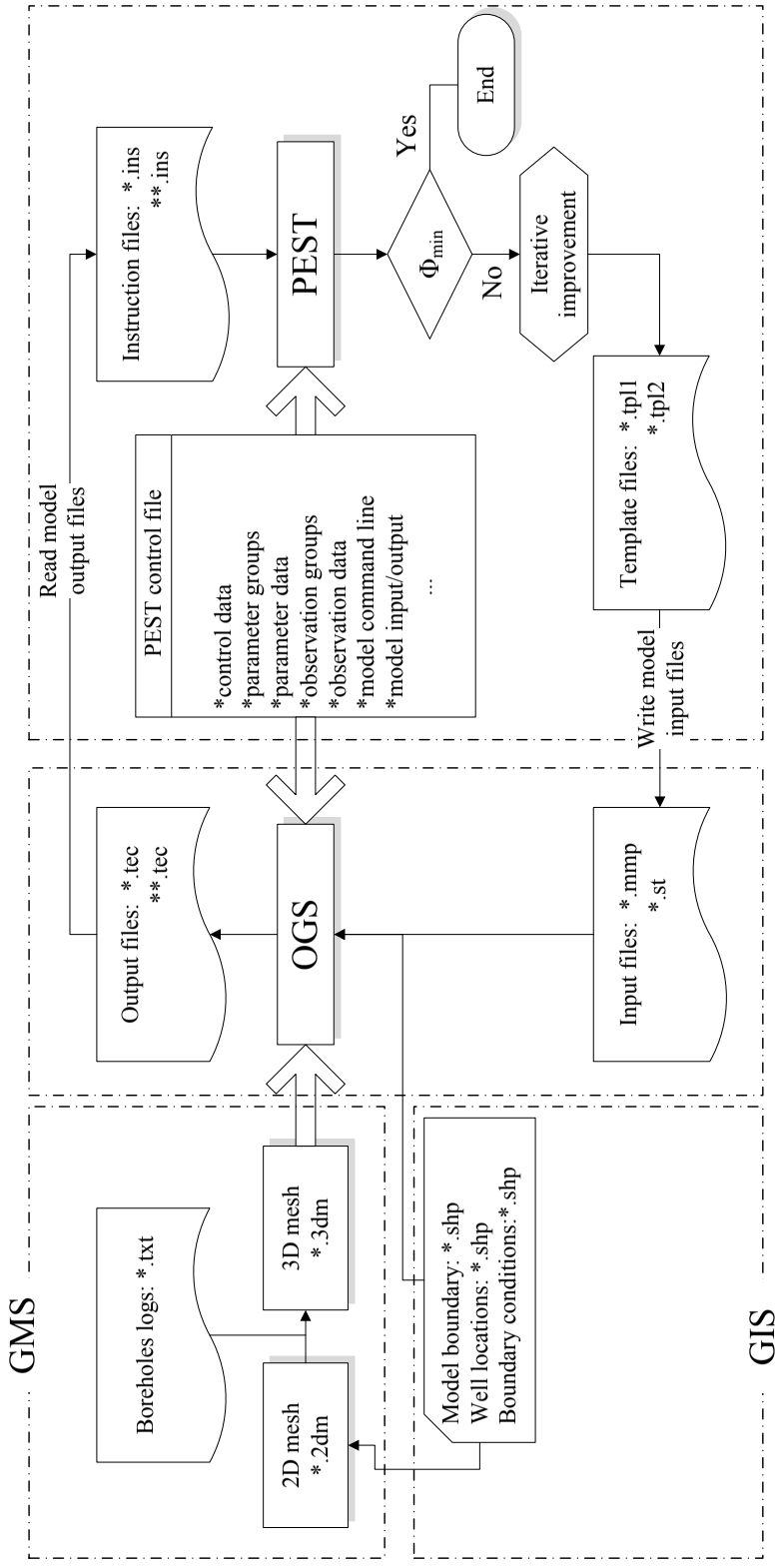

Figure 4.16: The workflow of GMS/OGS/PEST integration.

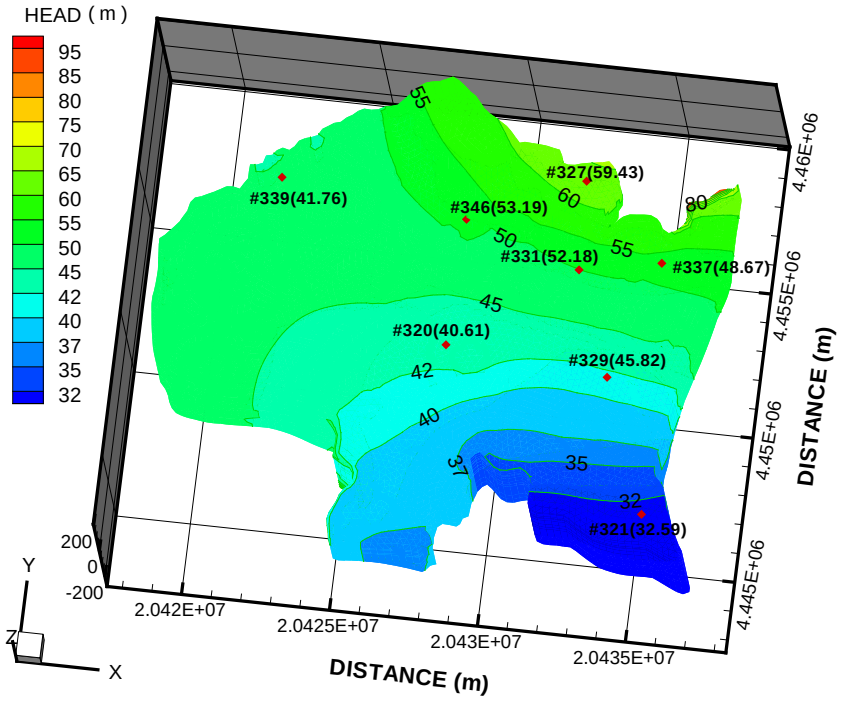

Figure 4.17: Comparison between simulated groundwater contour map and observed heads in specified wells (The projected coordinate system in this figure is Pulkovo_1942 transverse mercator).

goodness of fit, is 0.9452. Generally, correlation coefficients above 0.9 can be considered as acceptable [Hill, 1998]. The results of the parameter calibration (hydraulic conductivities and storage coefficients) are shown in Table 4.1. The estimated recharge fluxes at the northern boundary range from 6.0×10^{-2} to 1.5×10^{-1} m/d and the estimated recharge flux at the western border is 1.7×10^{-2} m/d.

Fig. 4.17 shows the computed hydraulic head distribution in the steady-state model and Fig. 4.18 depicts a comparison between the observed and computed groundwater levels in 8 observation wells. There is a fairly good overall agreement between the computed groundwater heads and observed values. In Fig. 4.17, the calculated groundwater head gradient changes more smoothly in the western part of the domain compared to the gradient in Fig. 4.10. The contour map in Fig. 4.10 includes monitoring wells in the mountain areas,

Table 4.1: Estimated initial values and ranges of the parameters induced to the model before calibration procedure and the optimized values afterwards.

Parameters	Category/Zone	Initial values	Ranges	Optimized values
Hydraulic	kh0	6.25×10^{-4}	$1.0 \times 10^{-4} \sim 1.0 \times 10^{-3}$	6.0×10^{-4}
conductivity	kv0	6.25×10^{-5}	$1.0 \times 10^{-5} \sim 1.0 \times 10^{-4}$	1.0×10^{-4}
(m/s)	kh1	1.85×10^{-4}	$1.0 \times 10^{-4} \sim 1.0 \times 10^{-3}$	7.0×10^{-4}
	kv1	1.85×10^{-5}	$1.0 \times 10^{-5} \sim 1.0 \times 10^{-4}$	7.0×10^{-5}
	kh2	1.0×10^{-5}	$5.0 \times 10^{-6} \sim 5.0 \times 10^{-5}$	6.0×10^{-6}
	kv2	1.0×10^{-6}	$5.0 \times 10^{-8} \sim 8.0 \times 10^{-6}$	9.0×10^{-8}
Lateral flux	st_l1	1.0×10^{-4}	$1.0 \times 10^{-5} \sim 6.0 \times 10^{-2}$	1.7×10^{-2}
(m/d)	st_l2	1.0×10^{-1}	$5.0 \times 10^{-2} \sim 2.0 \times 10^{-1}$	1.5×10^{-1}
	st_l3	4.0×10^{-2}	$5.0 \times 10^{-3} \sim 1.0 \times 10^{-1}$	6.0×10^{-2}
Specific storage	stor1	1.0×10^{-3}	$1.0 \times 10^{-5} \sim 1.0 \times 10^{-1}$	7.9×10^{-4}
(-)	stor2	1.0×10^{-3}	$1.0 \times 10^{-5} \sim 1.0 \times 10^{-1}$	7.9×10^{-4}
	stor3	1.0×10^{-3}	$1.0 \times 10^{-5} \sim 1.0 \times 10^{-1}$	1.0×10^{-5}

which are highly influenced by the local geological structures. Therefore we have excluded them from our model. To improve model quality, one or two monitoring wells in this area should be included in the future. In Fig. 4.18, the computed hydraulic heads are a bit higher than observed values in 3 observation wells (#320, #339, #337) and lower in observation well #329 and #346. This phenomenon may due to the pumping activities at some centralized locations. To reflect these local intensive pumping activities, the equal distribution of pumping rates shall be changed once the data on such activities are available.

Sensitivity analysis

In order to analyse the sensitivity of the model to changes of the input parameters, a model independent sensitivity analyser SENSAN in the PEST packages was applied. In the optimization process, the sensitivity of each input parameter is recorded to a specified file, which is updated during every iteration. In this study, the sensitivity of the hydraulic conductivities and lateral fluxes to the response of simulated hydraulic heads were evaluated. In the first running of PEST, the results (Sensitivity_1, Table 4.2) show that the most sensitive parameter in those composite input parameters is the lateral flux 2 (st_l2, Table 4.2) and the correlation coefficient is 0.8997. But the parameters of hydraulic conductivities seemed not so reasonable as the natural materials. Then the PEST was conducted again with the fixed hydraulic conductivities, a new set of lateral fluxes (value_2, Table 4.2) was

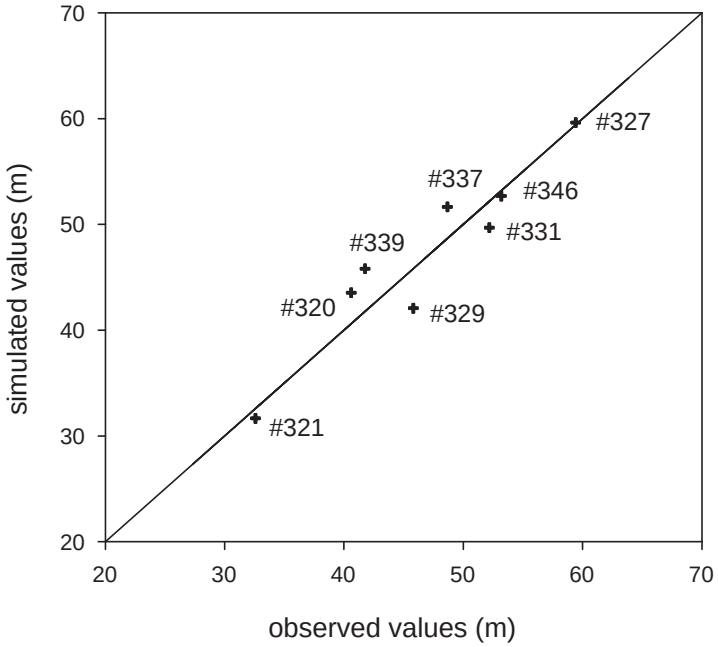

Figure 4.18: Observed vs. simulated groundwater level in 8 wells (see Fig. 4.17 for location).

achieved and the correlation coefficient was improved to 0.9324. For the same reason, the PEST was conducted for the third time with the fixed new lateral fluxes and the correlation coefficient was improved to 0.9452 with a new hydraulic conductivity parameter set (value_3, Table 4.2). The sensitivity analysis shows that the model is more sensitive to horizontal hydraulic conductivities than to vertical ones, more sensitive to the lateral flux 2 than to hydraulic conductivities.

Transient flow simulation

Based on the preliminary hydraulic conductivities and boundary conditions obtained from the steady-state calibration, a transient flow model is developed to simulate the groundwater level changes in the time period 1999-2007.

The calibration of the transient model is performed in PEST similar to the steady-state one. It takes into account the specific storages in different material groups and applies the

Table 4.2: Estimated parameters and sensitivity achieved by calibration with PEST in the Nankou area.

Category/zone	Parameters	value_1	Sensitivity_1	value_2	value_3
kh0	Hydraulic	4.0×10^{-4}	2.39	4.0×10^{-4}	6.0×10^{-4}
kv0	conductivity	1.0×10^{-4}	1.75×10^{-3}	1.0×10^{-4}	1.0×10^{-4}
kh1	(m/s)	8.0×10^{-4}	2.02	8.0×10^{-4}	7.0×10^{-4}
kv1		1.0×10^{-4}	9.93×10^{-4}	1.0×10^{-4}	7.0×10^{-5}
kh2		1.0×10^{-4}	0.82	1.0×10^{-4}	6.0×10^{-6}
kv2		1.0×10^{-6}	4.55×10^{-2}	1.0×10^{-6}	9.0×10^{-8}
st_l1	Lateral flux	5.0×10^{-3}	0.13	1.709×10^{-2}	1.709×10^{-2}
st_l2	(m/d)	0.1	3.62	0.150	0.150
st_l3		3.1×10^{-2}	1.55	6.016×10^{-2}	6.016×10^{-2}
correlation coefficient		0.8997	-	0.9324	0.9452

same hydraulic conductivities and the lateral recharge fluxes as in the steady-state model. The calibrated specific storage coefficients of different material groups (Table 4.1) are obtained with a correlation coefficient of 0.9716.

Fig. 4.19 (a) shows a scatter diagram of the observed vs. calculated heads at the observation wells over the simulation period. The mean difference between the observed values and the calculated groundwater heads for the total 45 data points is 0.14m. This small mean error suggests that there is no significant bias in the model results for the transient condition. Even though the mean difference is a reasonable low value, the calculated time series hydraulic heads in well #320 are overestimated as shown in Fig. 4.19 (a). The potential reason for this overestimation could be also the meanly distributed pumping rate input being used. In order to compare the temporal trends of simulated and monitored groundwater levels, two observation wells (# 321 and # 346, see location in Fig. 4.17) are selected from the different parts of the domain. Fig. 4.19 (b) shows that the increasing drawdown trends in the calculated heads are in a good agreement with that of the observed values. Generally, the regional groundwater flows from the northwest to southeast (Fig. 4.20a). However, in 2007 it reversed the direction in the northwestern part (Fig. 4.20b) it could be caused by the centralized agricultural pumping activities. A cone of depression in the south (Fig. 4.20b, red circle) developed in June 2006 due to the increasing pumping activities.

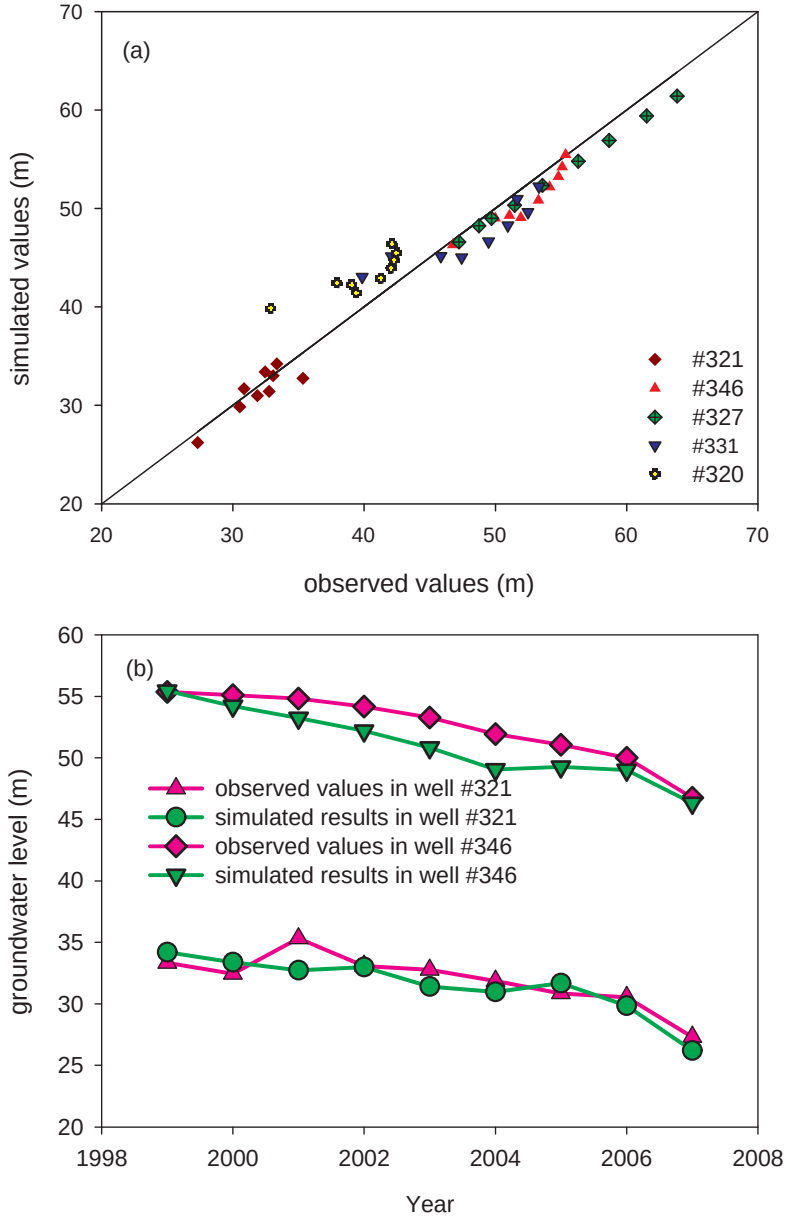

Figure 4.19: (a) Scatter plot of observed vs. simulated heads and (b) observed vs. simulated hydraulic heads temporal trends in selected monitoring wells as the result of model calibration (1999-2007).

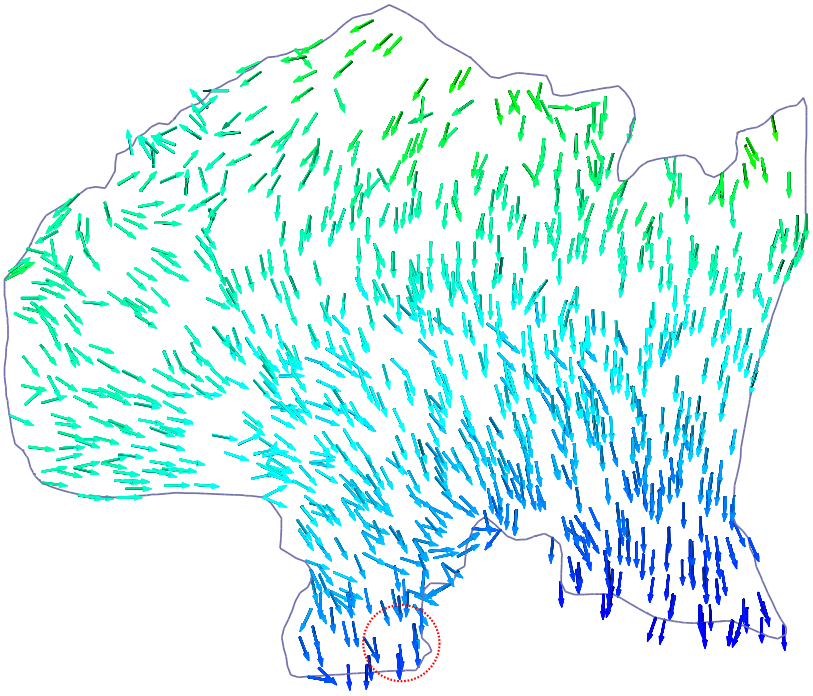

(a) 2006

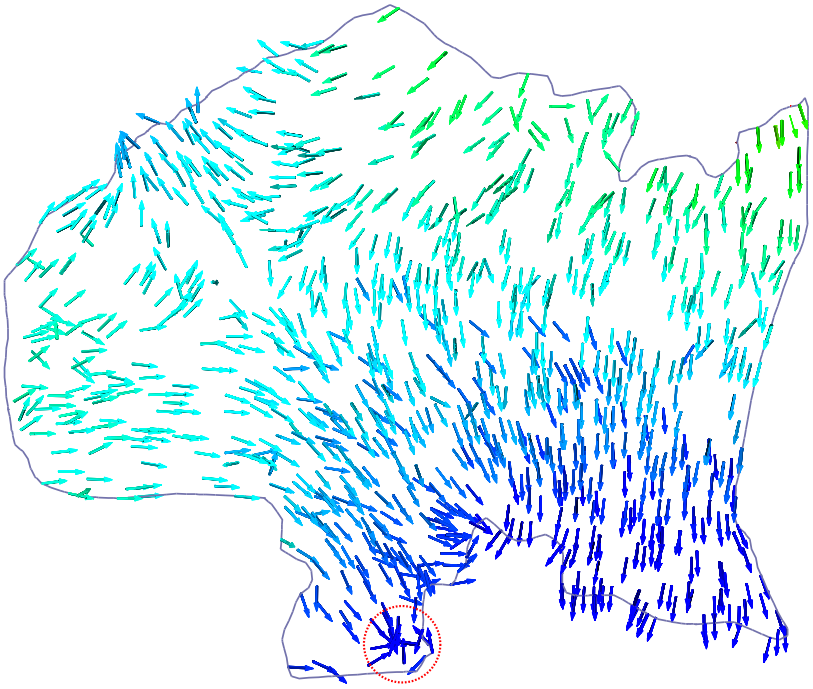

(b) 2007

Figure 4.20: Comparison between groundwater flow nets of 2006 and 2007.

Discussion

Before this groundwater model is used for the water resources management and contaminant transport modeling, the model uncertainty should be recognized. The sources of the total uncertainty in the modeling process can be divided into several categories, including input data, model structure, parameters and model technology etc. [Refsgaard et al., 2007]. In this study, the data sparse is the main source of the model uncertainty. The input data of the infiltration from precipitation and the pumping rates was assumed being uniformly distributed in the surface, which might cause the overcalculation or undercalculation in some observation wells. The density of boreholes in the study site is far less than that required in the Chinese standard for hydrogeological investigation of water-supply (GB50027-2001), so the hydrogeological structure model must have some deviation with that in reality. In addition, there are some data such as river seepage and agricultural irrigation regression missing. The model can be improved by introducing more historic data or increasing the number of observation wells properly.

4.2.5 Conclusions and outlook

There is a dramatic deterioration of groundwater in the Beijing area where groundwater is the most important resource for drinking water supply. In this work for the first time a groundwater model was developed for the Nankou site within the Beijing Plain. Gaining a better understanding of the transient groundwater system under an enormous pumping stress and drought conditions is of highest importance for a sustainable water resource management of Beijing City.

A 3-D groundwater flow model was developed for the Nankou area. The model was calibrated with all available data and the groundwater flow regime was investigated under steady and transient conditions. The groundwater level changes are resulting from interacting hydrological processes and anthropogenic activities, i.e. the recharges from precipitation, groundwater abstraction and so on. All available data relevant to these processes were used to analyse the groundwater flow regime in the study area but still not enough to identify all hydrogeological features. In order to reduce the uncertainties, the presented hydrogeological model will be improved in the future by developing appropriate monitoring

strategies and integrating more detailed data when available.

As prerequisites to the hydrogeological study, GMS (for data pre-processing) and PEST (for inverse parameter estimation) were integrated into the OGS code for groundwater finite element analysis. The code communication GMS / OGS / PEST is the technical achievement of this work. The inverse method embedded in PEST was applied to enhance the accuracy of the modeling in the present study by preparing control files, corresponding input and output files.

From the groundwater flow model described in this paper, it can be seen that the decreasing trend of ground water levels in the study area shows that the current groundwater utilization scheme is unsustainable under the drought climate conditions. This detailed 3-D groundwater model is only the first step toward a comprehensive effort to the scenario analysis for a sustainable water resources management in the Beijing Plain, including climate change, land use and social-economic factors. The research on the groundwater contamination and remediation in this area will soon be carried out based on this model.

4.3 Groundwater quality deterioration at Nankou site

4.3.1 Background

Generally, in order to assess and report on the quality of Beijing City's groundwater, 2∼3 samples taken from each suburban district are analyzed in April and September every year since 1970's. Based on these data, a long-term groundwater quality trend (Fig. 4.21) is identified in the sampling well #346. The limitation values of hardness and nitrate for drinking water sources are 450 mg/L and 20 mg/L respectively according to the Quality Standard for Ground Water (QSGW, GB/T 14848-93) in China. Compared with this criterion, the nitrate concentrations in the flood season are over 20 mg/L and after 1995 it increased higher both in the flood and dry seasons. The values of hardness were also increased much higher than the criterion (450 mg/L) after 1995. In order to figure out what is wrong with the groundwater quality in the site of well #346, a groundwater quality monitoring network (Fig. 4.22) was established in 2009. The measurements in this monitoring network show that the nitrate concentrations in other wells are still staying below the safe limitation.

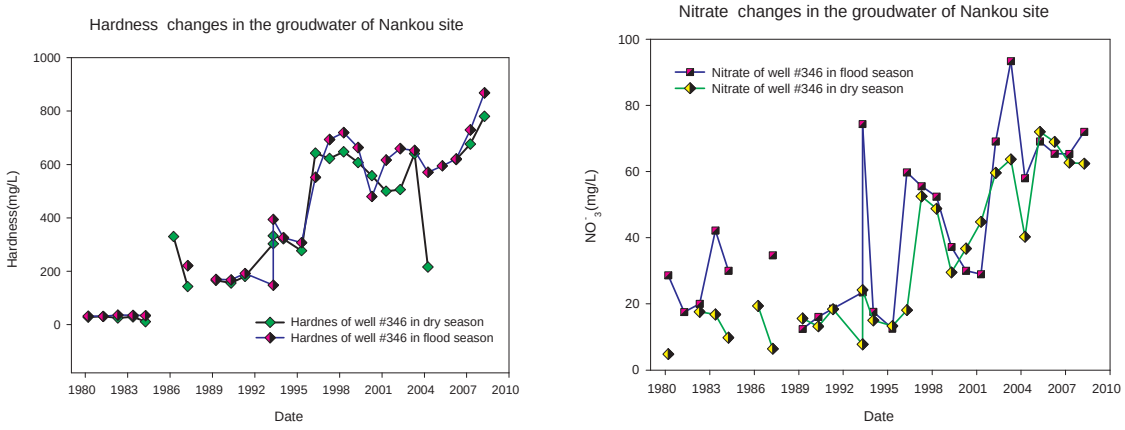

(a) Hardness (b) Nitrate

Figure 4.21: Long term groundwater quality trend at the Nankou site. (see Fig. 4.17 for the location of well #346).

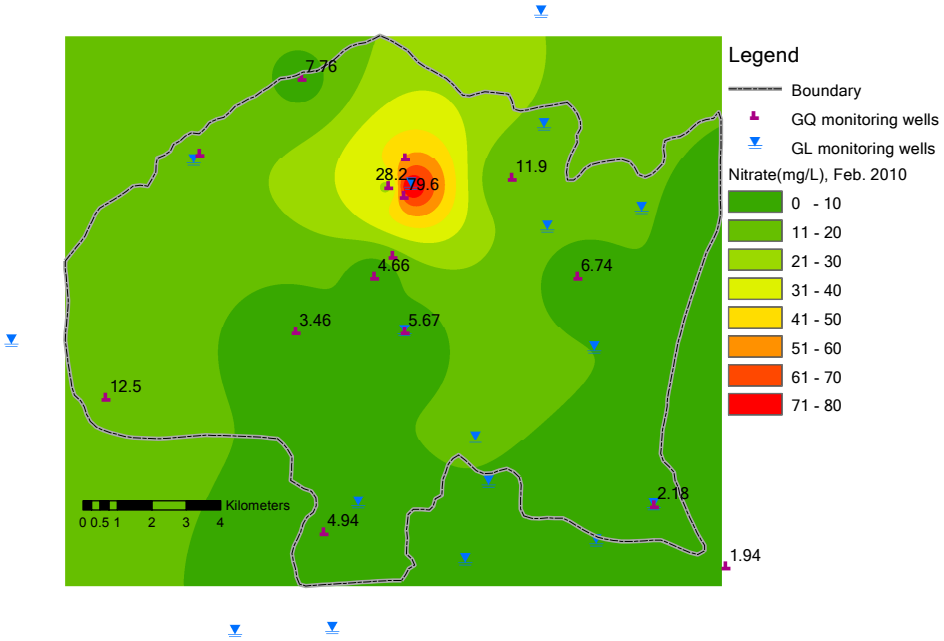

Figure 4.22: Nitrate concentration at the Nankou site in Feb. 2010.

4.3.2 Potential sources of groundwater pollution

Groundwater contamination can occur in many ways and from many sources, both natural- and human-induced. Groundwater contains some impurities, even if it is unaffected by human activities. The types and concentrations of natural impurities depend on the nature of the geological material through which the groundwater moves and the quality of the recharge water. Groundwater moving through sedimentary rocks and soils may pick up a wide range of compounds such as magnesium, calcium, and chloride. Most concern over groundwater contamination in the study area has centered on pollution associated with human activities. Human groundwater contamination can be related to the following 6 categories: pumping wells (abandoned wells included), waste disposal sites, agricultural activities, livestock & poultry waste, industrial wastewater and residential sewage.

(1) pumped wells

Most pumped wells (614) in the Nankou area are in the use of supplying drinking water or irrigation. Only 40 wells are abandoned for different purposes. All of the abandoned

wells were sealed completely. Therefore they are not vulnerable to be considered as the paths for the regional aquifer pollution.

(2) waste disposal sites

There are 6 waste disposal sites in the study area, and all of them are distributed inside of the Machikou town (Fig. 4.23). These waste disposal sites started to be used in 2006 or 2007. The total amount of the disposed waste from the above sites is about 19310 m^3 per year. The leachate from these waste disposal sites is a potential threat to the regional aquifer.

(3) agricultural activities

According to land use distribution, irrigated agriculture field accounts for about 22% (43.45 km^2) of the total land area of the Nankou site. The source of water for irrigation is mainly from the existing aquifers. Intensive fertilization of farmland or orchards (see Fig. 4.24) brought exceeding nitrate to the vadose zone. The average application of fertilizer is 210 kg N/ha·a and the inorganic nitrate accounts for about 61%.

(4) livestock and poultry waste

Livestock wastes could either be solid or liquid. Livestock wastes are described as liquid if the moisture content is more than 96%, between 90% and 96% moisture content, it is described as slurry while if the moisture content is below 84%, it is considered as solid. The solid waste is normally used as soil conditioner in this area, and the liquid waste are also irrigated as organic fertilizer in the farmlands. Many farms discharge their untreated sewage to nearby streams and canals which results in the pollution of regional shallow aquifer. Table. 4.3 shows the populations of livestock and poultry in the towns and Fig. 4.23. shows their distribution.

Table 4.3: The populations and sewages of livestock and poultry in the Nankou area.

Towns/Animals	Pigs	Cattle	Chickens	Sewage(ton/a)
Nankou	11771	3225	67398	68073
Chengnan	1500	868	7000	1300
Machikou	1500	198	120578	14446
Liucun	150	173	-	-
Shisanling	-	1570	-	6700
Total	14921	6034	194972	88519

(5) industrial and enterprise sewage

There are total 109 factories and enterprises in the study area, most of the wastewater is treated before it is discharged to Beishahe River. But there are still 17 factories or enterprises discharging the untreated wastewater into nearby streams or channels. The discharged untreated water accounts for 84.56 ton ammonium (NH_4^+) per year.

(6) residential sewage

According to the report of pollution sources investigation, only 9.23% residential wastewater is collected and conveyed to a central location for treatment or disposal in the study area. In other discentralized residential spot, the wastewater is disposed on-site or flows through some channels to surface water finally. The most dangerous strategy is to dispose the wastewater to some unsealed pits, which is a direct threat to the regional aquifer system. The total ammonium from the residential sewage accounts for about 119 ton per year.

Based on the above analysis, the nitrogen discharge could be placed in the following order by different sources: agricultural activities > livestock and poultry waste > residential sewage > industrial and enterprise wastewater > waste disposal sites.

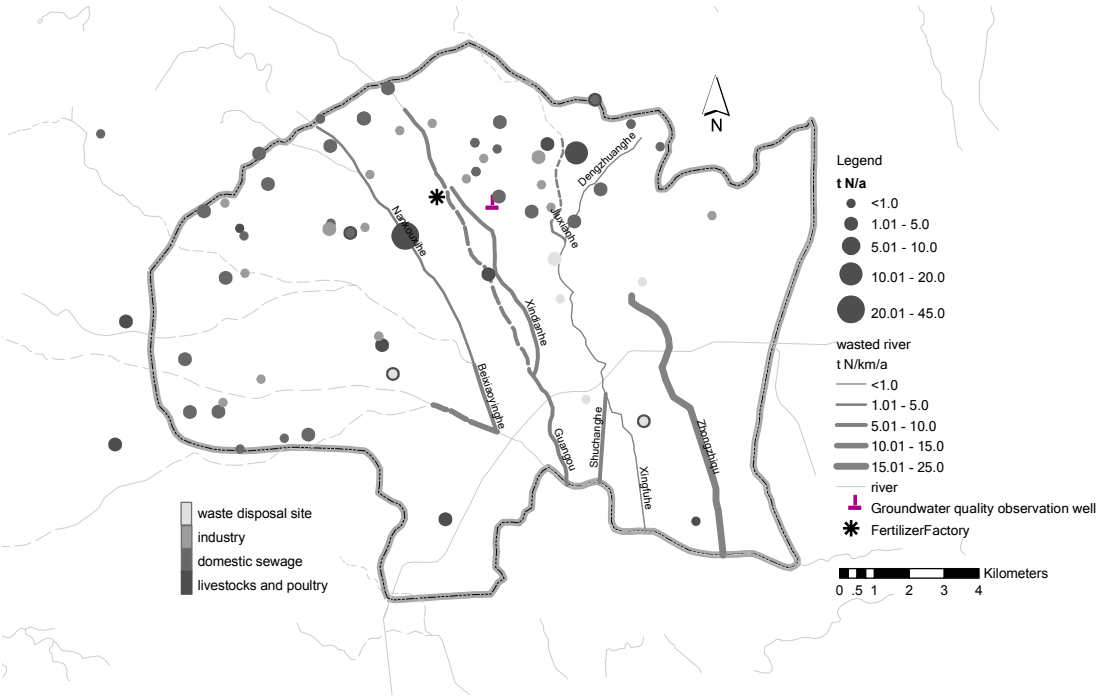

Figure 4.23: The distribution of potential pollution sources to the aquifer.

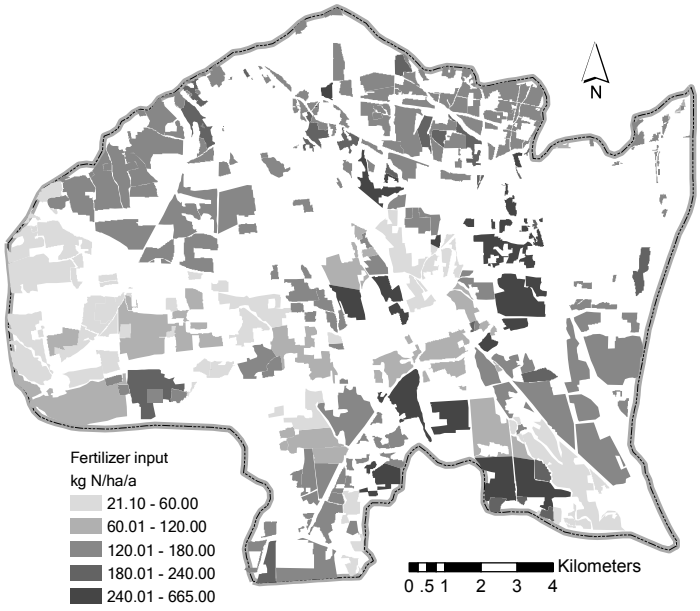

Figure 4.24: The distribution of fertilizer input to the farmlands and orchards.

4.3.3 Hydrochemistry

Chemical analysis of the groundwater samples produces the statistical values as shown in Table. 4.4 and 4.5. These results show that after 1995, the average concentrations of hardness and nitrate in the well #346 surpass those highest limits permitted for drinking water by the QSGW criteria, 450 mg/l and 20 mg/l respectively.

Table. 4.6 shows the evolution of the average concentrations of pH, nitrate, ammonium, and total nitrogen with depth in the 19 soil column samples. Profiles of the chemical concentrations vs. depth show almost the same trend. Most of the chemicals have higher concentrations in the surface layer and the layer of 50 cm. The profiles in Fig. 4.25 were constructed from the analysis of the samples taken in the location of well #346.

4.3.4 Concept model: nitrogen transformations

According to the historical chronology of Changping County [Zhao and Sun, 1979], there was a fertilizer factory (location see Fig. 4.26) founded in 1974, about 8 km from

Table 4.4: Statistical parameters of the groundwater chemical analysis (1980-1995).

Parameters	Unit	Mean	Minimum	Maximum	Standard Deviation
pH	-	7.5	6.8	8.1	0.3
Hardness	mg/l	164	11	394	124
Diss. solid	mg/l	531	120	998	308
SO_4^{2-}	mg/l	49.6	10.8	130.0	36.6
Cl^-	mg/l	50.1	9.7	132	28.44
NH_4^+	mg/l	0.07	0.01	0.20	0.06
NO_3^-	mg/l	20.1	4.8	74.4	14.0
MnO_4^-	mg/l	0.92	0.20	2.60	0.54
E.C.	μ S/cm	671	300	1250	312

Table 4.5: Statistical parameters of the groundwater chemical analysis (1996-2010).

Parameters	Unit	Mean	Minimum	Maximum	Standard Deviation
pH	-	7.3	6.6	7.9	0.3
Hardness	mg/l	627.4	216	868	132
Diss. solid	mg/l	1052	225	1742	315
SO_4^{2-}	mg/l	94	42	156	23.7
Cl^-	mg/l	134.9	68.4	219	34.8
NH_4^+	mg/l	0.2	0.05	0.58	0.15
NO_3^-	mg/l	54.8	18.1	93.4	19.35
MnO_4^-	mg/l	0.8	0.5	2.1	0.38
E.C.	μ S/cm	1241	245	1850	401
Fe	mg/l	0.3	0.03	1.14	0.28
Diss.DO	mg/l	6.7	5.0	8.5	1.48
K^+	mg/l	2.9	0.9	5.3	1.79
Na^+	mg/l	45.4	21.4	94	30.53
Ca^{2+}	mg/l	162.7	55.1	227	71.13
Mg^{2+}	mg/l	185.8	19.4	460.14	239.39
CO_3^{2-}	mg/l	271.0	154	398	118.4

the Changping County center with an annual output of 15,000 tons of synthetic ammonia. The untreated wastewater containing high concentration ammonium (250 mg/L) was directly discharged to the nearby Guangou river through an underground pipe. If the amount of wastewater discharge was 150 m^3/t ammonium, the total ammonium emission from the

Table 4.6: The soil chemicals with depth in the Nankou area (2010).

Depth	pH	NO_3^--N(mg/kg)	NH_4^+-N (mg/kg)	MnO_4^- (mg/kg)	TN (mg/kg)
10 cm	7.2	13.4	1.0	22.7	18.5
30 cm	7.2	12.9	1.0	14.8	17.2
50 cm	7.2	13.9	1.6	13.4	19.9
100 cm	7.2	11.5	0.8	11.6	15.9
150 cm	7.1	11.4	1.2	15.5	16.1
200 cm	7.2	8.7	2.0	14.2	13.5

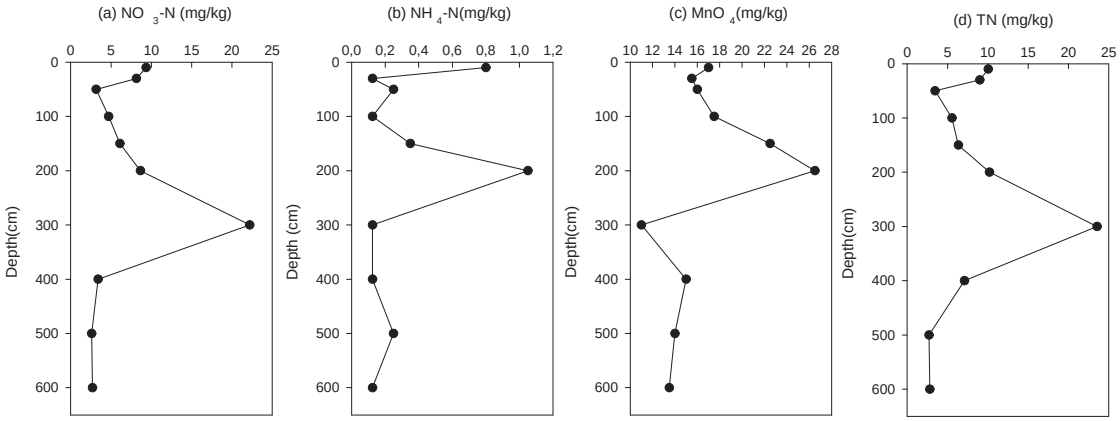

Figure 4.25: The profiles of chemicals in the soil column sample #346 with depth.

factory amounts to 562.5 t/a. In 1990, the factory stopped to manufacture fertilizer. Therefore in the 17 years when the fertilizer factory was running, it was a possible pollution source for the vicinity groundwater.

The bulk of the nitrogen in wastewater from the fertilizer factory is in the form of aqueous ammonium (NH_4^+). Most sediment and soil colloid surfaces are negatively charged, giving them the ability to act as cation exchangers. The ammonium cation can therefore be immobilized geochemically by adsorption to the soil particles. Otherwise, ammonium may be rapidly oxidized to nitrite (NO_2^-) in the presence of oxygen by the autotrophic ammonia-oxidizing bacteria. This is the first step in the process of nitrification, which is a two stage oxidation process mediated by the autotrophic ammonia-oxidizing bacteria. In the second step, the autotrophic nitrite-oxidizing bacteria oxidize nitrite to nitrate (NO_3^-). The over all chemical reaction for nitrification can be represented by the reaction 4.7 showing that 1 mg

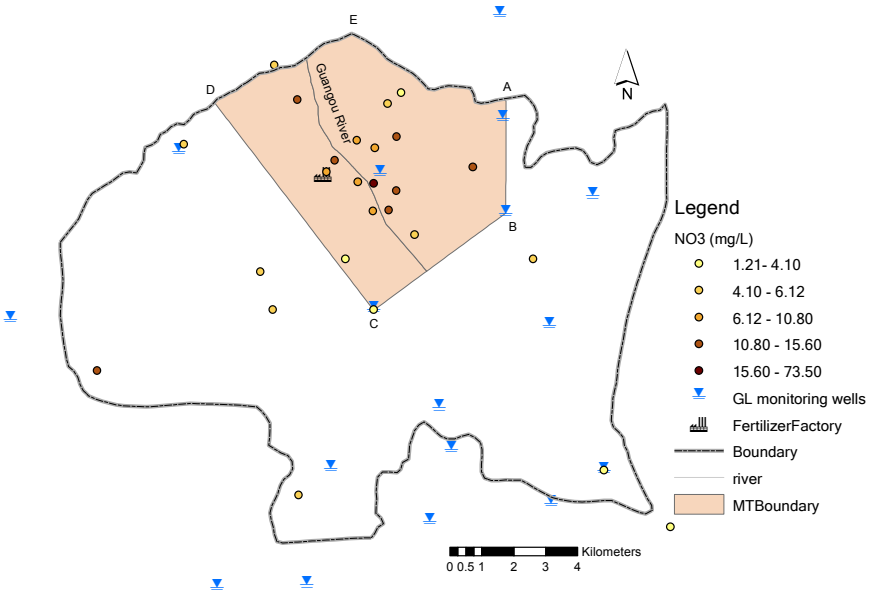

Figure 4.26: The redefined domain for contaminant transport model and the location of additional water quality monitoring wells.

NH_4^+ produces about 3.6 mg NO_3^-.

$$\begin{aligned} 2NH_4^+ + 3O_2 &\rightarrow 2NO_2^- + 2H_2O + 4H^+ \\ 2NO_2^- + O_2 &\rightarrow 2NO_3^- \end{aligned} \tag{4.7}$$

The ammonia-oxidizing bacteria are effective in converting ammonium to nitrite. Nitrite is a rather unstable nitrogen species, which will generally be reduced or oxidized. The nitrite-oxidizing bacteria then oxidize nitrite to nitrate. Nitrate is quite soluble in water and is not significantly adsorbed by clay-rich soils because it is an anion. In addition to the processes of adsorption and nitrification, ammonium in the unsaturated soil also can be removed by volatilization as gaseous status (NH_3) and plant uptaking as nutrient material. In the saturated aquifer, nitrate is reduced to nitrogen gas by denitrification. This process occurs primarily in anoxic conditions and involves heterotrophic bacteria. All these processes of ammonia and nitrate transformations in the unsaturated and saturated zones depend on the chemical redox conditions of the medium and the involvement of relative bacteria.

From the above theory of nitrogen transformation, most of the ammonium discharged

from the fertilizer factory could be oxidized by the autotrophic ammonia-oxidizing bacteria and infiltrated into to groundwater as nitrate species. This is in agreement with the results of chemical analysis in the groundwater, which shows that the concentration of ammonium remains a lower level (Table. 4.5).

Based on the hydrochemistry analysis in Section. 4.3.3, the concentrations of ferrous iron and sulfate in the groundwater keep at a lower level compared with the nitrate. In such an environment, the reduction of nitrate by chemical oxidation of ferrous iron or sulfur compounds such as iron sulfide and pyrite could be neglected. The denitrification processes dependent on the organic matter and heterotrophic bacteria also could not take place. Therefore the nitrate transport through the saturated zones in the study area follows the advection-dispersion transport equation (Eq. 2.50).

4.3.5 Groundwater model

The groundwater flow velocity in the aquifer is about 0.03 m/d based on Section. 4.2. By simple arithmetic, the advective transport velocity of the solutes in the aquifer will be 10 m/year. Therefore, the research should be more focused on the northern part of the Nankou area, where the well#346 is located. The domain for the contaminant transport modeling is accordingly redefined as shown in Fig. 4.26.

A three-dimensional, steady state local groundwater flow model is set up for the re-defined area (Fig. 4.26). Based on this local domain, a refined 3-D mesh is created with the methods mentioned in Section. 4.2. The number of the horizontal triangle elements is 27772. The vertical layers are created based on the borehole data. The total number of the prism and tetrahedra elements in the 3-D domain is 191766.

The boundaries of DE and EA (Fig. 4.26) are defined by the contact zone between the Beijing Plain Quaternary sediments and limestone formations of the mountain terrains as the catchment groundwater model. The AB and CD boundaries are defined as no flow conditions based on the catchment groundwater flow analysis in the Section. 4.2. The BC boundary is defined as a general head boundary. The head values at the nodes along the boundary BC is calculated by linear interpolation between the observed head of the start point and that of the endpoint. The top boundary is the precipitation recharge and

groundwater abstraction rates; the bottom boundary is treated as no flow.

The hydraulic conductivities in different materials are taken from the calibration results (Table. 4.2). The lateral fluxes through DE and EA boundaries are readjusted when the local groundwater flow model is calibrated against the observed groundwater levels.

4.3.6 Mass transport model

The 3-D mass transport model is developed based on the advection-dispersion equation (Eq. 2.50). The longitudinal dispersivity and transversal dispersivity are tried with the values of 50 m and 10 m respectively depending on the scale of observation, which is defined as the distance between the observation points and the source [Zheng and Bennett, 2002]. The boundary and initial conditions of groundwater flow are set as a steady state in 1998. The initial nitrate concentration within the domain is set to 4 mg/L. The total simulation period is 30 years. The discharge of nitrate from the fertilizer factory is estimated with the values of 5.058×10^6 g/d under the assumption that most ammonium was oxidized into nitrate based on the analysis in Section. 4.3.4. The simulation results after 30 years are shown in Fig. 4.27. From Fig. 4.27c and Fig. 4.27d, we can see that the contamination plum transport slows down apparently in the clay layer (red one). Therefore, the clay layer can block the plum extension to the deeper aquifer, but in the other hand, the pollutant will accumulate in the current aquifer layer and become a potential source if there is no remediation strategy applied.

Because there are no vertical concentration data for the 3-D model calibration, this model is considered to be simplified into a two-dimensional representation of an idealized catchment afterwards. The 2-D heterogeneous hydraulic conductivity K distribution is generated with GSTAT [Pebesma and Wesseling, 1998] based on the available 20 pumping test results. The nitrate discharge from the fertilizer factory is estimated with PEST. The calculated and observed concentrations from 1974 to 2008 in well $\#346$ are shown in Fig. 4.28. After 2008, the simulation is continued for 15 years under the different precipitation assumption (5 years 450 mm / year rainfall, 5 years 600 mm and 5 years 750 mm). From Fig. 4.28a and Fig. 4.28b, we can see that the influence on the contaminant transport by the precipitation change can be neglected. The concentration down trend (Fig. 4.28a) is

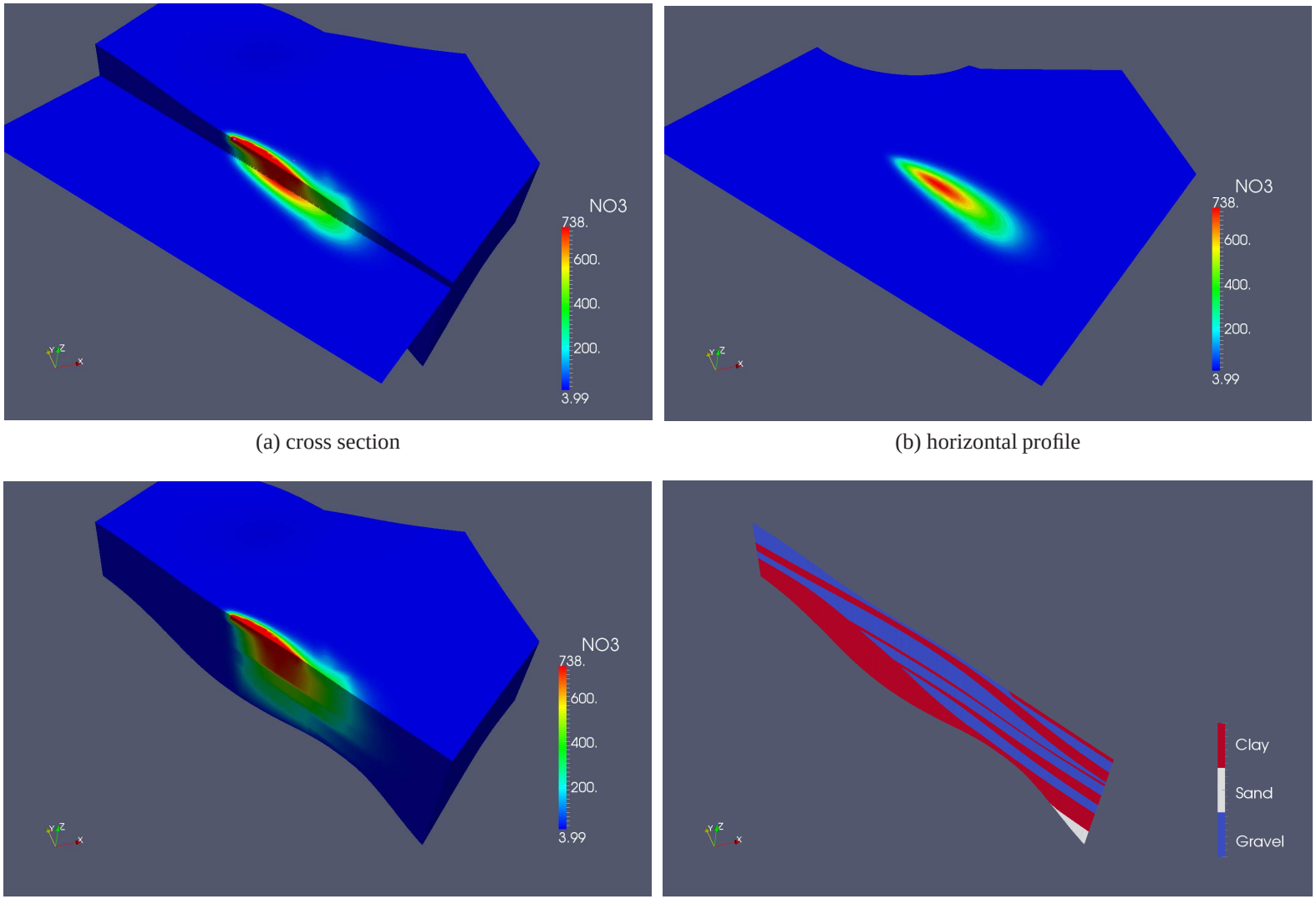

(a) cross section

(b) horizontal profile

(c) vertical profile

(d) vertical profile for material group

Figure 4.27: The simulation results of the contamination plume after 30 years (unit: mg/L).

mainly caused by the removal of the pollution source.

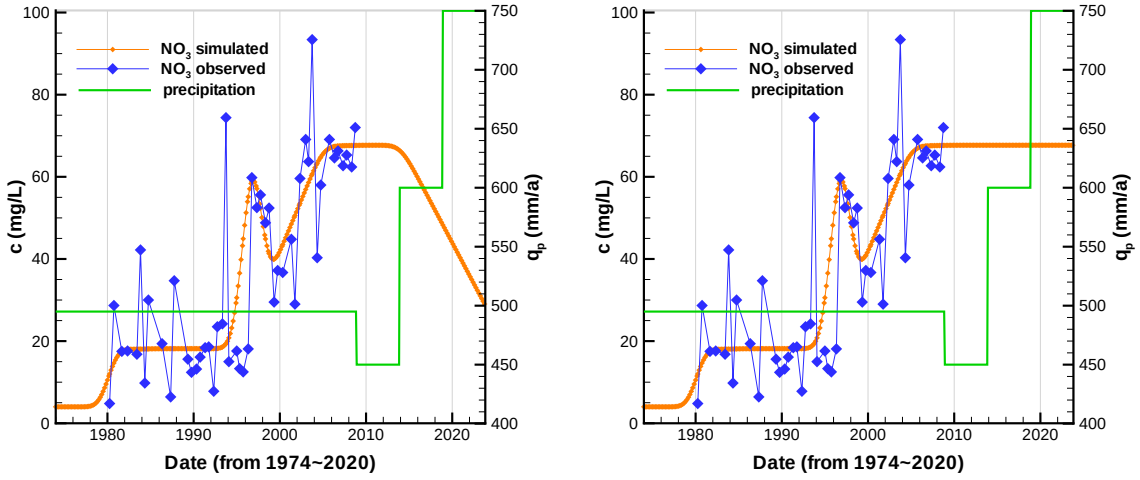

(a) after 2008 without pollution source

(b) after 2008 with pollution source

Figure 4.28: The calculated and observed concentration in well #346 under different precipitation.

4.3.7 Pump and treat scenario analysis

Groundwater that contains dissolved chemicals can be removed from the aquifer so that the contaminated water can be treated at the surface with the conventional methods of wastewater treatment. After reducing the concentration of contaminants in the water below a certain level, the treated water is either injected back into the aquifer or released to a surface water body. The finite maximum length of a steady state contaminant plume can be determined by developing and employing a new analytical solution considering of the finite aquifer thickness [Liedl et al., 2005]. In order to capture a plume of contaminated groundwater, it is necessary to have one or more pumping wells located down-gradient of the source area. The area contributing flow to that particular well is known as capture zone. The contaminants within the capture zone will flow to the pumping well once it starts working. Bayer-Raich et al. [2004] presented an analytical framework for estimation of representative field-scale average concentrations and mass flows on the basis of much larger sampling volumes that are obtained through so-called integral pumping tests. A

method for determining the optimum number of extraction wells, their locations and the rate at which each should be pumped has been developed by Javandel and Tsang [1985], in which a series of capture zone type curves (Fig. 4.29) are presented which can be used as tools for the design of aquifer cleanup projects.

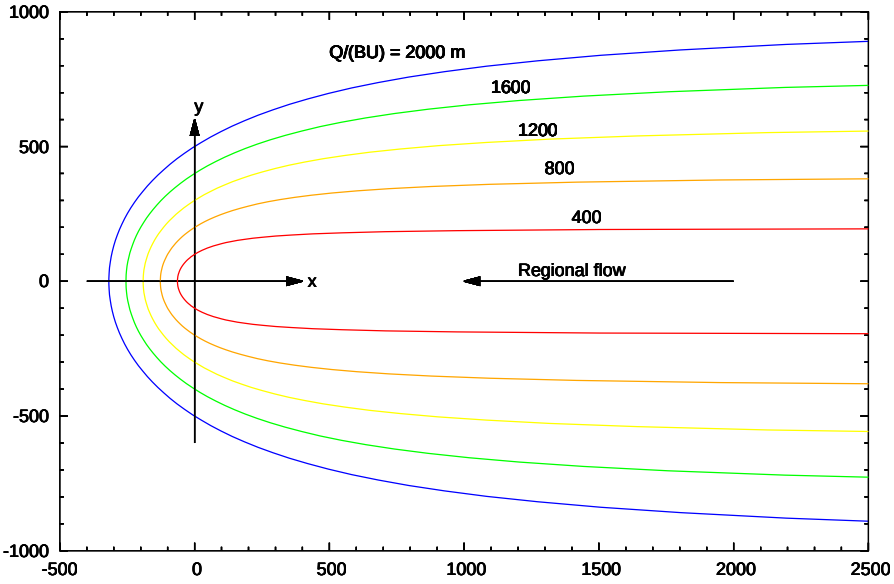

Figure 4.29: A set of type curves showing the capture zones of a single pumping well located at the origin for various values of (Q/BU).

Computation theory of capture zone

Consider a homogeneous and isotropic aquifer with a uniform thickness B[L]. A uniform and steady regional flow with a Darcy velocity U[L/T] is parallel to and in the direction of the negative x-axis. The position of a single pumping well is assumed at the origin and the well discharge is Q[L^3/T]. The equation of the line that divides the area that will be captured by the well from the rest of the flow field is

$$y + \frac{Q}{2\pi BU} tan^{-1}\frac{y}{x} = \pm\frac{Q}{2BU} \tag{4.8}$$

The only parameter in Eq. 4.8 is the ratio $(Q/(BU))$. Fig. 4.29 illustrates a set of type

curves for five values of parameter ($Q/(BU)$), all the water particles within the corresponding type curve will eventually go to the pumping well. In the reality there is a maximum quantity of water that can be pumped from a single extraction well. If the plume is wider than the capture zone developed by the maximum pumping rate, then multiple extraction wells are needed. Multiple extractions may lead to the overlapping of their capture zones or groundwater flow passing between them. If the distance between extraction wells (d) is less than or equal to $Q/\pi BU$, then the capture zones will overlap and the dividing streamlines can be defined as

$$y + \frac{Q}{2\pi BU}\left(tan^{-1}\frac{y-d}{x} + tan^{-1}\frac{y+d}{x}\right) = \pm\frac{Q}{BU} \tag{4.9}$$

If there are three wells , then the well in the middle can be located at the origin and the other two wells at the distances +d and -d on the y axis. The optimum well spacing is $\frac{\sqrt[3]{2}Q}{\pi BU}$. The equation for the dividing streamlines is

$$y + \frac{Q}{2\pi BU}\left(tan^{-1}\frac{y}{x} + tan^{-1}\frac{y-d}{x} + tan^{-1}\frac{y+d}{x}\right) = \pm\frac{3Q}{2BU} \tag{4.10}$$

Since cleanup operation usually lasts for several years, corresponding drawdown at the well bore may be calculated using either the equilibrium or nonequilibrium equation for large values of time is

$$\Delta h = \frac{2.3Q}{4\pi KB} log\frac{2.25KBt}{r_w^2 S} \tag{4.11}$$

$$\Delta h = \frac{2.3Q}{4\pi KB}\left\{log\frac{2.25KBt}{r_w^2 S} + log\frac{2.25KBt}{(2d)^2 S}\right\} \tag{4.12}$$

Eq.4.11 is for the drawdown induced by the single well pumping and Eq. 4.12 is for the drawdown at each of two pumping wells which distance is set as $2d$. In the above equations (Eq.4.11 and 4.12), Δh is the draw down in the aquifer [L], r_w is the effective well radius [L], K is the hydraulic conductivity [L/T], Q is the pumping rate [L^3/T], S is the storage coefficient and t is the elapsed time since the start of pumping [T].

Application to the nitrate polluted site

In order to identify the nitrate pollution plume in the vicinity area of well #346, an in-depth groundwater quality investigation was carried out by Beijing Hydrological Center in October, 2010. The water samples from additional 16 wells focused on this site (see location in Fig. 4.26) were analyzed in the laboratory. The nitrate plume contour lines interpolated with IDW method is shown in Fig. 4.30.

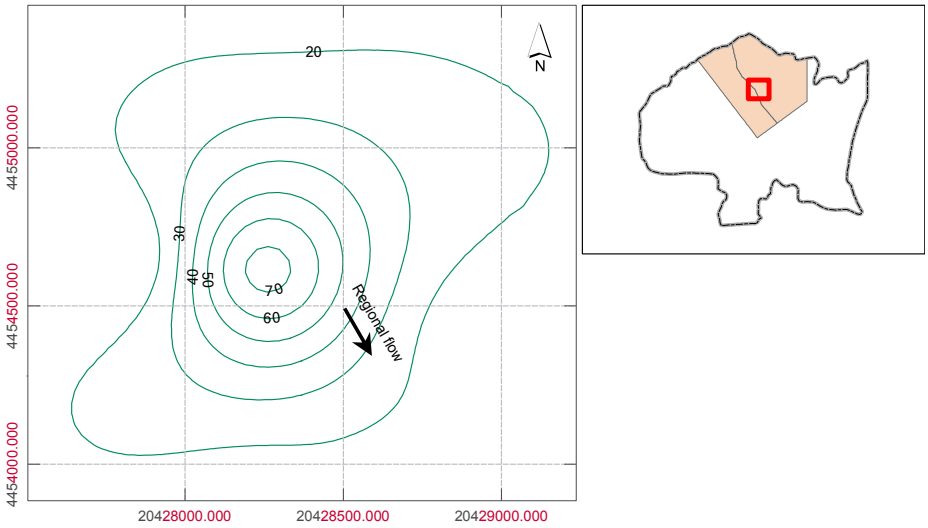

Figure 4.30: The nitrate plume contour map.

Based on the steady state groundwater flow model, the Darcy's flow velocity through the well # 346 is in the direction of 60 ° counterclockwise to the positive x-axis direction. The regional velocity of 6.0×10^{-7} m/s can be estimated by Darcy's law (Eq. 2.1).

Table 4.7: The characteristics of the pump and treat scenarios for one or two pumping wells.

Number of pumping wells	Location of well#346	Pumping rate at each well (m^3/s)	Drawdown at each well after 360 days (m)	
			analytical	numerical
1	(2300,140)	6.0e-2	3.96	4.15
2	(350,140)	4.8e-2	4.34	4.57

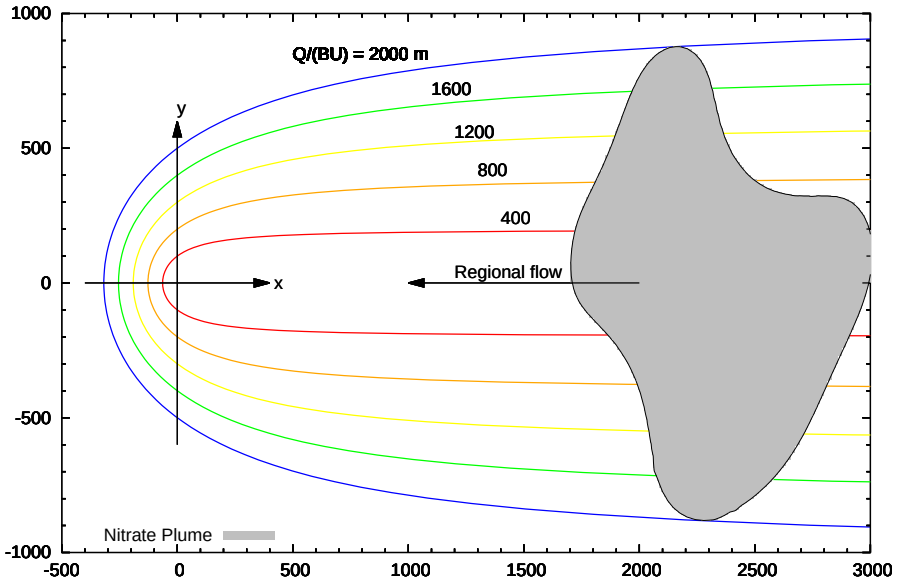

Figure 4.31: The nitrate plume combined with type curves map in the regional flow direction (single pumping well).

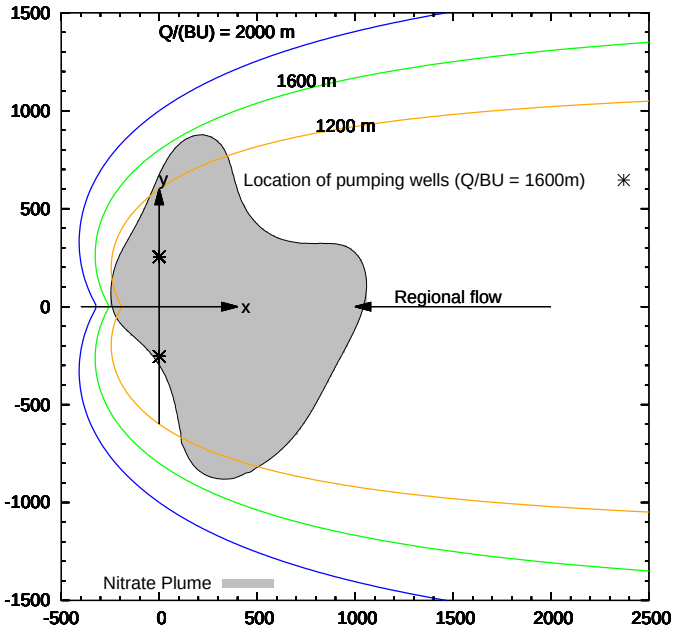

Figure 4.32: The nitrate plume combined with type curves map in the regional flow direction (double pumping well).

In the case of Fig. 4.32, the parameter Q/BU is 2000 m. According to the borehole log in this site, the average aquifer thickness is 50 m. Then based on the above relationship of Q, B and U, the pumping rate for one well is equal to 0.06 m^3/s. Other results with two pumping wells are list in Table. 4.7, and the location coordinates in Table. 4.7 mean the transformations of the well$\#$346 in the local coordinate system (Fig. 4.31 and 4.32). Pumping with two wells will take away the contaminant plume in a shorter time period but will induce much deeper drawdown in this case. The optimization with multi-pumping wells in reasonable locations will be carried out in future study.

Chapter 5

Summary and outlook

In this work, an integrated computational hydrosystem analysis methodology is applied to the Meijiang and Nankou catchments in China. In order to reproduce the complex hydrogeological structure of the case study site, GMS was used to do the geometrical modeling based on the available borehole data, and an interface that connects GMS and the numerical simulator OGS was developed to finish this data communication. A GIS based relational database model GHDB designed to create a specialized set of geo- and hydro-objects is also integrated with OGS.

In the Meijiang catchment, the regional soil water distribution and its response from surface infiltration was studied. The soil water Darcy's velocities achieved from RHSM can be used as source terms for calculating groundwater recharge by using a numerical integration scheme. In the Nankou case study, a 3-D groundwater flow model was developed and the pollution sources were investigated . The model was calibrated with all available data and the groundwater flow regime was investigated under steady and transient conditions. The groundwater level changes are resulting from interacting hydrological processes and anthropogenic activities, e.g. the recharges from precipitation, groundwater abstraction and so on. All available data relevant to these processes were used to analyse the groundwater flow regime in the study area but still not enough to identify all hydrogeological features. In order to reduce the uncertainties, the presented hydrogeological model will be improved in the future by developing appropriate monitoring strategies and integrating more detailed data when available.

With these two case study, the hydrosystem processes in the unsaturated vadzone and saturated aquifer were analysed respectively dependent on the available data. The coupling of the flow in the unsaturated and saturated zone applied to the reality could be a future work. In the Nankou case study, the treat and pump remediation scenario analysis is still on the way. The optimization with the total pumping rate and the clean-up time as objectives for multi-pumping wells will be the future research focus.

Appendix A

Publications list

1. **F. Sun**, C. Chen, W. Wang, Y. Wu, G. Lai and O. Kolditz. Compartment approach for regional hydrological analysis: Application to the Meijang catchment. In peer reviewed proceedings of the 7th International Conference on Calibration and Reliability in Groundwater Modeling (MODELCARE), Wuhan, China, 20-23 September, 2009, pages 191-194. IAHS Publ. 341-26, 2011.

2. **F. Sun**, H. Shao, T. Kalbacher, W. Wang, Z. Yang, Z. Huang and O. Kolditz. The groundwater flow regime at the Nankou site in the greater Beijing area. In Proceedings of the 9th International Conference on Hydroinformatics, Tianjin, China, 6-10 September, 2010. ISBN 978-7-89472-324-6, Chemical Industry Press, pages 485-493.

3. **F. Sun**, H. Shao, T. Kalbacher, W. Wang, Z. Yang, Z. Huang and O. Kolditz. Groundwater drawdown at Nankou site of Beijing Plain: model development and calibration. *Environmental Earth Sciences*, 2011. DOI: 10.1007/s12665-011-0957-4.

4. **F. Sun**. Groundwater flow. Chapter 5 in book: OpenGeoSys developer benchmark book, O. Kolditz, U. Görke and H. Shao, Eds, Springer-Verlag Berlin Heidelberg, in press, 2011.

REFERENCES

M. B. Abbott, J. C. Bathurst, J. A. Cunge, P. E. O'Connell, and J. Rasmussen. An introduction to the european hydrological system – systeme hydrologique europeen, "SHE", 2: Structure of a physically-based, distributed modelling system. *Journal of Hydrology*, 87(1-2):61 – 77, 1986.

R. G. Allen, L. S. Pereira, D. Raes, and M. Smith. Crop evapotranspiration: Guidelines for computing crop water requirements. In *FAO Irrigation & Drainage Paper No.56*, 1998.

J. G. Arnold, R. Srinivasan, R. S. Muttiah, and J. R. Williams. Large area hydrologic modeling and assessment part I: model development. *Journal of the American Water Resources Association*, 34(1):73–89, 1998.

M. Bayer-Raich, J. Jarsjö, R. Liedl, T. Ptak, and G. Teutsch. Average contaminant concentration and mass flow in aquifers from time-dependent pumping well data: Analytical framework. *Water Resour. Res.*, 40:W08303, 2004.

J. Bear. *Dynamics of Fluids in Porous Media*. American Elsevier Publishing Company, 1972.

Beijing Hydrogeology & Engineering Geology Center. *Beijing Hydrogeological Maps*. Beijing, 1980.

G. Bertoldi, D. Tamanini, F. Zanotti, and R. Rigon. Geotop, a hydrological balance model, technical description and programs guide (v0.875). Technical report, Department of Civil and Environmental Engineering, University of Trento, 2004.

G. Booch, J. Rumbaugh, and I. Jacobson. *Unified Modeling Language User Guide, The (2nd Edition) (Addison-Wesley Object Technology Series)*. Addison-Wesley Professional, 2005. ISBN 0321267974.

R. H. Brooks and A. T. Corey. Hydraulic properties of porous media, 1964.

C. Chen, A. Sawarieh, T. Kalbacher, M. Beinhorn, W. Wang, and O. Kolditz. A GIS based 3-D hydrosystem model of the Zarqa Ma'in-jiza areas in central Jordan. *Journal of Environmental Hydrology*, 13, 2005.

V. T. Chow, D. R. Maidment, and L. W. Mays. *Applied hydrology*. McGraw-Hill, New York, 1988.

A. T. Corey. The interrelation between gas and oil relative permeabilities. *Prod. Monthly*, 19(1):38–41, 1954.

H. A. R. de Bruin. From Penman to Makkink. In J. C Hoogart, editor, *Evaporation and weather: Proceedings and Information No. 39*, pages 5–27, 1987.

H. A. R. de Bruin and W. N Lablans. Reference crop evapotranspiration determined with a modified makkink equation. *Hydrological Processes*, 12:1053–1062, 1998.

J. Doherty. *MODINV-MODFLOW Parameter Optimization Manual Version 1.05*. Australian Center for Tropical Freshwater Research, Townsville, Queensland, 1990.

J. Doherty. *PEST:Model Independent Parameter Estimation*. Watermark Numerical Computing, Brisbane, Australia, 5 edition, 2004.

P. A. Domenico. An analytical model for multidimensional transport of a decaying contaminant species. *Journal of Hydrology*, 91(1-2):49–58, 1987.

W. Duan. Beijing water resources and the south to north water diversion project. *Canadian Journal of Civil Engineering*, 32:159–163, 2005.

E. Eichhorn. Modeling the dynamics of slope water as a source in Eastern basin with GeoSys. Master's thesis, Dresden University of Technology, Dresden, Germany, 2010.

C. W. Fetter. *Contaminant Hydrogeology*. Prentice Hall Publishing Company, Upper Saddle River, N.J., 2 edition, 1998.

R. A. Freeze and J. A. Cherry. *Groundwater*. Prentice Hall Inc., Englewood Cliffs, N.J., 1979.

L. W. Gelhar, C. Welty, and K. R. Rehfeldt. A critical review of data on field-scale dispersion in aquifers. *Water Resour. Res.*, 28(7):1955–1974, 1992.

R. E. Glover. *Transient Ground Water Hydraulics*. Water Resources Publications, 1978.

O. Gunduz and M. M. Aral. River networks and groundwater flow: a simultaneous solution of a coupled system. *Journal of Hydrology*, 301(1-4):216 – 234, 2005.

A. W. Harbaugh, E. R. Banta, M. C. Hill, and M. G. McDonald. Modflow-2000, the u.s. geological survey modular ground-water model: User guide to modularization concepts and the groundwater flow process. Technical report, U.S. Geological Survey, 2000.

T. Hewson. Simulation of leachate movement in the areal plane-a finite element approach. Master's thesis, Princeton University, 1976.

M. C. Hill. A computer program (MODFLOWP) for estimating parameters of a transient, threedimensional, ground-water flow model using nonlinear regression: U.S. Geological Survey Open-File Report 91–484. Technical report, 1992.

M. C. Hill. Methods and guidelines for effective model calibration with application to UCODE, a computer code for universal inverse modeling. U.S. Geological Survey Water Resources Report 98–4005. Technical report, 1998.

I. Javandel and C. Tsang. Capture-zone type curves: A tool for aquifer cleanup. *Ground Water*, 24(5):616 – 625, 1985.

O. Kolditz. Modelling flow and heat transfer in fractured rocks: dimensional effect of matrix heat diffusion. *Geothermics*, 24(3):421–437, 1995. ISSN 0375-6505.

O. Kolditz and H. Shao, editors. *OpenGeoSys Developer Benchmark Book*. 2010. `http://www.opengeosys.net`.

O. Kolditz, Y. Du, C. Buerger, J. Delfs, D. Kuntz, M. Beinhorn, M. Hess, W. Wang, B. van der Grift, and C. te Stroet. Development of a regional hydrologic soil model and application to the beerze-reusel drainage basin. *Environmental Pollution*, 148(3): 855 – 866, 2007.

O. Kolditz, J. O. Delfs, C. Buerger, M. Beinhorn, and C. H. Park. Numerical analysis of coupled hydrosystems based on an object-oriented compartment approach. *Journal of Hydroinformatics*, 10:227–244, 2008.

A. M. Lemon and N. L. Jones. Building solid models from boreholes and user-defined cross-sections. *Computers & Geosciences*, 29(5):547–555, 2003. ISSN 0098-3004.

R. Liedl, A. J. Valocchi, P. Dietrich, and P. Grathwohl. Finiteness of steady state plumes. *Water Resour. Res.*, 41:W12501, 2005.

H. J. Liu, N. S. Hsu, and T. H. Lee. Simultaneous identification of parameter, initial condition, and boundary condition in groundwater modeling. *Hydrological Processes*, 23: 2358–2367, 2009.

J. Liu, C. M. Zheng, L. Zheng, and Y. P. Lei. Ground water sustainability: methodology and application to the north china plain. *Ground Water*, 46:897–909, 2008.

F. Lomeland, E. Ebeltoft, and W. Hammervold Thomas. A new versatile relative permeability correlation. *Reviewed Proceedings of the 2005 International Symposium of the SCA*,, 32, 2005.

G. F. Makkink. Testing the Penman formula by means of lysimeters. *International Journal of Water Engineering*, 11:277–288, 1957.

M. G. McDonald and A. W. Harbaugh. *A modular three-dimensional finite-difference ground-water flow model*. Techniques of Water-Resources Investigations, Book 6. U.S. Geological Survey, 1988.

B. Miles, T. Kalbacher, O. Kolditz, C. Chen, J. Gronewold, W. Wang, and A. Peter. Development and parameterisation of a complex hydrogeological model based on high-resolution direct-push data. *Environmental Geology*, 52(7):1399–1412, 2007.

S. J. Owen, N. L. Jones, and J. P. Holland. A comprehensive modeling environment for the simulation of groundwater flow and transport. *Engineering with Computers*, 12: 235–242, 1996.

E. J. Pebesma and C. G. Wesseling. Gstat: a program for geostatistical modelling, prediction and simulation. *Computers & Geosciences*, 24(1):17 – 31, 1998.

E. P. Poeter and M. C. Hill. Inverse models: a necessary next step in ground-water modeling. *Ground Water*, 35:250–260, 1997.

E. P. Poeter, M. C. Hill, E. R. Banta, S. Mehl, and S. Christensen. Ucode_2005 and six other computer codes for universal sensitivity analysis, calibration, and uncertainty evaluation: U.S. Geological Survey Techniques and Methods 6-A11, 283p. Technical report, 2005.

Probe International Beijing Group. Beijing's Water Crisis: 1949-2008 Olympics. `http://old.probeinternational.org/catalog/pdfs/BeijingWaterCrisis1949-2008.pdf`, 2008.

J. C. Refsgaard, J. P. van der Sluijs, A. L. Højberg, and P. A. Vanrolleghem. Uncertainty in the environmental modelling process - a framework and guidance. *Environmental Modelling & Software*, 22(11):1543 – 1556, 2007.

L. A. Richards. Capillary conduction of liquids through porous mediums. *Physics*, 1(5): 318–333, 1931.

K. E. Saxton and P. H. Willey. *The SPAW model for agricultural field and pond hydrologic simulation*, chapter 17, pages 401–435. Taylor & Francis Group, U.S., 2006.

E. A. Sudicky, J. E. Vanderkwaak, J. P. Jones, J. P. Keizer, R. G. Mclaren, and G. B. Matanga. Fully-integrated modelling of surface and subsurface water flow and solute transport: Model overview and application. In A. S. Alsharhan and W. W. Wood, editors, *Water Resources Perspectives: Evaluation, Management and Policy*, volume 50 of *Developments in Water Science*, pages 313 – 318. Elsevier, 2003.

M. T. van Genuchten. A closed-form equation for predicting the hydraulic conductivity of unsaturated soils. *Soil Sci. Soc. Am. J.*, 44(5):892–898, 1980.

L. Y. Wang, J. P. Han, J. R. Liu, C. Ye, Y. J. Zhen, L. Q. Wan, W. P. Li, and Y. X. Zhou. Modelling of regional groundwater flow in Beijing Plain. *Hydrogeology & Engineering Geology*, 36(1):11–17, 2009a.

S. Q. Wang, J. L. Shao, X. F. Song, Y. B. Zhang, Z. B. Huo, and X. Y. Zhou. Application of MODFLOW and geographic information system to groundwater flow simulation in North China Plain, China. *Environmental Geology*, 36(1):11–17, 2008.

W. Wang, G. Kosakowski, and O. Kolditz. A parallel finite element scheme for thermo-hydro-mechanical (THM) coupled problems in porous media. *Computers & Geosciences*, 35:1631–1641, 2009b.

A. W. Warrick, J. W. Biggar, and D. R. Nielsen. Simultaneous solute and water transfer for an unsaturated soil. *Water Resources Research*, 7(5):1216–1225, 1971.

Wasy Software. *Wasy Software, IFMMIKE11 1.1, User Manual*. Wasy GmbH, Institute for Water Resources Planning and System Research, 2004.

E. B. Wylie and V. L. Streter. *Fluid transients*. Republished with minor corrections by FEB Press, Ann Arbor, NY, 1983. New York: McGraw Hill, 1978.

Z. Xie, Z. Zhang, G. Xing, M. Xu, and F. Zhang. Analysis of the groundwater-supply security about the representative cities in North China Plain. *Resources Sciences*, 31: 400–405, 2009.

X. K. Xu. A study of numerical simulation for groundwater flow in the Beijing plain. Master's thesis, China University of Geosciences, Beijing, 2006.

Z. J. Zhang and Y. H. Fei. *Investigation and evaluation on the sustainable utilization of groundwater in North China Plain*. Geological Publishing House, Beijing, 2009.

D. Zhao and B. Sun. *The gazetteer of Changping county, Beijing*. Beijing Publishing Group, Beijing, 1979.

C. Zheng and G.D. Bennett. *Applied contaminant transport modeling*. Wiley-Interscience, 2002. ISBN 9780471384779.

Feng Sun

I certify that I have read this dissertation and that, in my opinion, it is fully adequate in scope and quality as a dissertation for the degree of Doctor of Philosophy.

(Prof. Dr. Olaf Kolditz) Principal Adviser

Approved for the University Committee on Graduate Studies